Clumped isotope thermometry as a new tool for reconstructing Miocene climate change

Thomas Jan Leutert

Thesis for the degree of Philosophiae Doctor (PhD)
University of Bergen, Norway
2020

UNIVERSITY OF BERGEN

Clumped isotope thermometry as a new tool for reconstructing Miocene climate change

Thomas Jan Leutert

Thesis for the degree of Philosophiae Doctor (PhD)
at the University of Bergen

Date of defense: 27.01.2020

Year: 2020

Title: Clumped isotope thermometry as a new tool for reconstructing Miocene climate change

Name: Thomas Jan Leutert

Print: Skipnes Kommunikasjon / University of Bergen

Scientific environment

The research leading to this dissertation was performed at the Department of Earth Science and the Bjerknes Centre for Climate Research, University of Bergen, Norway. The PhD study was part of the C^4T project financed by the European Research Council (ERC) under the European Union's Horizon 2020 research and innovation programme (grant agreement No 638467). Additional funding came from the Trond Mohn Foundation. The supervisory committee consisted of Nele Meckler (University of Bergen) as the main supervisor and the co-supervisors Alison Piasecki (Harvard University) and Aradhna Tripati (University of California, Los Angeles).

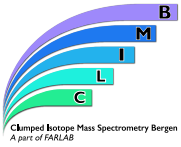

Acknowledgements

First and foremost, I would like to express my sincere gratitude to Nele Meckler for giving me the opportunity to carry out this research. I feel very lucky to have had her as my main supervisor, and thank her for many stimulating discussions, ideas, patience and support throughout the whole project. Thanks to Nele, my PhD study time was very colorful including various group retreats, dinners, conferences, research stays and a cruise. I would also like to thank my co-supervisors Alison Piasecki and Aradhna Tripati for their guidance and detailed input especially on Paper I.

Furthermore, I would like to thank all present and past members of the clumped isotope group. Thank you for the team spirit and countless hours together in the laboratory. Ling, thank you for the friendship and the encouragement in difficult times. You have been the best office mate one could imagine. Niklas, we have shared many ups and downs during our time in Bergen. I am very grateful to have had you as a PhD buddy almost from the beginning, and thank you for sharing your knowledge reaching far beyond science. Alison, I learned a lot about isotope measurements from you, many thanks for that. Sevi, thank you for all the fun we had inside and outside our office and your support, also during evenings and weekends. Anna, thank you for the delightful conversations we had during lunchtime. Alvaro, your enthusiasm for science really inspired me during the last phase of my PhD. I am very grateful for this source of motivation. In addition, I want to thank my office mate Yves Krüger (and his familiy) for brightening up my every day office life and the lunches we had together.

Philip Sexton, Robin van der Ploeg, Alfredo Martínez-García, Alexandra Auderset and Stefano Bernasconi are thanked for fruitful collaboration, support and help with writing. In particular, I would like to acknowledge Alfredo and Alexandra for providing TEX_{86}-based temperature data for Paper II. Also, I am grateful to Carrie Lear for providing sample material as well as Ann Holbourn and

Wolfgang Kuhnt who provided sediment samples and offered the opportunity to join R/V Sonne Expedition SO-257 in the Indian Ocean.

During my PhD, I had the chance to co-supervise a master project. Kristine, I thank you for the enthusiasm and the great job you have done.

I would like to further thank Enver Alagoz, Anna Kieu-Diem Tran, Pål Tore Mørkved and Inigo Müller for technical support in the isotope laboratories at the University of Bergen and ETH Zurich, Andreas Rasmussen and Jordan Donn Holl for help with sample washing and Irene Heggstad for support with the scanning electron microscope. I have shared the last years with numerous great colleagues in the Quaternary Earth Systems group and the Bjerknes Centre for Climate Research at the University of Bergen. In particular, I would like to thank Lisa Griem, Lukas Becker, Henrik Sadatzki, Eirik Vinje Galaasen, Nil Irvali, Raúl Tapia, Andreas Plach, Yongbiao Weng, Carl Regnéll, Fanny Ekblom Johansson, Torgeir Opeland Røthe, Tobias Zolles, Sunniva Rutledal, Willem van der Bilt, Johannes Werner and Alexios Theofilopoulos for accompanying me during the last four years. A special thanks goes to Alvaro and Eirik for proofreading my thesis.

I am deeply grateful to my wonderful family always supporting me on my way. Thank you very much for having helped me to get settled in Bergen, and always making me feel loved and at home when staying in Switzerland. I also thank my friends in Norway, Switzerland and Germany, especially Benjamin, Erica, Lukas, Marc, Nicole, Martin, Steffen, Mischa and Sebastian. Numerous hikes, barbecues, beers, cinema and play evenings made this time unforgettable for me. Last but not least, I thank my dear girlfriend Janika for her endless support. You did not only provide invaluable scientific help, for example with taxonomic issues, but you were also there for me when I was frustrated and listened to my complaints with patience. I am especially grateful for our weekend escapes in Kiel and many other places in Europe giving me rest, warmth and the strength to go on in stressful times. Without your love, this would have not been possible.

Abstract

This PhD thesis focuses on the clumped isotope paleothermometer and its application to foraminiferal carbonates buried in ocean sediments. Based on new proxy evidence for ocean temperature, the thesis aims at improving our understanding of the mechanisms driving the climate system in a warmer world.

In the first paper, the effects of diagenetic processes on clumped isotope temperatures are examined in order to assess the fidelity and robustness of the paleothermometer for applications deeper in geological time. For this purpose, clumped isotope temperature data measured on middle Eocene benthic and planktic foraminifera from six ODP/IODP sites in the Atlantic Ocean are compared. Our results demonstrate that benthic and well-preserved planktic foraminiferal carbonates are likely to yield robust temperature estimates of initial calcification, whereas temperatures derived from planktic foraminiferal tests with clear signs of diagenetic alteration appear to be biased towards cool temperatures. These observations are supplemented with end-member mixing modeling.

In the second paper, we use planktic foraminiferal clumped isotope and organic biomarker-based temperature records from ODP Site 1171 on the South Tasman Rise to constrain the thermal evolution of the upper waters of the Southern Ocean across the middle Miocene climate transition, which is a large-scale climate shift towards colder conditions. Our results suggest that upper ocean cooling was gradual and coupled to the expansion of the Antarctic ice sheet. These observations contrast with previous Mg/Ca-based temperature reconstructions that indicate much more abrupt cooling preceding ice sheet expansion. We show that Mg/Ca-based paleotemperature estimates can be brought into agreement with those based on clumped isotopes and TEX_{86} when taking into account pH as a non-thermal influence on Mg/Ca in planktic foraminifera. Integrating our upper ocean temperature records with recent reconstructions of atmospheric CO_2 indicates that the effect of CO_2 forcing on southern high latitude climate may have been more

important than previously assumed.

In the third paper, the focus is on middle Miocene bottom water temperatures and ice volume. We present clumped as well as oxygen and carbon isotope data measured on benthic foraminiferal tests from ODP Site 747 located on the Kerguelen Plateau in the Southern Ocean. Our results suggest that Middle Miocene Southern Ocean bottom waters were substantially warmer than today, and then cooled by ~3-5°C. This cooling seems to precede ice growth during the middle Miocene climate transition, and was followed by a transient warming. We hypothesize that bottom water temperatures at Site 747 may have been influenced by regional processes, and specifically changes in heat transport between the upper and deep ocean.

Taken together, the results of this thesis provide new constraints on the robustness of the clumped isotope paleothermometer towards burial diagenesis, and demonstrate the potential of the paleothermometer to provide key insights into Earth's climate history. Continued clumped isotope analyses on foraminiferal carbonates from past greenhouse climates may further improve our understanding of the impacts of future warming on sensitive regions such as Antarctica.

List of publications

Paper I

Leutert T.J., Sexton P.F., Tripati A., Piasecki A., Ho S.L. and Meckler A.N. Sensitivity of clumped isotope temperatures in fossil benthic and planktic foraminifera to diagenetic alteration. *Geochimica et Cosmochimica Acta* **257**, 354-372 (2019).

Paper II

Leutert T.J., Auderset A., Martínez-García A., Modestou S. and Meckler A.N. Southern Ocean temperature evolution coupled to middle Miocene ice sheet expansion. *Manuscript in preparation for Nature Geoscience*.

Paper III

Leutert T.J., Modestou S., Bernasconi S.M. and Meckler A.N. Southern Ocean bottom water cooling and ice sheet expansion during the middle Miocene climate transition. *Manuscript in preparation for Earth and Planetary Science Letters*.

Table of Contents

Introduction

The Intergovernmental Panel on Climate Change (IPCC) has noted in its fifth Assessment Report that globally averaged land and ocean surface temperatures increased by approximately 1°C from 1880 to 2012 (IPCC, 2013; see also IPCC, 2018). Positive radiative forcing, leading to surface warming, global ice loss and a rising sea level, has been primarily attributed to the observed increase in the atmospheric concentration of greenhouse gases, in particular anthropogenic carbon dioxide (CO_2) (e.g., Foster et al., 2017). This greenhouse gas has risen from a pre-industrial level of ~280 ppm to ~410 ppm during the last 250 years (IPCC, 2013; https://www.co2.earth), and will likely continue to do so. Depending on the emission scenario, projected CO_2 concentrations for 2100 range from ~420 ppm (RCP2.6) to ~940 ppm (RCP8.5) (Bopp et al., 2013). In addition to direct radiative forcing, a number of feedback mechanisms play a role in determining the effects of climate change on global and regional scales. Examples are positive carbon-cycle feedbacks associated with a reduced CO_2 sink in the ocean that may reinforce the expected temperature increase (e.g., Joos et al., 1999; Sabine et al., 2004; IPCC, 2013). Other types of feedbacks such the surface albedo feedback are related to sea ice and ice sheets (e.g., Hall, 2004; Goosse et al., 2018). A better understanding of such feedbacks, their underlying processes and the response of the climate system to high atmospheric CO_2 concentrations is required to reduce uncertainties and improve our predictions of future climate change.

Middle Miocene climate transition in the context of Cenozoic cooling

Climate observations and reconstructions for the last few thousand years have yielded important insights into actual climate trends and the fundamental

mechanisms of the climate system (e.g., Rahmstorf et al., 2007; Neukom et al., 2019). However, such data can provide only limited constraints on the effects of future warming because the projected scale of change is unlike anything seen on Earth during the last millions of years. By contrast, sedimentary archives of past warm climates further back in time offer great potential for increasing our basic understanding of future climate forcings, feedbacks and thresholds.

During the Cenozoic era, the past 65 million years, the Earth System has transitioned from a warm and likely ice-free "greenhouse" to a cooler "icehouse" state. Climate change during this era is revealed by the oxygen isotopic composition ($\delta^{18}O$) of fossil benthic foraminiferal tests buried in ocean sediments (Figs. 1 and 2b), reflecting a combination of changes in bottom water temperature (BWT) and continental ice volume (e.g., Zachos et al., 2001; Zachos et al., 2008; Cramer et al., 2011; Veizer and Prokoph, 2015; De Vleeschouwer et al., 2017). Early Cenozoic warming (indicated by the decrease in benthic $\delta^{18}O$ in Fig. 2b) and the early Eocene climatic optimum (EECO, benthic $\delta^{18}O$ minimum) were followed by a long-term cooling trend (increase in benthic $\delta^{18}O$) continuing through most of the remaining Cenozoic. This long-term cooling pattern is complex, including both gradual and relatively abrupt changes, while also being interrupted by a number of transient warm periods. The effect of ice volume on benthic $\delta^{18}O$ is thought to have been significant only from around 34 Ma, when Antarctic ice sheets expanded rapidly during the Eocene-Oligocene transition (EOT) (e.g., Lear et al., 2000; Zachos et al., 2001; Coxall et al., 2005).

The Pliocene is the most recent period where atmospheric CO_2 reached close to present-day or even slightly higher levels (Fig. 2a; Martínez-Botí et al., 2015; Sosdian et al., 2018). Future CO_2 levels in the atmosphere are however projected to be substantially higher in low mitigation scenarios, causing a need to go further back in time when looking for geological precedents for future CO_2 forcing (Bopp et al., 2013; Foster et al., 2017; Burke et al., 2018; Sosdian et al., 2018). The Miocene climatic optimum (MCO, ~17-14 Ma) and the EECO (~52-52 Ma) were likely characterized by maximum CO_2 levels well above 500 and 1000 ppm,

respectively (Anagnostou et al., 2016; Foster et al., 2017; Sosdian et al., 2018). These warm periods may thus represent more useful analogues for predictions of future warm states.

The middle Miocene is particularly interesting for studying the interactions between ocean temperature, ice sheets, sea level and CO_2 in the near future, as warm climate conditions coincide with a continental configuration that is relatively close to modern (Herold et al., 2008; Goldner et al., 2014; Matthews et al., 2016). The most striking glaciation event of the middle Miocene, as expressed by a benthic $\delta^{18}O$ increase of ~1‰, occurred around 14 Ma (e.g., Flower and Kennett, 1993; Holbourn et al., 2005). The middle Miocene climate transition (MMCT) terminated the MCO, and initiated the overall cooling trend characterizing the last 14 Myr. Recent reassessments of alkenone- and boron isotope-based CO_2 estimates suggest a CO_2 decrease of ~100-300 ppm across the MMCT (Sosdian et al., 2018; Super et al., 2018), although disagreements between different CO_2 reconstruction techniques still exist.

Fig. 1: Foraminiferal test. Umbilical (left), apertural (middle) and spiral (right) view of the benthic species *Cibicidoides wuellerstorfi* (modified from Gottschalk et al. (2016)). This species has been widely used for paleoclimate reconstructions.

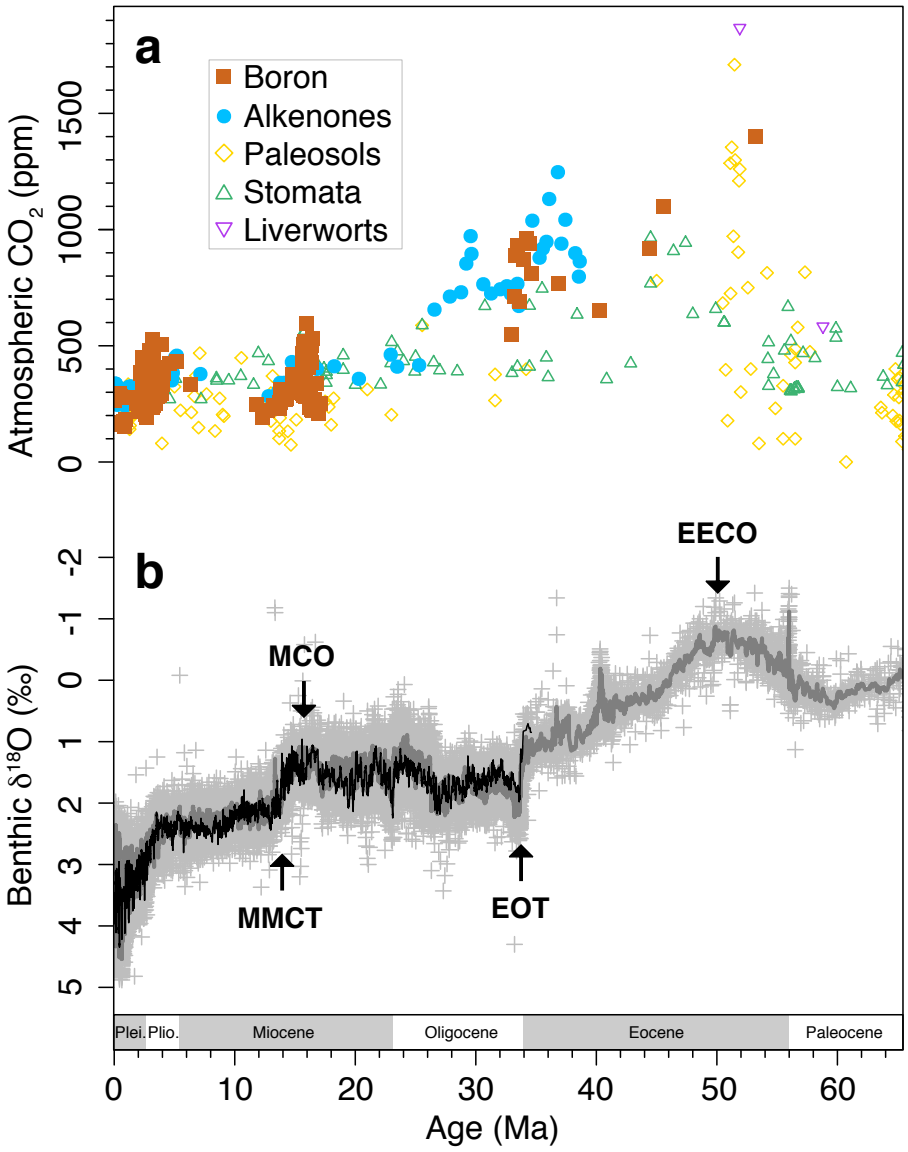

Fig. 2: Evolution of global climate during the last 65 Myr. **a**, Atmospheric CO_2 compiled by Foster et al. (2017). Estimates are based on boron isotopes (red filled squares), alkenones (blue filled circles), paleosols (yellow diamonds), stomata (green triangles), and liverworts (purple triangles). **b**, Deep-sea benthic foraminiferal $\delta^{18}O$ from the global compilation of Veizer and Prokoph (2015) (light grey crosses = raw data, dark grey line = 11-point running mean) and the 35 Myr-splice of high-resolution records of De Vleeschouwer et al. (2017) (black line = 11-point running mean). Major climate

optima and transitions are labelled as follows: MMCT = middle Miocene climate transition, MCO = Miocene climatic optimum, EOT = Eocene-Oligocene transition, EECO = early Eocene climatic optimum. Time scale after Gradstein et al. (2012).

Benthic foraminiferal $\delta^{18}O$ records (Fig. 2b) indicate that continental ice sheets were relatively small during the MCO, and then expanded abruptly on Antarctica and possibly also in the Arctic (e.g., DeConto et al., 2008). However, benthic foraminiferal $\delta^{18}O$ represents a convoluted signal affected by changes in both bottom water $\delta^{18}O$ (i.e., ice volume) and bottom water temperature (BWT) during the middle Miocene (e.g., Zachos et al., 2001). This dual control of ice volume and temperature limits the informative value of foraminiferal $\delta^{18}O$ in the absence of an independent constraint on either ice volume or temperature. Various reconstruction and modelling techniques have been used to isolate middle Miocene changes in sea level, ice volume and BWT (e.g., Kominz et al., 2008; Shevenell et al., 2008; Langebroek et al., 2009; de Boer et al., 2010; Lear et al., 2010; Lear et al., 2015; Frigola et al., 2018). Suggested changes in sea level across the MMCT span a wide range of values from around 20 to 90 m (Kominz et al., 2008; Langebroek et al., 2009; de Boer et al., 2010; Lear et al., 2010; Lear et al., 2015; Frigola et al., 2018). Independent estimates of middle Miocene BWTs are largely based on the Mg/Ca paleothermometer, and indicate a bottom water cooling of ~0.5-3°C (Lear et al., 2000; Billups and Schrag, 2002, 2003; Shevenell et al., 2008; Lear et al., 2010; Lear et al., 2015). These results appear consistent with the interpretation that a large fraction of the observed benthic $\delta^{18}O$ increase relates to Antarctic ice sheet expansion (e.g., Shevenell et al., 2008). Although the Mg/Ca proxy has shown high potential for revealing the BWT component of the benthic foraminiferal $\delta^{18}O$ signal, the proxy has been shown to be sensitive to a number of non-thermal controls including bottom water carbonate saturation (e.g., Elderfield et al., 2006) and seawater Mg/Ca (e.g., Evans and Müller, 2012). These complications have been addressed (e.g., Lear et al., 2010; Evans and Müller, 2012), but uncertainties regarding middle Miocene BWTs remain.

Our knowledge of upper ocean temperature change across the MMCT depends on several measurement techniques, each with its own strengths and weaknesses. The most commonly used upper ocean temperature proxies are Mg/Ca and organic biomarkers. Applied to planktic foraminifera, the Mg/Ca thermometer suggests pronounced (~6-7°C) upper ocean cooling at southern high latitudes (Shevenell et al., 2004; Kuhnert et al., 2009) and much smaller cooling at low latitudes (Holbourn et al., 2010) during the MMCT. In addition to calcification temperature, however, non-thermal controls such as pH (e.g., Russell et al., 2004; Evans et al., 2016), salinity (e.g., Hönisch et al., 2013) and seawater Mg/Ca (e.g., Evans and Müller, 2012) have been shown to impact planktic foraminiferal Mg/Ca in certain settings. Further factors with the potential to alter primary Mg/Ca ratios in planktic foraminiferal tests are dissolution and diagenesis (e.g., Sexton et al., 2006b; Regenberg et al., 2007; Regenberg et al., 2014). Biomarkers such as the alkenone unsaturation index ($U_{37}^{K'}$) and the tetraether index of tetraethers (TEX_{86}) represent alternative approaches to derive past upper ocean temperatures (e.g., Brassell et al., 1986; Prahl and Wakeham, 1987; Schouten et al., 2002). TEX_{86}-based upper ocean temperatures from the Southern Ocean offshore East Antarctica suggest ocean conditions that are overall warmer during the MCO than after this climatic optimum, supported by palynological proxy data (Bijl et al., 2018; Hartman et al., 2018; Sangiorgi et al., 2018). Similarly, a North Atlantic temperature reconstruction based on TEX_{86} indicates warm conditions during the MCO, followed by an upper ocean cooling of ~6°C across the MMCT (Super et al., 2018). Other TEX_{86}- and $U_{37}^{K'}$-based ocean temperature records from the western tropical Atlantic are of low temporal resolution (e.g., Zhang et al., 2013). In any case, the TEX_{86} and $U_{37}^{K'}$ methods are not without their own complications. For TEX_{86}, uncertainty is caused by the lack of clarity about the exact depth of the origin of the temperature signal below sea surface (e.g., Lipp et al., 2008; Ho and Laepple, 2016), whereas the application of the $U_{37}^{K'}$ proxy is limited to settings with temperatures below ~28°C (e.g., Müller et al., 1998; Herbert et al., 2016). Furthermore, $U_{37}^{K'}$-based temperature values can be strongly biased to late summer/autumn (e.g., Haug et al., 2005).

The difficulty in reconstructing ocean temperatures during the MMCT has become an impediment to understanding the driving mechanisms of global climate change during this key interval. A large part of the scientific debate centers on processes related to global carbon cycling, orbital forcing, Southern Ocean hydrography and Antarctic ice sheet dynamics. Notably, Southern Ocean cooling reconstructed from planktic foraminiferal Mg/Ca appears to precede the stepped increase in ice volume by ~100-300 kyr (Shevenell et al., 2004; Kuhnert et al., 2009). This observation was linked to orbital forcing and changes in atmospheric and oceanic circulation controlling meridional heat/vapor transport (e.g., Shevenell et al., 2004; Holbourn et al., 2005; Kuhnert et al., 2009). Circulation hypotheses (e.g., relating oceanic circulation patterns to tectonic events such as the closing of the Tethys) have also been made earlier for the MMCT (e.g., Schnitker, 1980; Woodruff and Savin, 1989). Other studies have suggested a more direct link between atmospheric CO_2 and climate during that interval (e.g., Vincent and Berger, 1985; Tripati et al., 2009; Foster et al., 2012; Holbourn et al., 2014; Super et al., 2018). Thorough testing of these hypotheses has remained difficult, also due to the ambiguity inherent in existing ocean temperature reconstructions. Independent ocean temperature records from well-dated sedimentary sequences are urgently needed to assess the roles of circulation patterns and CO_2 as potential drivers of the MMCT.

Clumped isotope thermometer

Carbonate clumped isotope thermometry is based on measuring the extent to which ^{13}C and ^{18}O isotopes are bound to one another in a carbonate mineral lattice (e.g., Eiler and Schauble, 2004; Wang et al., 2004; Ghosh et al., 2006; Schauble et al., 2006; Eiler, 2007, 2011, 2013). This chemical bonding (or "clumping") of ^{13}C and ^{18}O in carbonate ion (CO_3^{2-}) groups can be described by the following homogeneous isotope exchange reaction:

$$^{13}C^{16}O_3^{-2} + {}^{12}C^{18}O^{16}O_2^{-2} \rightleftharpoons {}^{13}C^{18}O^{16}O_2^{-2} + {}^{12}C^{16}O_3^{-2} \quad (1)$$

At present, it is not possible to measure ^{13}C–^{18}O bond abundances directly in solid carbonate minerals (i.e., CO_3^{2-}). Instead, abundances of species containing both ^{13}C and ^{18}O (mostly $^{13}C^{18}O^{16}O$) are measured on CO_2 gas extracted from carbonate powder by phosphoric acid digestion (Ghosh et al., 2006; Huntington et al., 2009). If temperature is controlled during carbonate acid digestion, then the degree of ^{13}C-^{18}O ordering in a carbonate mineral can be estimated from the measured clumped isotope signature of the released CO_2 gas (e.g., Ghosh et al., 2006; Schauble et al., 2006; Eiler, 2007; Guo et al., 2009; Eiler, 2011, 2013; Defliese et al., 2015). The Δ_{47} value (reported in units of per mil) measures the temperature-dependent excess of mass 47 isotopologues relative to the abundances expected for a stochastic isotope distribution (Wang et al., 2004; Eiler, 2007, 2011):

$$\Delta_{47} = \left[\left(\frac{R^{47}}{R^{47*}} - 1\right) - \left(\frac{R^{46}}{R^{46*}} - 1\right) - \left(\frac{R^{45}}{R^{45*}} - 1\right)\right] \times 1000 \quad (2)$$

R^{45}, R^{46} and R^{47} are the measured ratios of the masses 45, 46 and 47 relative to mass 44, respectively. R^{45*}, R^{46*} and R^{47*} are the corresponding ratios expected for stochastic distribution of all isotopes among all possible CO_2 isotopologues. These latter ratios are derived from the abundance ratios $^{17}O/^{16}O$, $^{18}O/^{16}O$ and $^{13}C/^{12}C$ (Eiler, 2007).

The clumped isotope method is technically challenging, because multiply-substituted isotopologues are naturally scarce and the excess abundances of these isotopologues relative to stochastic isotope distribution low (e.g., Eiler, 2007; Eiler, 2011; Spencer and Kim, 2015). Contaminants such as hydrocarbons and chlorocarbons can lead to isobaric interferences during measurement (e.g., Eiler, 2007, 2011). Therefore, the method relies on highly pure CO_2 gas. Furthermore, the isotope signal is controlled by composition (i.e., δ^{47})-dependent (non-linearity) effects related to negative backgrounds on the Faraday collectors of the mass spectrometer as well as composition-independent (scale compression) effects

associated with electron ionization source processes (e.g., Huntington et al., 2009; Dennis et al., 2011; He et al., 2012; Bernasconi et al., 2013). Most clumped isotope data produced until now have been corrected and standardized based on CO_2 gases of different bulk isotopic compositions (δ^{47}) that are heated to >1000°C or isotopically equilibrated to a certain temperature (e.g., Huntington et al., 2009; Dennis et al., 2011). Analyzing these gases of different isotopic composition and ordering states allows for the determination of Δ_{47} versus δ^{47} regressions (gas lines), whose slopes can be used to assess δ^{47}-dependent biases in Δ_{47} measurements. Composition-independent biases can be accounted for by applying an empirical transfer function (based on the gas line intercepts at different temperatures) to normalize the measured values to an absolute reference frame and enable inter-laboratory data comparison (Wang et al., 2004; Dennis et al., 2011). A number of recent studies have demonstrated that the comparability of clumped isotope data from different laboratories can be further improved through use of the ^{17}O abundance correction parameters from Brand et al. (2010), daily background monitoring for pressure-proportional background correction and consistent carbonate-based correction schemes (e.g., Bernasconi et al., 2013; Meckler et al., 2014; Daëron et al., 2016; Bernasconi et al., 2018). Importantly, using a micro-volume (e.g., Bernasconi et al., 2013) and the long-integration dual-inlet (LIDI) method of Hu et al. (2014) for the measurements has helped reduce sample size requirements, improving the applicability of the clumped isotope thermometer in settings where sample amount is a limiting factor.

The key feature of the carbonate clumped isotope thermometer is that the clumped isotope signature of a carbonate mineral is independent of the isotopic composition of its parent water at thermodynamic equilibrium (e.g., Ghosh et al., 2006; Eiler, 2013). In spite of comparably large measurement uncertainties, this paleothermometer thus has the potential to yield accurate carbonate formation temperatures, even in settings where the isotopic composition of the parent water body is poorly constrained. Empirical data and theoretical modeling support the assumption that primary clumped isotope signatures of benthic and planktic foraminiferal carbonates are largely uncompromised by non-equilibrium

fractionation processes, related to solution pH and isotope exchange kinetics, as well as species-specific vital effects (e.g., Tripati et al., 2010; Grauel et al., 2013; Kele et al., 2015; Tripati et al., 2015; Watkins and Hunt, 2015; Breitenbach et al., 2018; Peral et al., 2018; Piasecki et al., 2019; Meinicke et al., in review). For other more widely used foraminifera-based paleothermometers (e.g., $\delta^{18}O$, Mg/Ca), differential vital effects (e.g., Bemis et al., 1998; Lear et al., 2002) introduce uncertainties, particularly in intervals of taxonomic turnover and/or intervals with rare extant species. Also, the clumped isotope method yields carbonate $\delta^{18}O$ values in parallel to carbonate formation temperatures. Measured $\delta^{18}O$ and temperature values can be combined in order to estimate water $\delta^{18}O$ compositions. Constraints on seawater $\delta^{18}O$ may be used to infer changes in salinity or global ice volume. Separation of the ice volume and temperature contributions to the $\delta^{18}O$ signal recorded in deep-sea carbonates has been a goal for a long time (e.g., Lear et al., 2000; Zachos et al., 2001). We further note that no significant ^{13}C–^{18}O bond reordering has been observed in the solid carbonate mineral lattice below ~100°C on 10^6 year-timescales (e.g., Dennis and Schrag, 2010; Henkes et al., 2014). This enhances confidence in the application of the clumped isotope approach to sample material from far back in time for long-term temperature studies.

The clumped isotope method has a number of drawbacks. Relatively large samples sizes are required to produce Δ_{47} data with an analytical error that is small enough for paleoclimate applications, limiting the use of the clumped isotope method in many settings (for example, at high latitudes where foraminiferal abundances are often low). Measurements are time-consuming, and larger analytical random errors in clumped isotope temperature estimates, compared to other proxies, make it difficult to assess small and rapid changes in temperature and their exact timing. Furthermore, the primary state of isotopic ordering can be altered by structural changes during burial diagenesis (e.g., recrystallization, secondary calcite precipitation), with the degree of alteration depending on the depositional setting (Stolper et al., 2018). Last, it is important to note that the clumped isotope method is still in its infancy, compared to other more established paleoceanographic temperature proxies. There is a lot more left to explore.

To sum up, the carbonate clumped isotope thermometer represents a promising tool to reconstruct past ocean temperatures, because it circumvents major limitations of other more established paleotemperature proxies. But, the application of this relatively new method to fossil foraminiferal carbonates also poses some challenges including potential diagenetic effects on clumped isotope signatures.

Objectives

The main purpose of this PhD project was to use the clumped isotope method to contribute to solving long-standing questions about Miocene climate. First, the potential of diagenetic biases in clumped isotope temperature reconstructions was explored to provide a foundation and offer guidelines for the paleoceanographic application of the clumped isotope temperature proxy. Then, clumped isotope signatures were measured on middle Miocene benthic and planktic foraminifera in order to reconstruct Southern Ocean temperature change across the MMCT.

The specific objectives were to:

1) Constrain the resistance of the primary clumped isotope temperature signal hosted within benthic and planktic foraminiferal tests to post-depositional diagenesis (e.g., recrystallization) and assess which degree of foraminiferal preservation is required for meaningful ocean temperature reconstructions (Paper I).

2) Reconstruct upper ocean temperature evolution in the Southern Ocean across the MMCT based on planktic foraminiferal Δ_{47} in combination with TEX_{86} to study the roles of climate feedbacks and forcings, especially ocean circulation and atmospheric CO_2, in controlling Southern Ocean and Antarctic climate (Paper II).

3) Quantify middle Miocene bottom water cooling and ice volume changes through benthic foraminiferal Δ_{47} and $\delta^{18}O$, and integrate these results with existing proxy records to further understand the mechanisms driving high southern latitude climate (Paper III).

Material and methods

Sediment samples were obtained from the core repositories of the Ocean Drilling Program (ODP) and Integrated Ocean Drilling Program (IODP) from a number of study sites (Fig. 3). Coordinates, water depths, and relevant references for each study site are provided in Table 1. For our study on diagenetic effects (**Objective 1**), ODP/IODP Sites 1408, 1409, 1410, 1050, 1260 and 1263 were chosen. These sites are all located in the Atlantic Ocean basin but are characterized by different burial histories and a wide range of foraminiferal preservation states. Clumped isotope values were measured on coeval middle Eocene tests of upper ocean mixed layer-dwelling planktic foraminifera *Acarinina bullbrooki* and *Morozovelloides coronatus* as well as those of shallow infaunal benthic foraminifera *Nuttalides truempyi*, allowing to constrain diagenetic effects on clumped isotope temperatures. The primary nature of foraminiferal calcite was assessed by means of scanning electron microscopy (SEM).

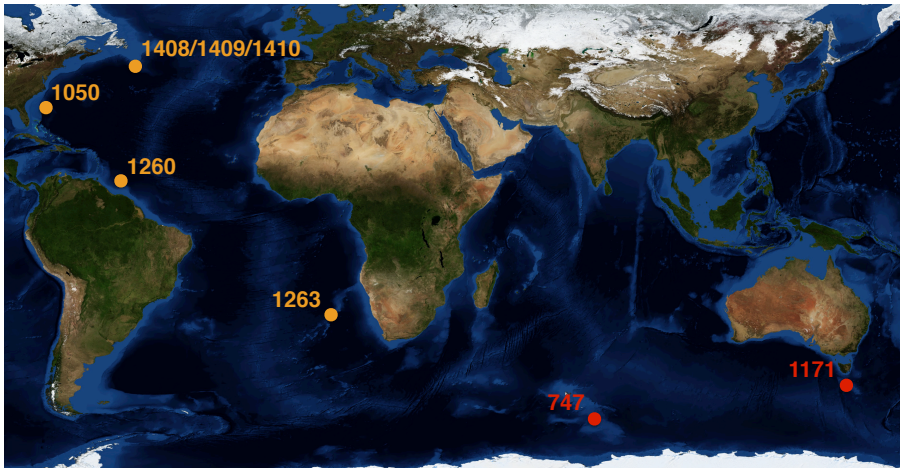

Fig. 3: Locations of ODP/IODP sites. Sites used for Eocene (Paper I) and Miocene (Papers II and III) temperature reconstructions are marked orange and red, respectively (map from NASA (2004)).

Middle Miocene upper ocean temperatures (**Objective 2**) were reconstructed at ODP Site 1171 located on the South Tasman Rise in the Southern Ocean. The Hole 1171C section covering the MMCT is characterized by carbonate-rich nannofossil ooze with foraminifera, relatively constant sedimentation and good foraminiferal preservation, and has been previously used for middle Miocene climate reconstructions (Exon et al., 2001; Shevenell and Kennett, 2004; Shevenell et al., 2004, 2008). Notably, the Mg/Ca-based high-resolution upper ocean temperature record from Site 1171 (Shevenell et al., 2004) has served as a middle Miocene Southern Ocean reference for more than a decade. In this PhD project, Δ_{47} measurements were performed on the same planktic foraminiferal species (*Globigerina bulloides*) as has been used for Mg/Ca analysis (Shevenell et al., 2004). This allows for a direct comparison of the Δ_{47} and Mg/Ca paleotemperature proxies. Efforts to reconstruct Southern Ocean BWTs (**Objective 3**) were concentrated on ODP Site 747 located on the Kerguelen Plateau. Middle Miocene sediments at this site predominantly consist of nannofossil ooze and contain well-preserved foraminifera of the genus *Cibicidoides* (Schlich et al., 1989; Billups and Schrag, 2002). Here, we picked benthic foraminifera *Cibicidoides wuellerstorfi* and *Cibicidoides mundulus* for Δ_{47} analysis.

All picked foraminiferal tests were cracked between glass plates. The cleaning procedure involved ultrasonication in deionized water and methanol followed by extensive rinsing with deionized water. We followed a clumped isotope measurement approach using a large number of replicates of very small (~100 µg each) carbonate samples (Schmid and Bernasconi, 2010; Hu et al., 2014; Meckler et al., 2014; Müller et al., 2017). Clumped isotope measurements were carried out on Thermo Scientific MAT 253 (Plus) mass spectrometers coupled to Kiel IV carbonate preparation devices (see Schmid and Bernasconi (2010) for details). A Porapak trap was included in each Kiel device to eliminate contaminants (Schmid et al., 2012). Four different carbonate standards were used for standardization and monitoring of the measured sample values. The precision required for paleoceanographic interpretation was obtained by pooling >30 Δ_{47} measurements from adjacent samples (e.g., Grauel et al., 2013; Fernandez et al., 2017).

Table 1: Locations, water depths and references for the ODP/IODP study sites used in this PhD project.

	No.	Site	Latitude (°N)	Longitude (°E)	Water depth (m)	References
Paper I	1	**1408**	41.43	-49.78	3020	Norris et al. (2014a)
	2	**1409**	41.3	-49.23	3500	Norris et al. (2014b)
	3	**1410**	41.33	-49.17	3390	Norris et al. (2014c); Vahlenkamp et al. (2018)
	4	**1050**	30.1	-76.23	2300	Norris et al. (1998)
	5	**1260**	9.27	-54.55	2550	Erbacher et al. (2004); Edgar et al. (2007); Westerhold and Röhl (2013); Sexton et al. (2006a)
	6	**1263**	-28.53	2.78	2720	Zachos et al. (2004); Westerhold et al. (2015)
Paper II	7	**1171**	-48.5	149.11	2150	Exon et al. (2001); Shevenell et al. (2004); Shevenell and Kennett (2004); Shevenell et al. (2008)
Paper III	8	**747**	-54.81	76.79	1695	Schlich et al. (1989); Majewski and Bohaty (2010); Abrajevitch et al. (2014); Verducci et al. (2009)

Temperatures were calculated from mean Δ_{47} values based on the recalculated (Bernasconi et al., 2018) travertine-based calibration of Kele et al. (2015). This very well constrained calibration from inorganic carbonates spans a large temperature range and agrees well with foraminifera-based calibrations, including several calibrations produced in-house (Peral et al., 2018; Piasecki et al., 2019; Meinicke et al., in review). Sample dating largely builds on published age models (e.g., Shevenell and Kennett, 2004; Westerhold and Röhl, 2013; Abrajevitch et al.,

2014; Westerhold et al., 2015). Further details on study sites, sample processing, geochemical analyses, age models and statistical methods are provided in the manuscripts (Papers I-III).

Summary of papers

Paper I: *Sensitivity of clumped isotope temperatures in fossil benthic and planktic foraminifera to diagenetic alteration*

Paper I investigates the potential of post-depositional diagenetic processes to alter primary Δ_{47} signatures in benthic and planktic foraminiferal tests. For this purpose, we compare middle Eocene foraminiferal Δ_{47}-based deep and surface ocean temperatures from six Atlantic ODP/IODP sites with different states of preservation. For benthic and well-preserved planktic foraminiferal tests, we find no evidence of a diagenetically induced bias in reconstructed paleotemperatures. In contrast, Δ_{47}-derived paleotemperatures calculated from planktic foraminiferal tests with apparent signs of diagenetic alteration are unreasonably low, similar to what has been previously observed for classic $\delta^{18}O$-based paleothermometry. The diagenetic cool bias appears to be most visible in the tropics. We support the interpretation of these observations with theoretical modelling of diagenetic calcite contributions with different end-member compositions, and propose an approach to correct for secondary diagenetic overprints. At the same time, our Δ_{47} measurements on benthic and well-preserved planktic foraminifera provide improved constraints on middle Eocene ocean temperatures.

Paper II: *Southern Ocean temperature evolution coupled to middle Miocene ice sheet expansion*

In Paper II, we reconstruct the temperature evolution in the upper waters of the Southern Ocean across the MMCT following a multi-proxy approach. We use clumped isotope and lipid biomarker thermometry to revisit upper ocean temperatures at ODP Site 1171 located on the South Tasman Rise. Site 1171 has become a well-studied Southern Ocean reference for the middle Miocene because of its upper ocean temperature record based on Mg/Ca signatures of planktic foraminiferal tests (Shevenell et al., 2004). This benchmark upper ocean

temperature record shows a cooling of ~6-7°C in the Southern Ocean preceding Antarctic cryosphere expansion. The authors of the study have interpreted their results to reflect orbitally paced changes in meridional heat/vapor transport and a thermal isolation of Antarctica starting well before the onset of ice growth (Shevenell et al., 2004). At the same time, they challenged the notion that atmospheric CO_2 was the primary driver of the MMCT. Our multiproxy temperature record indicates that the change seen in planktic foraminiferal Mg/Ca may have been partly caused by pH as an additional, non-thermal control on Mg/Ca in planktic foraminifera. Both Δ_{47}- and TEX_{86}-based upper ocean temperatures show a gradual cooling, which is in phase with Antarctic cryosphere expansion. Upper ocean temperatures and Antarctic ice volume appear to largely follow CO_2 trends, suggesting a more dominant role of atmospheric CO_2 in driving middle Miocene ice growth than previously assumed.

Paper III: *Southern Ocean bottom water cooling and ice sheet expansion during the middle Miocene climate transition*

Paper III focuses on reconstructing bottom water conditions in the Southern Ocean during the middle Miocene. New clumped isotope temperature as well as $\delta^{18}O$ and $\delta^{13}C$ data are presented from ODP Site 747 located on the Kerguelen Plateau around 55°S. Our dataset appears to confirm that peak BWTs during the Miocene climatic optimum were considerably (roughly 5-10°C) warmer than today, not only at low latitudes (e.g., Lear et al., 2010; Modestou et al., in prep.) but also at southern high latitudes. Nevertheless, bottom water $\delta^{18}O$ values calculated from benthic foraminiferal $\delta^{18}O$ and Δ_{47}-based ocean temperatures suggest substantial global ice volume during the time interval covered by the study. Our results further indicate that the middle Miocene period of widespread warmth was followed by a Southern Ocean bottom water cooling of ~3-5°C and an increase in global ice volume. Interestingly, the reconstructed cooling at Site 747 precedes the ice volume increase (as deduced from bottom water $\delta^{18}O$ obtained from the same measurements) by roughly 500 kyr, whereas the ice volume increase itself is accompanied by a transient bottom water warming. We relate these observations

primarily to regional factors affecting bottom water conditions at Site 747. Specifically, we hypothesize that a freshening of upper ocean waters relative to bottom waters during ice sheet expansion on Antarctica may have resulted in increased stratification reducing convective vertical mixing and upward heat flux in the Southern Ocean. Changes in vertical mixing of the water column may also help explain the lead of bottom water cooling versus ice growth, in addition to potential thresholds for Antarctic cryosphere expansion. Data from other study sites are needed for a more conclusive interpretation.

Synthesis and outlook

Recent advances in clumped isotope methodology, particularly in reducing sample size requirements, have formed the basis for the application of this method to fossil foraminiferal carbonates. Spanning the range from method "ground-truthing" to application, this thesis demonstrates that clumped isotope temperatures from well-preserved foraminifera are relatively robust to controls other than primary calcification temperature, providing an ideal supplement to higher-resolution Mg/Ca- and organic biomarker-based temperature estimates. Clumped isotope data generated from southern high latitude sedimentary sequences reveal new insights into the magnitude and timing of Southern Ocean temperature change during the middle Miocene.

The results documented in Paper I provide essential constraints on the fidelity of the clumped isotope thermometer when being applied to middle Eocene benthic and planktic foraminiferal tests. In addition, we propose an approach for correcting fossil foraminiferal Δ_{47} for diagenetic alteration. However, this approach relies on knowledge of the percentage of diagenetic calcite in a foraminiferal test. Independent quantitative estimates of diagenetic calcite contributions are thus needed. Characterizing these contributions (e.g., by electron backscatter diffraction) is challenging, but would be an important next step to further improve our estimates of absolute ocean temperatures, especially for ODP Sites 1260 and 1263 where foraminiferal tests showed clear signs of diagenetic alteration. Correction for diagenetic effects would also benefit from direct measurement of the isotopic composition ($\delta^{18}O$ and $\delta^{13}C$) of diagenetic calcite (e.g., by in situ secondary ion mass spectrometry). We did not assess effects on primary clumped isotope signatures purely from dissolution. These dissolution effects could be studied by analysing coeval foraminiferal carbonates with different states of dissolution from a water depth transect, or by dissolution experiments. Finally, it would be interesting to carry out further analyses of diagenetic effects on clumped

isotopes values with older samples (e.g., from the Cretaceous) to test the robustness of temperature reconstructions further back in time.

Our multiproxy upper ocean temperature record from ODP Site 1171 in the Southern Ocean suggests that temperature was closely coupled with Antarctic ice volume during the MMCT (Paper II). This finding is in contrast with previous observations that had suggested temporal lags (Shevenell et al., 2004; Kuhnert et al., 2009), and thus provides a new view of middle Miocene Southern Ocean temperature evolution. Although existing CO_2 records are of low temporal resolution, upper ocean temperature and ice volume both appear to broadly follow changes in atmospheric CO_2 (e.g., Sosdian et al., 2018). This observation suggests a high sensitivity of Southern Ocean and Antarctic climate to atmospheric CO_2 changes in a greenhouse climate. The hypothesis of a decline in atmospheric CO_2 triggering the MMCT should be further tested with higher-resolution CO_2 proxy records. Southern high latitude records of marine productivity (e.g., opal fluxes) may help test the hypothesis of a decrease in Southern Ocean upwelling, acting as a positive ocean circulation feedback that contributed to the observed (e.g., Sosdian et al., 2018) drawdown of CO_2 during the middle Miocene.

In Paper III, we present clumped isotope data from middle Miocene benthic foraminifera providing new constraints on Southern Ocean BWT evolution and global ice volume, but also raising new questions. BWT records from other sites may help answering the question whether the strong and early bottom water cooling observed at Site 747 was limited to the region around the Kerguelen Plateau, or whether this cooling was a more widespread feature. More BWT data may also help clarify the spatial extent of the observed transient warming after the MMCT and assess the role of dissolution at Site 747. Adding benthic foraminiferal Mg/Ca measurements at Site 747 would make our comparison of Δ_{47}- and Mg/Ca-based BWTs more informative.

In general, there is a strong need to better understand the climate response to past and future CO_2 forcing. Reliable paleotemperature records from additional

low and high latitude sites are required, not only for the Miocene but also for other intervals of elevated atmospheric CO_2. I am involved in several studies including clumped isotope thermometry that are currently in preparation. I co-supervised the MSc thesis of Kristin Sleen Jenssen focusing on the subtropical northwestern Pacific during the middle Miocene (presented in MSc thesis Sleen Jenssen (2017)), and have continued her work as a side project. This effort will allow assessing low latitude climate variability during the middle Miocene, complementing the Southern Ocean studies of this thesis (Papers II and III). Furthermore, I have contributed clumped isotope data to a project targeting the North Atlantic during the middle Eocene climatic optimum with a multiproxy approach (van der Ploeg et al., in prep.). I am moreover involved in the middle Miocene BWT study of Modestou et al. (in prep.) comparing Δ_{47}-based BWTs off Northwest Australia with previously published Mg/Ca-based BWTs (Lear et al., 2010).

The focus of my work has been on analyzing clumped isotope compositions of foraminiferal carbonates. Compared to foraminifera, calcite platelets produced by coccolithophore algae have been less used for paleoclimate reconstructions. Nevertheless, the Δ_{47} signatures of these coccoliths hold potential to yield reliable sea surface temperature estimates (Tripati et al., 2010; Tripati et al., 2014; Drury and John, 2016; Katz et al., 2017). Available sedimentary fine fractions from the samples studied here could be used to assess whether reasonable sea surface temperature values can be obtained for the middle Eocene and/or the middle Miocene. Coccolithophores and foraminifera tend to have different seasonal preferences in certain settings (e.g., Haug et al., 2005). Depending on the setting, combining coccolith and foraminiferal Δ_{47} measurements may thus allow for reconstruction of vertical temperature gradients or seasonality.

References

Abrajevitch, A., Roberts, A.P. and Kodama, K. (2014) Volcanic iron fertilization of primary productivity at Kerguelen Plateau, Southern Ocean, through the Middle Miocene Climate Transition. *Palaeogeography, Palaeoclimatology, Palaeoecology* **410,** 1-13.

Anagnostou, E., John, E.H., Edgar, K.M., Foster, G.L., Ridgwell, A., Inglis, G.N., Pancost, R.D., Lunt, D.J. and Pearson, P.N. (2016) Changing atmospheric CO_2 concentration was the primary driver of early Cenozoic climate. *Nature* **533,** 380-384.

Bemis, B.E., Spero, H.J., Bijma, J. and Lea, D.W. (1998) Reevaluation of the oxygen isotopic composition of planktonic foraminifera: Experimental results and revised paleotemperature equations. *Paleoceanography* **13,** 150-160.

Bernasconi, S.M., Hu, B., Wacker, U., Fiebig, J., Breitenbach, S.F.M. and Rutz, T. (2013) Background effects on Faraday collectors in gas-source mass spectrometry and implications for clumped isotope measurements. *Rapid Communications in Mass Spectrometry* **27,** 603-612.

Bernasconi, S.M., Müller, I.A., Bergmann, K.D., Breitenbach, S.F.M., Fernandez, A., Hodell, D.A., Jaggi, M., Meckler, A.N., Millan, I. and Ziegler, M. (2018) Reducing uncertainties in carbonate clumped isotope analysis through consistent carbonate-based standardization. *Geochemistry, Geophysics, Geosystems* **19,** 2895-2914.

Bijl, P.K., Houben, A.J.P., Hartman, J.D., Pross, J., Salabarnada, A., Escutia, C. and Sangiorgi, F. (2018) Paleoceanography and ice sheet variability offshore Wilkes Land, Antarctica - Part 2: Insights from Oligocene-Miocene dinoflagellate cyst assemblages. *Climate of the Past* **14,** 1015-1033.

Billups, K. and Schrag, D.P. (2002) Paleotemperatures and ice volume of the past 27 Myr revisited with paired Mg/Ca and $^{18}O/^{16}O$ measurements on benthic foraminifera. *Paleoceanography* **17,** 3-1-3-11.

Billups, K. and Schrag, D.P. (2003) Application of benthic foraminiferal Mg/Ca ratios to questions of Cenozoic climate change. *Earth and Planetary Science Letters* **209,** 181-195.

Bopp, L., Resplandy, L., Orr, J.C., Doney, S.C., Dunne, J.P., Gehlen, M., Halloran, P., Heinze, C., Ilyina, T., Séférian, R., Tjiputra, J. and Vichi, M. (2013) Multiple stressors of ocean ecosystems in the 21st century: projections with CMIP5 models. *Biogeosciences* **10,** 6225-6245.

Brand, W.A., Assonov, S.S. and Coplen, T.B. (2010) Correction for the ^{17}O interference in $\delta^{13}C$ measurements when analyzing CO_2 with stable isotope mass spectrometry (IUPAC Technical Report). *Pure and Applied Chemistry* **82,** 1719-1733.

Brassell, S.C., Eglinton, G., Marlowe, I.T., Pflaumann, U. and Sarnthein, M. (1986) Molecular Stratigraphy - a new Tool for Climatic Assessment. *Nature* **320,** 129-133.

Breitenbach, S.F.M., Mleneck-Vautravers, M.J., Grauel, A.-L., Lo, L., Bernasconi, S.M., Müller, I.A., Rolfe, J., Gázquez, F., Greaves, M. and Hodell, D.A. (2018) Coupled Mg/Ca and clumped isotope analyses of foraminifera provide consistent water temperatures. *Geochimica et Cosmochimica Acta* **236,** 283-296.

Burke, K.D., Williams, J.W., Chandler, M.A., Haywood, A.M., Lunt, D.J. and Otto-Bliesner, B.L. (2018) Pliocene and Eocene provide best analogs for near-future climates. *Proceedings of the National Academy of Sciences of the United States of America* **115,** 13288-13293.

Coxall, H.K., Wilson, P.A., Pälike, H., Lear, C.H. and Backman, J. (2005) Rapid stepwise onset of Antarctic glaciation and deeper calcite compensation in the Pacific Ocean. *Nature* **433,** 53-57.

Cramer, B.S., Miller, K.G., Barrett, P.J. and Wright, J.D. (2011) Late Cretaceous-Neogene trends in deep ocean temperature and continental ice volume: Reconciling records of benthic foraminiferal geochemistry ($\delta^{18}O$ and Mg/Ca) with sea level history. *Journal of Geophysical Research-Oceans* **116,** 1-23.

Daëron, M., Blamart, D., Peral, M. and Affek, H.P. (2016) Absolute isotopic abundance ratios and the accuracy of Δ_{47} measurements. *Chemical Geology* **442,** 83-96.

de Boer, B., van de Wal, R.S.W., Bintanja, R., Lourens, L.J. and Tuenter, E. (2010) Cenozoic global ice-volume and temperature simulations with 1-D ice-sheet models forced by benthic $\delta^{18}O$ records. *Annals of Glaciology* **51,** 23-33.

De Vleeschouwer, D., Vahlenkamp, M., Crucifix, M. and Pälike, H. (2017) Alternating Southern and Northern Hemisphere climate response to astronomical forcing during the past 35 m.y. *Geology* **45,** 375-378.

DeConto, R.M., Pollard, D., Wilson, P.A., Pälike, H., Lear, C.H. and Pagani, M. (2008) Thresholds for Cenozoic bipolar glaciation. *Nature* **455,** 652-656.

Defliese, W.F., Hren, M.T. and Lohmann, K.C. (2015) Compositional and temperature effects of phosphoric acid fractionation on Δ_{47} analysis and implications for discrepant calibrations. *Chemical Geology* **396,** 51-60.

Dennis, K.J., Affek, H.P., Passey, B.H., Schrag, D.P. and Eiler, J.M. (2011) Defining an absolute reference frame for 'clumped' isotope studies of CO_2. *Geochimica et Cosmochimica Acta* **75,** 7117-7131.

Dennis, K.J. and Schrag, D.P. (2010) Clumped isotope thermometry of carbonatites as an indicator of diagenetic alteration. *Geochimica et Cosmochimica Acta* **74,** 4110-4122.

Drury, A.J. and John, C.M. (2016) Exploring the potential of clumped isotope thermometry on coccolith-rich sediments as a sea surface temperature proxy. *Geochemistry Geophysics Geosystems* **17,** 4092-4104.

Edgar, K.M., Wilson, P.A., Sexton, P.F. and Suganuma, Y. (2007) No extreme bipolar glaciation during the main Eocene calcite compensation shift. *Nature* **448,** 908-911.

Eiler, J.M. (2007) "Clumped-isotope" geochemistry—The study of naturally-occurring, multiply-substituted isotopologues. *Earth and Planetary Science Letters* **262,** 309-327.

Eiler, J.M. (2011) Paleoclimate reconstruction using carbonate clumped isotope thermometry. *Quaternary Science Reviews* **30,** 3575-3588.

Eiler, J.M. (2013) The Isotopic Anatomies of Molecules and Minerals. *Annual Review of Earth and Planetary Sciences* **41,** 411-441.

Eiler, J.M. and Schauble, E. (2004) $^{18}O^{13}C^{16}O$ in Earth's atmosphere. *Geochimica et Cosmochimica Acta* **68,** 4767-4777.

Elderfield, H., Yu, J., Anand, P., Kiefer, T. and Nyland, B. (2006) Calibrations for benthic foraminiferal Mg/Ca paleothermometry and the carbonate ion hypothesis. *Earth and Planetary Science Letters* **250,** 633-649.

Erbacher, J., Mosher, D.C., Malone, M.J. and the Expedition 207 Scientists (2004) Site 1260, *Proceedings of the Ocean Drilling Program, Initial Reports Volume 207*, pp. 1-113.

Evans, D. and Müller, W. (2012) Deep time foraminifera Mg/Ca paleothermometry: Nonlinear correction for secular change in seawater Mg/Ca. *Paleoceanography* **27,** 1-11.

Evans, D., Wade, B.S., Henehan, M., Erez, J. and Müller, W. (2016) Revisiting carbonate chemistry controls on planktic foraminifera Mg/Ca: implications for sea surface temperature and hydrology shifts over the Paleocene Eocene Thermal Maximum and Eocene Oligocene transition. *Climate of the Past* **12,** 819-835.

Exon, N.F., Kennett, J.P., Malone, M.J. and the Expedition 189 Scientists (2001) Site 1171, *Proceedings of the Ocean Drilling Program, Initial Reports Volume 189*.

Fernandez, A., Müller, I.A., Rodríguez-Sanz, L., van Dijk, J., Looser, N. and Bernasconi, S.M. (2017) A Reassessment of the Precision of Carbonate Clumped Isotope Measurements: Implications for Calibrations and Paleoclimate Reconstructions. *Geochemistry Geophysics Geosystems* **18,** 4375-4386.

Flower, B.P. and Kennett, J.P. (1993) Middle Miocene Ocean-Climate Transition - High-Resolution Oxygen and Carbon Isotopic Records from Deep-Sea Drilling Project Site 588A, Southwest Pacific. *Paleoceanography* **8,** 811-843.

Foster, G.L., Lear, C.H. and Rae, J.W.B. (2012) The evolution of pCO_2, ice volume and climate during the middle Miocene. *Earth and Planetary Science Letters* **341-344,** 243-254.

Foster, G.L., Royer, D.L. and Lunt, D.J. (2017) Future climate forcing potentially without precedent in the last 420 million years. *Nature Communications* **8,** 1-8.

Frigola, A., Prange, M. and Schulz, M. (2018) Boundary conditions for the Middle Miocene Climate Transition (MMCT v1.0). *Geoscientific Model Development* **11,** 1607-1626.

Ghosh, P., Adkins, J., Affek, H., Balta, B., Guo, W., Schauble, E.A., Schrag, D. and Eiler, J.M. (2006) ^{13}C-^{18}O bonds in carbonate minerals: A new kind of paleothermometer. *Geochimica et Cosmochimica Acta* **70,** 1439-1456.

Goldner, A., Herold, N. and Huber, M. (2014) The challenge of simulating the warmth of the mid-Miocene climatic optimum in CESM1. *Climate of the Past* **10,** 523-536.

Goosse, H., Kay, J.E., Armour, K.C., Bodas-Salcedo, A., Chepfer, H., Docquier, D., Jonko, A., Kushner, P.J., Lecomte, O., Massonnet, F., Park, H.S., Pithan, F., Svensson, G. and Vancoppenolle, M. (2018) Quantifying climate feedbacks in polar regions. *Nature Communications* **9,** 1-13.

Gottschalk, J., Riveiros, N.V., Waelbroeck, C., Skinner, L.C., Michel, E., Duplessy, J.C., Hodell, D. and Mackensen, A. (2016) Carbon isotope offsets between benthic foraminifer species of the genus Cibicides (Cibicidoides) in the glacial sub-Antarctic Atlantic. *Paleoceanography* **31,** 1583-1602.

Gradstein, F.M., Ogg, J.G., Schmitz, M. and Ogg, G. (2012) *The Geologic Time Scale 2012*. Elsevier, Oxford.

Grauel, A.L., Schmid, T.W., Hu, B., Bergami, C., Capotondi, L., Zhou, L. and Bernasconi, S.M. (2013) Calibration and application of the 'clumped isotope' thermometer to foraminifera for high-resolution climate reconstructions. *Geochimica et Cosmochimica Acta* **108,** 125-140.

Guo, W., Mosenfelder, J.L., Goddard III, W.A. and Eiler, J.M. (2009) Isotopic fractionations associated with phosphoric acid digestion of carbonate minerals: Insights from first-principles theoretical modeling and clumped isotope measurements. *Geochimica et Cosmochimica Acta* **73,** 7203-7225.

Hall, A. (2004) The role of surface albedo feedback in climate. *Journal of Climate* **17,** 1550-1568.

Hartman, J.D., Sangiorgi, F., Salabarnada, A., Peterse, F., Houben, A.J.P., Schouten, S., Brinkhuis, H., Escutia, C. and Bijl, P.K. (2018) Paleoceanography and ice sheet variability offshore Wilkes Land, Antarctica - Part 3: Insights from Oligocene-Miocene TEX_{86}-based sea surface temperature reconstructions. *Climate of the Past* **14,** 1275-1297.

Haug, G.H., Ganopolski, A., Sigman, D.M., Rosell-Mele, A., Swann, G.E.A., Tiedemann, R., Jaccard, S.L., Bollmann, J., Maslin, M.A., Leng, M.J. and Eglinton, G. (2005) North Pacific seasonality and the glaciation of North America 2.7 million years ago. *Nature* **433,** 821-825.

He, B., Olack, G.A. and Colman, A.S. (2012) Pressure baseline correction and high-precision CO_2 clumped-isotope (Δ_{47}) measurements in bellows and micro-volume modes. *Rapid Communications in Mass Spectrometry* **26,** 2837-2853.

Henkes, G.A., Passey, B.H., Grossman, E.L., Shenton, B.J., Perez-Huerta, A. and Yancey, T.E. (2014) Temperature limits for preservation of primary calcite clumped isotope paleotemperatures. *Geochimica et Cosmochimica Acta* **139,** 362-382.

Herbert, T.D., Lawrence, K.T., Tzanova, A., Peterson, L.C., Caballero-Gill, R. and Kelly, C.S. (2016) Late Miocene global cooling and the rise of modern ecosystems. *Nature Geoscience* **9,** 843-847.

Herold, N., Seton, M., Müller, R.D., You, Y. and Huber, M. (2008) Middle Miocene tectonic boundary conditions for use in climate models. *Geochemistry Geophysics Geosystems* **9,** 1-10.

Ho, S.L. and Laepple, T. (2016) Flat meridional temperature gradient in the early Eocene in the subsurface rather than surface ocean. *Nature Geoscience* **9,** 606-610.

Holbourn, A., Kuhnt, W., Lyle, M., Schneider, L., Romero, O. and Andersen, N. (2014) Middle Miocene climate cooling linked to intensification of eastern equatorial Pacific upwelling. *Geology* **42,** 19-22.

Holbourn, A., Kuhnt, W., Regenberg, M., Schulz, M., Mix, A. and Andersen, N. (2010) Does Antarctic glaciation force migration of the tropical rain belt? *Geology* **38,** 783-786.

Holbourn, A., Kuhnt, W., Schulz, M. and Erlenkeuser, H. (2005) Impacts of orbital forcing and atmospheric carbon dioxide on Miocene ice-sheet expansion. *Nature* **438,** 483-487.

Hönisch, B., Allen, K.A., Lea, D.W., Spero, H.J., Eggins, S.M., Arbuszewski, J., deMenocal, P., Rosenthal, Y., Russell, A.D. and Elderfield, H. (2013) The influence of salinity on Mg/Ca in planktic foraminifers - Evidence from cultures, core-top sediments and complementary $\delta^{18}O$. *Geochimica et Cosmochimica Acta* **121,** 196-213.

Hu, B., Radke, J., Schlüter, H.J., Heine, F.T., Zhou, L. and Bernasconi, S.M. (2014) A modified procedure for gas-source isotope ratio mass spectrometry: the long-integration dual-inlet (LIDI) methodology and implications for clumped isotope measurements. *Rapid Communications in Mass Spectrometry* **28,** 1413-1425.

Huntington, K.W., Eiler, J.M., Affek, H.P., Guo, W., Bonifacie, M., Yeung, L.Y., Thiagarajan, N., Passey, B.H., Tripati, A.K., Daëron, M. and Came, R. (2009) Methods and limitations of 'clumped' CO_2 isotope (Δ_{47}) analysis by gas-source isotope ratio mass spectrometry. *Journal of Mass Spectrometry* **44,** 1318-1329.

IPCC (2013) *Climate Change 2013: The Physical Science Basis: Contribution of Working Group I to the Fifth Assessment Report of the Intergovernmental Panel on Climate Change*. Cambridge University Press, Cambridge, United Kingdom and New York, NY, USA.

IPCC (2018) *An IPCC Special Report on the impacts of global warming of 1.5°C above pre-industrial levels and related global greenhouse gas emission pathways, in the context of strengthening the global response to the threat of climate change, sustainable development, and efforts to eradicate poverty*. IPCC, Geneva, Switzerland.

Joos, F., Plattner, G.K., Stocker, T.F., Marchal, O. and Schmittner, A. (1999) Global warming and marine carbon cycle feedbacks on future atmospheric CO_2. *Science* **284,** 464-467.

Katz, A., Bonifacie, M., Hermoso, M., Cartigny, P. and Calmels, D. (2017) Laboratory-grown coccoliths exhibit no vital effect in clumped isotope (Δ_{47}) composition on a range of geologically relevant temperatures. *Geochimica et Cosmochimica Acta* **208,** 335-353.

Kele, S., Breitenbach, S.F.M., Capezzuoli, E., Meckler, A.N., Ziegler, M., Millan, I.M., Kluge, T., Deák, J., Hanselmann, K., John, C.M., Yan, H., Liu, Z. and Bernasconi, S.M. (2015) Temperature dependence of oxygen- and clumped isotope fractionation in carbonates: A study of travertines and tufas in the 6–95 °C temperature range. *Geochimica et Cosmochimica Acta* **168,** 172-192.

Kominz, M.A., Browning, J.V., Miller, K.G., Sugarman, P.J., Mizintseva, S. and Scotese, C.R. (2008) Late Cretaceous to Miocene sea-level estimates from the New Jersey and Delaware coastal plain coreholes: an error analysis. *Basin Research* **20,** 211-226.

Kuhnert, H., Bickert, T. and Paulsen, H. (2009) Southern Ocean frontal system changes precede Antarctic ice sheet growth during the middle Miocene. *Earth and Planetary Science Letters* **284,** 630-638.

Langebroek, P.M., Paul, A. and Schulz, M. (2009) Antarctic ice-sheet response to atmospheric CO_2 and insolation in the Middle Miocene. *Climate of the Past* **5,** 633-646.

Lear, C.H., Coxall, H.K., Foster, G.L., Lunt, D.J., Mawbey, E.M., Rosenthal, Y., Sosdian, S.M., Thomas, E. and Wilson, P.A. (2015) Neogene ice volume and ocean temperatures: Insights from infaunal foraminiferal Mg/Ca paleothermometry. *Paleoceanography***,** 1-18.

Lear, C.H., Elderfield, H. and Wilson, P.A. (2000) Cenozoic Deep-Sea Temperatures and Global Ice Volumes from Mg/Ca in Benthic Foraminiferal Calcite. *Science* **287,** 269-272.

Lear, C.H., Mawbey, E.M. and Rosenthal, Y. (2010) Cenozoic benthic foraminiferal Mg/Ca and Li/Ca records: Toward unlocking temperatures and saturation states. *Paleoceanography* **25,** 1-11.

Lear, C.H., Rosenthal, Y. and Slowey, N. (2002) Benthic foraminiferal Mg/Ca-paleothermometry: A revised core-top calibration. *Geochimica et Cosmochimica Acta* **66,** 3375-3387.

Lipp, J.S., Morono, Y., Inagaki, F. and Hinrichs, K.U. (2008) Significant contribution of Archaea to extant biomass in marine subsurface sediments. *Nature* **454,** 991-994.

Majewski, W. and Bohaty, S.M. (2010) Surface-water cooling and salinity decrease during the Middle Miocene climate transition at Southern Ocean ODP Site 747 (Kerguelen Plateau). *Marine Micropaleontology* **74,** 1-14.

Martínez-Botí, M.A., Foster, G.L., Chalk, T.B., Rohling, E.J., Sexton, P.F., Lunt, D.J., Pancost, R.D., Badger, M.P.S. and Schmidt, D.N. (2015) Plio-Pleistocene climate sensitivity evaluated using high-resolution CO_2 records. *Nature* **518,** 49-54.

Matthews, K.J., Maloney, K.T., Zahirovic, S., Williams, S.E., Seton, M. and Müller, D. (2016) Global plate boundary evolution and kinematics since the late Paleozoic. *Global and Planetary Change* **146,** 226-250.

Meckler, A.N., Ziegler, M., Millan, M.I., Breitenbach, S.F.M. and Bernasconi, S.M. (2014) Long-term performance of the Kiel carbonate device with a

new correction scheme for clumped isotope measurements. *Rapid Communications in Mass Spectrometry* **28,** 1705-1715.

Meinicke, N., Ho, S.L., Hannisdal, B., Nürnberg, D., Tripati, A., Schiebel, R. and Meckler, A.N. (in review) A robust calibration of the Δ_{47}-T relationship for foraminifers. *Geochimica et Cosmochimica Acta*.

Modestou, S., Leutert, T.J., Lear, C.H. and Meckler, A.N. (in prep.) Middle Miocene Indian Ocean bottom water temperatures: comparison of clumped isotope and Mg/Ca records.

Müller, I.A., Fernandez, A., Radke, J., van Dijk, J., Bowen, D., Schwieters, J. and Bernasconi, S.M. (2017) Carbonate clumped isotope analyses with the long-integration dual-inlet (LIDI) workflow: scratching at the lower sample weight boundaries. *Rapid Communications in Mass Spectrometry* **31,** 1057-1066.

Müller, P.J., Kirst, G., Ruhland, G., von Storch, I. and Rosell-Melé, A. (1998) Calibration of the alkenone paleotemperature index $U_{37}^{K'}$ based on core-tops from the eastern South Atlantic and the global ocean (60°N-60°S). *Geochimica et Cosmochimica Acta* **62,** 1757-1772.

NASA (2004) World Map.

Neukom, R., Steiger, N., Gómez-Navarro, J.J., Wang, J. and Werner, J.P. (2019) No evidence for globally coherent warm and cold periods over the preindustrial Common Era. *Nature* **571,** 550-554.

Norris, R.D., Kroon, D., Klaus, A. and the Expedition 171B Scientists (1998) Site 1050, *Proceedings of the Ocean Drilling Program, Initial Reports, Vol. 171B*, pp. 93-169.

Norris, R.D., Wilson, P.A., Blum, P. and the Expedition 342 Scientists (2014a) Site U1408, *Proceedings of the Integrated Ocean Drilling Program, Volume 342*, pp. 1-91.

Norris, R.D., Wilson, P.A., Blum, P. and the Expedition 342 Scientists (2014b) Site U1409, *Proceedings of the Integrated Ocean Drilling Program, Volume 342*, pp. 1-104.

Norris, R.D., Wilson, P.A., Blum, P. and the Expedition 342 Scientists (2014c) Site U1410, *Proceedings of the Integrated Ocean Drilling Program, Volume 342*, pp. 1-87.

Peral, M., Daëron, M., Blamart, D., Bassinot, F., Dewilde, F., Smialkowski, N., Isguder, G., Bonnin, J., Jorissen, F., Kissel, C., Michel, E., Vázquez Riveiros, N. and Waelbroeck, C. (2018) Updated calibration of the clumped isotope thermometer in planktonic and benthic foraminifera. *Geochimica et Cosmochimica Acta* **239,** 1-16.

Piasecki, A., Bernasconi, S.M., Grauel, A.L., Hannisdal, B., Ho, S.L., Leutert, T.J., Marchitto, T.M., Meinicke, N., Tisserand, A. and Meckler, A.N. (2019) Application of Clumped Isotope Thermometry to Benthic Foraminifera. *Geochemistry, Geophysics, Geosystems* **20,** 1-9.

Prahl, F.G. and Wakeham, S.G. (1987) Calibration of Unsaturation Patterns in Long-Chain Ketone Compositions for Paleotemperature Assessment. *Nature* **330,** 367-369.

Rahmstorf, S., Cazenave, A., Church, J.A., Hansen, J.E., Keeling, R.F., Parker, D.E. and Somerville, R.C.J. (2007) Recent climate observations compared to projections. *Science* **316,** 709.

Regenberg, M., Nürnberg, D., Schönfeld, J. and Reichart, G.J. (2007) Early diagenetic overprint in Caribbean sediment cores and its effect on the geochemical composition of planktonic foraminifera. *Biogeosciences* **4,** 957-973.

Regenberg, M., Regenberg, A., Garbe-Schönberg, D. and Lea, D.W. (2014) Global dissolution effects on planktonic foraminiferal Mg/Ca ratios controlled by

the calcite-saturation state of bottom waters. *Paleoceanography* **29,** 127-142.

Russell, A.D., Hönisch, B., Spero, H.J. and Lea, D.W. (2004) Effects of seawater carbonate ion concentration and temperature on shell U, Mg, and Sr in cultured planktonic foraminifera. *Geochimica et Cosmochimica Acta* **68,** 4347-4361.

Sabine, C.L., Feely, R.A., Gruber, N., Key, R.M., Lee, K., Bullister, J.L., Wanninkhof, R., Wong, C.S., Wallace, D.W.R., Tilbrook, B., Millero, F.J., Peng, T.H., Kozyr, A., Ono, T. and Rios, A.F. (2004) The oceanic sink for anthropogenic CO_2. *Science* **305,** 367-371.

Sangiorgi, F., Bijl, P.K., Passchier, S., Salzmann, U., Schouten, S., McKay, R., Cody, R.D., Pross, J., van de Flierdt, T., Bohaty, S.M., Levy, R., Williams, T., Escutia, C. and Brinkhuis, H. (2018) Southern Ocean warming and Wilkes Land ice sheet retreat during the mid-Miocene. *Nature Communications* **9,** 1-11.

Schauble, E.A., Ghosh, P. and Eiler, J.M. (2006) Preferential formation of ^{13}C-^{18}O bonds in carbonate minerals, estimated using first-principles lattice dynamics. *Geochimica et Cosmochimica Acta* **70,** 2510-2529.

Schlich, R., Wise, S.W. and the Expedition 120 Scientists (1989) Site 747, *Proceedings of the Ocean Drilling Program, Initial Reports, 120*, pp. 89-156.

Schmid, T.W. and Bernasconi, S.M. (2010) An automated method for 'clumped-isotope' measurements on small carbonate samples. *Rapid Communications in Mass Spectrometry* **24,** 1955-1963.

Schmid, T.W., Radke, J. and Bernasconi, S.M. (2012) Clumped-isotope measurements on small carbonate samples with a Kiel IV carbonate device and a MAT 253 mass spectrometer. *Thermo Fisher Application Note*.

Schnitker, D. (1980) North Atlantic oceanography as possible cause of Antarctic glaciation and eutrophication. *Nature* **284,** 615-616.

Schouten, S., Hopmans, E.C., Schefuss, E. and Damsté, J.S.S. (2002) Distributional variations in marine crenarchaeotal membrane lipids: a new tool for reconstructing ancient sea water temperatures? *Earth and Planetary Science Letters* **204,** 265-274.

Sexton, P.F., Wilson, P.A. and Norris, R.D. (2006a) Testing the Cenozoic multisite composite $\delta^{18}O$ and $\delta^{13}C$ curves: New monospecific Eocene records from a single locality, Demerara Rise (Ocean Drilling Program Leg 207). *Paleoceanography* **21**.

Sexton, P.F., Wilson, P.A. and Pearson, P.N. (2006b) Microstructural and geochemical perspectives on planktic foraminiferal preservation: "Glassy" versus "Frosty". *Geochemistry Geophysics Geosystems* **7,** 1-29.

Shevenell, A.E. and Kennett, J.P. (2004) Paleoceanographic Change During the Middle Miocene Climate Revolution: An Antarctic Stable Isotope Perspective, in: Exon, N., Kennett, J., Malone, M. (Eds.), *The Cenozoic Southern Ocean: Tectonics, Sedimentation, and Climate Change Between Australia and Antarctica*. AGU, Washington, D. C., pp. 235-252.

Shevenell, A.E., Kennett, J.P. and Lea, D.W. (2004) Middle Miocene Southern Ocean Cooling and Antarctic Cryosphere Expansion. *Science* **305,** 1766-1770.

Shevenell, A.E., Kennett, J.P. and Lea, D.W. (2008) Middle Miocene ice sheet dynamics, deep-sea temperatures, and carbon cycling: A Southern Ocean perspective. *Geochemistry Geophysics Geosystems* **9,** 1-14.

Sleen Jenssen, K. (2017) Reconstructing Middle Miocene tropical sea surface temperatures with clumped isotope thermometry, Department of Earth Science. University of Bergen.

Sosdian, S.M., Greenop, R., Hain, M.P., Foster, G.L., Pearson, P.N. and Lear, C.H. (2018) Constraining the evolution of Neogene ocean carbonate chemistry using the boron isotope pH proxy. *Earth and Planetary Science Letters* **498,** 362-376.

Spencer, C. and Kim, S.T. (2015) Carbonate clumped isotope paleothermometry: a review of recent advances in CO_2 gas evolution, purification, measurement and standardization techniques. *Geosciences Journal* **19,** 357-374.

Stolper, D.A., Eiler, J.M. and Higgins, J.A. (2018) Modeling the effects of diagenesis on carbonate clumped-isotope values in deep- and shallow-water settings. *Geochimica et Cosmochimica Acta* **227,** 264-291.

Super, J.R., Thomas, E., Pagani, M., Huber, M., O'Brien, C. and Hull, P.M. (2018) North Atlantic temperature and pCO_2 coupling in the early-middle Miocene. *Geology* **46,** 519-522.

Tripati, A.K., Eagle, R.A., Thiagarajan, N., Gagnon, A.C., Bauch, H., Halloran, P.R. and Eiler, J.M. (2010) $^{13}C–^{18}O$ isotope signatures and 'clumped isotope' thermometry in foraminifera and coccoliths. *Geochimica et Cosmochimica Acta* **74,** 5697-5717.

Tripati, A.K., Hill, P.S., Eagle, R.A., Mosenfelder, J.L., Tang, J., Schauble, E.A., Eiler, J.M., Zeebe, R.E., Uchikawa, J., Coplen, T.B., Ries, J.B. and Henry, D. (2015) Beyond temperature: Clumped isotope signatures in dissolved inorganic carbon species and the influence of solution chemistry on carbonate mineral composition. *Geochimica et Cosmochimica Acta* **166,** 344-371.

Tripati, A.K., Roberts, C.D. and Eagle, R.A. (2009) Coupling of CO_2 and Ice Sheet Stability Over Major Climate Transitions of the Last 20 Million Years. *Science* **326,** 1394-1397.

Tripati, A.K., Sahany, S., Pittman, D., Eagle, R.A., Neelin, J.D., Mitchell, J.L. and Beaufort, L. (2014) Modern and glacial tropical snowlines controlled by sea surface temperature and atmospheric mixing. *Nature Geoscience* **7,** 205-209.

Vahlenkamp, M., Niezgodzki, I., De Vleeschouwer, D., Bickert, T., Harper, D., Turner, S.K., Lohmann, G., Sexton, P., Zachos, J. and Pälike, H. (2018) Astronomically paced changes in deep-water circulation in the western North Atlantic during the middle Eocene. *Earth and Planetary Science Letters* **484,** 329-340.

van der Ploeg, P., Cramwinckel, M.J., Leutert, T.J., Bohaty, S.M., Fokkema, C.D., Hidding, R.J., Kocken, I.J., Meckler, A.N., van der Meer, A.E., Middelburg, J.J., Müller, I.A., Peterse, F., Reichart, G.-J., Schouten, S., Sexton, P.F., Wilson, P.A., Ziegler, M. and Sluijs, A. (in prep.) Surface ocean warming and hydrographic change in the North Atlantic during the Middle Eocene Climatic Optimum.

Veizer, J. and Prokoph, A. (2015) Temperatures and oxygen isotopic composition of Phanerozoic oceans. *Earth-Science Reviews* **146,** 92-104.

Verducci, M., Foresi, L.M., Scott, G.H., Sprovieri, M., Lirer, F. and Pelosi, N. (2009) The Middle Miocene climatic transition in the Southern Ocean: Evidence of paleoclimatic and hydrographic changes at Kerguelen plateau from planktonic foraminifers and stable isotopes. *Palaeogeography Palaeoclimatology Palaeoecology* **280,** 371-386.

Vincent, E. and Berger, W.H. (1985) Carbon Dioxide and Polar Cooling in the Miocene: The Monterey Hypothesis, in: Sundquist, E., Broecker, W. (Eds.), *The Carbon Cycle and Atmospheric CO_2: Natural Variations Archean to Present*. AGU, Washington, D. C., pp. 455-468.

Wang, Z., Schauble, E.A. and Eiler, J.M. (2004) Equilibrium thermodynamics of multiply substituted isotopologues of molecular gases. *Geochimica et Cosmochimica Acta* **68,** 4779-4797.

Watkins, J.M. and Hunt, J.D. (2015) A process-based model for non-equilibrium clumped isotope effects in carbonates. *Earth and Planetary Science Letters* **432,** 152-165.

Westerhold, T. and Röhl, U. (2013) Orbital pacing of Eocene climate during the Middle Eocene Climate Optimum and the chron C19r event: Missing link found in the tropical western Atlantic. *Geochemistry Geophysics Geosystems* **14,** 4811-4825.

Westerhold, T., Röhl, U., Frederichs, T., Bohaty, S.M. and Zachos, J.C. (2015) Astronomical calibration of the geological timescale: closing the middle Eocene gap. *Climate of the Past* **11,** 1181-1195.

Woodruff, F. and Savin, S.M. (1989) Miocene Deepwater Oceanography. *Paleoceanography* **4,** 87-140.

Zachos, J.C., Dickens, G.R. and Zeebe, R.E. (2008) An early Cenozoic perspective on greenhouse warming and carbon-cycle dynamics. *Nature* **451,** 279-283.

Zachos, J.C., Kroon, D., Blum, P. and the Expedition 208 Scientists (2004) Site 1263, *Proceedings of the Ocean Drilling Program, Initial Reports Volume 208*, pp. 1-87.

Zachos, J.C., Pagani, M., Sloan, L., Thomas, E. and Billups, K. (2001) Trends, rhythms, and aberrations in global climate 65 Ma to present. *Science* **292,** 686-693.

Zhang, Y.G., Pagani, M., Liu, Z., Bohaty, S.M. and DeConto, R. (2013) A 40-million-year history of atmospheric CO_2. *Philosophical Transactions of the Royal Society of London A* **371**.

Paper I

I

Sensitivity of clumped isotope temperatures in fossil benthic and planktic foraminifera to diagenetic alteration

Thomas J. Leutert[1]*, Philip F. Sexton[2], Aradhna Tripati[3,4], Alison Piasecki[1,5], Sze Ling Ho[1,6] and A. Nele Meckler[1]

[1]Bjerknes Centre for Climate Research and Department of Earth Science, University of Bergen, 5007 Bergen, Norway
[2]School of Environment, Earth & Ecosystem Sciences, The Open University, Milton Keynes MK7 6AA, UK
[3]Department of Earth, Planetary, and Space Sciences, Department of Atmospheric and Oceanic Sciences, Institute of the Environment and Sustainability, Center for Diverse Leadership in Science, University of California, Los Angeles, CA 90095, USA
[4]European Institute of Marine Sciences (IUEM), Université de Brest, UMR 6538, Domaines Océaniques, Rue Dumont D'Urville, and IFREMER, Laboratoire Géophysique et enregistrement Sédimentaire, 29280 Plouzané, France
[5]Department of Earth and Planetary Sciences, Harvard University, Cambridge, MA 02138, USA
[6]Institute of Oceanography, National Taiwan University, 10617 Taipei, Taiwan

*Corresponding author:
E-mail: Thomas.Leutert@uib.no

Geochimica et Cosmochimica Acta **257**, 354-372 (2019).

Available online at www.sciencedirect.com

ScienceDirect

Geochimica et Cosmochimica Acta 257 (2019) 354–372

Geochimica et Cosmochimica Acta

www.elsevier.com/locate/gca

Sensitivity of clumped isotope temperatures in fossil benthic and planktic foraminifera to diagenetic alteration

Thomas J. Leutert [a,*], Philip F. Sexton [b], Aradhna Tripati [c,d], Alison Piasecki [a,e], Sze Ling Ho [a,f], A. Nele Meckler [a]

[a] Bjerknes Centre for Climate Research and Department of Earth Science, University of Bergen, 5007 Bergen, Norway
[b] School of Environment, Earth & Ecosystem Sciences, The Open University, Milton Keynes MK7 6AA, UK
[c] Department of Earth, Planetary, and Space Sciences, Department of Atmospheric and Oceanic Sciences, Institute of the Environment and Sustainability, Center for Diverse Leadership in Science, University of California, Los Angeles, CA 90095, USA
[d] European Institute of Marine Sciences (IUEM), Université de Brest, UMR 6538, Domaines Océaniques, Rue Dumont D'Urville, and IFREMER, Laboratoire Géophysique et enregistrement Sédimentaire, 29280 Plouzané, France
[e] Department of Earth and Planetary Sciences, Harvard University, Cambridge, MA 02138, USA
[f] Institute of Oceanography, National Taiwan University, 10617 Taipei, Taiwan

Received 27 November 2018; accepted in revised form 4 May 2019; available online 13 May 2019

Abstract

Applying the clumped isotope (Δ_{47}) thermometer to foraminifer microfossils offers the potential to significantly improve paleoclimate reconstructions, owing to its insensitivity to the isotopic composition of seawater (unlike traditional oxygen isotope ($\delta^{18}O$) analyses). However, the extent to which primary Δ_{47} signatures of foraminiferal calcites can be altered during diagenesis is not well known. Here, we present Δ_{47} data as well as high-resolution (~10 kyr) $\delta^{18}O$ and $\delta^{13}C$ middle Eocene time series, measured on benthic and planktic foraminifera from ODP/IODP Sites 1408, 1409, 1410, 1050, 1260 and 1263 in the Atlantic Ocean. The sites examined span various oceanographic regimes, including the western tropical to mid-latitude North Atlantic, and the eastern mid-latitude South Atlantic. Comparing data from contemporaneous foraminifera with different preservation states, we test the effects of diagenetic alteration on paleotemperature reconstructions for the deep and surface ocean. We find that overall, primary Δ_{47} signatures appear similarly sensitive to diagenetic overprinting as $\delta^{18}O$, with differences in sensitivity depending on pore fluid chemistry and the amount of secondary calcite. Where planktic foraminifera are significantly altered, sea surface temperatures derived from Δ_{47} and $\delta^{18}O$ values are biased towards cool temperatures. In comparison, Δ_{47} and $\delta^{18}O$ values of benthic and well preserved planktic foraminifera are less affected by diagenesis and thus likely to yield robust foraminiferal calcification temperatures. With independent estimates of diagenetic calcite fractions, secondary overprints could be corrected for, using end-member modeling and Δ_{47}-based temperatures from benthic foraminifera.

Keywords: Clumped isotopes; Foraminifera; Preservation; Diagenesis; Eocene; Stable-isotope geochemistry

1. INTRODUCTION

For decades, the geochemical composition of foraminiferal tests buried in ocean sediments has been used to reconstruct paleoceanographic conditions, addressing a large range of questions regarding forcing and response mechanisms in the climate system (e.g., Zachos et al., 2001).

* Corresponding author.
E-mail address: Thomas.Leutert@uib.no (T.J. Leutert).

https://doi.org/10.1016/j.gca.2019.05.005
0016-7037/

The carbonate clumped isotope (Δ_{47}) paleothermometer based on the ordering of two heavy isotopes (^{13}C and ^{18}O) in the carbonate lattice (Ghosh et al., 2006; Schauble et al., 2006) is increasingly being applied in paleoceanographic research (e.g., Rodríguez-Sanz et al., 2017; Evans et al., 2018; Henkes et al., 2018). Recent advances in the analytical technique, especially in reducing sample size requirements, have greatly improved the applicability of this thermometer to foraminiferal carbonates (e.g., Meckler et al., 2014; Müller et al., 2017). Unlike other foraminifera-based proxies (e.g., Mg/Ca, $\delta^{18}O$), the clumped isotope paleothermometer is independent of the chemical composition of the parent-water body, rendering it especially suitable for applications in deep time where secular changes in seawater composition occurred. In addition, foraminiferal species-specific vital effects seem to be negligible (Tripati et al., 2010; Grauel et al., 2013; Breitenbach et al., 2018; Peral et al., 2018; Piasecki et al., 2019).

However, the reconstruction of ocean temperatures from foraminiferal carbonates requires the preservation of primary Δ_{47} signatures established during initial biogenic calcite precipitation. Post-depositional diagenesis may alter primary geochemical compositions of carbonates buried in ocean sediments, and thus bias any derived paleoclimate signal (e.g., Killingley, 1983; Delaney, 1989; Schrag, 1999; Pearson et al., 2001; Rudnicki et al., 2001; Tripati et al., 2003; Sexton et al., 2006b; Sexton and Wilson, 2009; Kozdon et al., 2011; Kozdon et al., 2013; Edgar et al., 2015; Golreihan et al., 2018). Reconstructing tropical sea surface conditions has proven to be especially challenging. $\delta^{18}O$-based sea surface temperature (SST) reconstructions for the tropics in the Cretaceous and Paleogene greenhouse climates (with atmospheric CO_2 levels several times of the preindustrial level) were found to be substantially lower than expected from model simulations, and even often cooler than tropical SSTs today (e.g., Zachos et al., 1994). This "cool tropics paradox" (Dhondt and Arthur, 1996) became an impediment to understanding greenhouse climates for several decades (Crowley and Zachos, 1999). A solution to the discrepancies between model and proxy data was proposed when the validity of much of the data (mostly $\delta^{18}O$-based SST estimates) began to be called into question (Wilson and Opdyke, 1996; Pearson et al., 2001; Sexton et al., 2006b). It was hypothesized that planktic foraminiferal calcites from the pelagic carbonate-rich drill sites normally targeted for paleoceanographic studies were compromised by diagenesis in the cold seafloor environment. It is now understood that diagenetic precipitation of secondary inorganic calcite (Pearson et al., 2001) and/or recrystallization of primary biogenic calcite (Sexton et al., 2006b) at the seafloor can lead to planktic foraminifera with artificially high $\delta^{18}O$ values and thus unrealistically low calculated paleotemperatures. Although it is often assumed that benthic foraminiferal isotopic compositions are less impacted by these diagenetic processes (Edgar et al., 2013; Voigt et al., 2016), $\delta^{18}O$ values of benthic foraminiferal tests have been shown to be susceptible to diagenetic alteration, with the extent of alteration dependent upon sediment lithology and sedimentation rate (Sexton and Wilson, 2009). Diagenetic effects also remain problematic for most other foraminifer-based geochemical paleoproxies including Δ_{47} (e.g., Sexton et al., 2006b; Kozdon et al., 2013; Edgar et al., 2015; Stolper et al., 2018). A recent study by Stolper et al. (2018) showed that primary Δ_{47}-based SSTs measured on different size fractions of marine bulk carbonate sediments are biased towards sub-seafloor temperatures in a carbonate-rich pelagic setting, likely reflecting recrystallization and cementation in pore fluids under a geothermal gradient. To date, however, little is known about specifically how foraminiferal Δ_{47} signatures respond to diagenetic alteration on million-year timescales.

This study assesses the effects of diagenetic alteration on the foraminiferal Δ_{47} paleothermometer, using stable isotope data and Scanning Electron Microscope (SEM) imaging of middle Eocene foraminifera from multiple regions in the Atlantic Ocean. We apply the clumped isotope technique to planktic and benthic foraminifera from sediments retrieved from sites at a range of burial depths, sediment lithologies, and pore fluid chemistries, and compare the clumped isotope results with $\delta^{18}O$ data acquired from the same samples. We have two main goals with this work. First, we aim to test the reliability of Δ_{47}-based deep-sea temperature (DST) reconstructions. For that, we assume that bottom water conditions during biogenic calcite precipitation were similar at sites from similar water depths, and inter-site differences in benthic foraminiferal Δ_{47} values are attributable to diagenetic alteration. Second, we analyse planktic foraminifera from sites with contrasting sediment lithologies and burial histories to assess how resistant Δ_{47}-derived SSTs are to diagenetic alteration. The sensitivity of benthic and planktic foraminiferal paleotemperatures to diagenesis is further examined using end-member mixing modeling. Thereby, we assume varying amounts of diagenetic calcite. Finally, we compare the middle Eocene paleotemperature values of this study to existing data, exploring the possible impacts of diagenesis on reconstructions of latitudinal temperature gradients.

2. BACKGROUND: DIAGENESIS OF FORAMINIFERAL CALCITE

Post-depositional alteration of foraminiferal tests is complex and comprises several inter-related processes, which may potentially affect foraminiferal Δ_{47} signatures. The relevant processes include neomorphism, cementation, dissolution, and solid-state reordering. Neomorphism or recrystallization involves the replacement of primary biogenic calcite with larger inorganic calcite crystals (e.g., Killingley, 1983; Sexton et al., 2006b). Ultimately, the replacement of small biogenic microgranules with larger calcite crystals changes the reflective properties of a foraminiferal test (Pearson and Burgess, 2008). Non-recrystallized pristine tests without structural alteration or overgrowths tend to have a translucent ("glassy") appearance under the binocular microscope, whereas recrystallized tests appear opaque ("frosty") (Sexton et al., 2006b). However, surface microstructures such as pores and spines can be preserved even in the case of significant recrystallization. This makes it difficult to precisely assess neomorphic changes

under the light microscope. Instead, alternative analytical methods such as SEM imagery must be used for diagnosis (e.g., Sexton et al., 2006b). Cementation occurs when carbonate mineral overgrowths form on or within tests during burial. Like recrystallization, this process impacts the bulk chemistry of foraminiferal tests. Whole-test chemistry can also be affected in the water column and in sediments through partial dissolution in undersaturated waters (Brown and Elderfield, 1996). Finally, a series of studies have shown that the geochemical composition of fossils may also be altered without visually perceptible changes, for example through solid state diffusion of isotopes at high burial temperatures (Passey and Henkes, 2012; Henkes et al., 2014; Shenton et al., 2015).

The impact of most of these diagenetic processes on foraminiferal carbonate chemistry is largely controlled by factors that influence sediment-pore fluid exchange during early burial. This exchange can be intensified by low sedimentation rates and/or an overlying hiatus resulting in increased diagenetic alteration (Rudnicki et al., 2001; Sexton and Wilson, 2009). In contrast, fine clay and silt may "entomb" foraminifera limiting the interaction of their calcite with the surrounding pore fluids. It has been suggested that preservation is thus favoured by hemipelagic clay-rich lithologies and low porosities (e.g., Sexton et al., 2006b; Sexton and Wilson, 2009).

3. MATERIAL AND METHODS

3.1. Site selection

Clumped isotope data are presented from an interval spanning 500 kyr centered at magnetochron boundary 20n/20r at 43.432 Ma (Ogg, 2012; Vandenberghe et al., 2012). This time interval within the middle Eocene is characterized by a comparatively stable global climatic regime without major climate transitions or hyperthermal events (e.g., Sexton et al., 2006a; Zachos et al., 2008). 50–72 samples were taken at each study site for a temporal resolution of around 10 kyr.

We examined samples from six pelagic sites spanning a range of latitudes (Fig. 1). IODP Sites 1408 (41°26′N, 49° 47′W), 1409 (41°18′N, 49°14′W) and 1410 (41°20′N, 49° 10′W) were drilled on the Southeast Newfoundland Ridge (Fig. 1) representing the northernmost location of this study (Norris et al., 2014a, b, c). ODP Site 1050 (30°06′N, 76° 14′W) is located on Blake Nose in the western North Atlantic (Norris et al., 1998), whereas ODP Site 1260 (09°16′N, 54°33′W) was drilled on Demerara Rise in the western equatorial Atlantic Ocean (Erbacher et al., 2004). ODP Site 1263 (28°32′S, 02°47′E) on Walvis Ridge is located in the eastern South Atlantic (Zachos et al., 2004). Table 1 summarizes the main characteristics of the sites including paleowater depth, paleolatitude and lithology. Our 500 kyr target interval at Sites 1409 and 1050 is carbonate ooze at shallow burial depths and at Sites 1408, 1410 and 1263 is at greater burial depths, whereas Site 1260 is our only site that was sampled below the ooze-chalk transition.

We investigate the effect of diagenesis on the isotopic composition of benthic foraminiferal tests by comparing

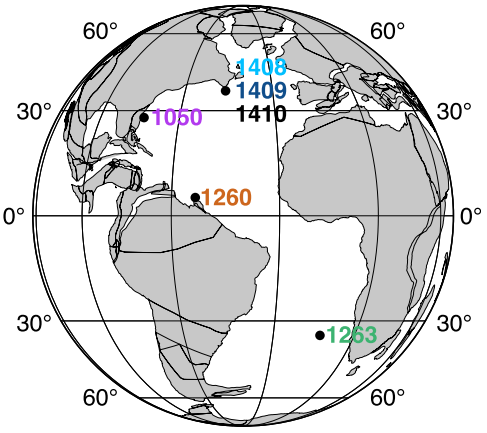

Fig. 1. Paleogeographic reconstruction of the Atlantic Ocean basin for the middle Eocene (45 Ma) showing the locations of the study sites. The base map is from the plate tectonic reconstruction service of the Ocean Drilling Stratigraphic Network (http://www.odsn.de).

results from Sites 1409, 1260 and 1263 (Fig. 1). The study sites host benthic foraminifera with different burial histories (Erbacher et al., 2004; Zachos et al., 2004; Norris et al., 2014b) but were all located in water depths between 2000 and 3000 m during the middle Eocene (Table 1). Modern bottom water temperatures are similar at each of the sites (around 2.5 to 3 °C, Fig. S1). Previous studies (e.g., Sexton et al., 2006a) suggest a relatively homogeneous Atlantic Ocean with respect to benthic foraminiferal $\delta^{18}O$ values in the time interval of this study, indicating minimal differences in DST and deep-sea water $\delta^{18}O$ values between our target sites.

Planktic foraminifera were analysed from Sites 1408, 1409, 1410, 1050, 1260 and 1263, covering a wide range of latitudes (Table 1) and preservation states, as indicated by new and previous SEM work as well as cruise report data (Norris et al., 1998; Erbacher et al., 2004; Zachos et al., 2004; Sexton et al., 2006a; Norris et al., 2014a, b, c). Sites 1050, 1260 and 1263 represent "typical" carbonate-rich pelagic ODP/IODP drill sites hosting frosty foraminifera in our target interval. Measured pore fluid Sr^{2+} profiles for Sites 1050, 1260 and 1263 are shown in Fig. S2, but not further discussed due to their limited informative value in terms of foraminiferal preservation. The foraminifera buried in the clay-rich drift sediments offshore Newfoundland at Sites 1408, 1409 and 1410 (Boyle et al., 2017) appear exceptionally well preserved. Notably, preservation may be slightly better at Sites 1408 and 1410 in comparison to Site 1409, owing to their higher sedimentation rates (e.g., Sexton and Wilson, 2009).

The benthic species used in this study was the shallow infaunal species *Nuttalides truempyi*. For planktic foraminifera, we used *Morozovelloides coronatus* (junior synonym *M. spinulosa*) at the low latitude sites (Sites 1050 and 1260) and *Acarinina bullbrooki* at the high latitude sites

Table 1
Characteristics of the study sites.

Site	Modern water depth[a] (m)	Paleowater depth[b] (m)	Paleolatitude[c]	Splice depth[d] (m)	Lithology	Porosity[a] (vol%)	Mean sedimentation rate (cm/kyr)	$CaCO_3$[a] (wt%)
1408	~3020	~2580	29.1–34.8°N	154.51–166.21	Nannofossil clay and ooze	~60	2.95	~40–50
1409	~3500	~3050	28.9–34.6°N	56.90–66.21	Nannofossil clay and ooze	~70	2.42	~40–50
1410	~3390	~2950	28.9–34.6°N	159.25–170.28	Nannofossil clay and ooze	~60	3.07	~40–50
1050	~2300	~1000–2000	21.7–27.4°N	57.04–72.84	Nannofossil ooze	~60	3.31	~70
1260	~2550	~2500–3200	2.5°S–3.2°N	117.21–128.88	Radiolarian and nannofossil chalk	~60–70	2.34	~70–80
1263	~2720	~2000–3000	37.1–42.8°S	169.82–174.22	Nannofossil ooze	~50	0.88	~90

[a] Shipboard measurements (Norris et al., 1998; Erbacher et al., 2004; Zachos et al., 2004; Norris et al., 2014a, b, c).
[b] From Tucholke and Vogt, 1979 (Sites 1408, 1409, 1410; around 50 Ma), Norris et al., 1998 (Site 1050), Sexton et al., 2006a (Site 1260) and Zachos et al., 2004 (Site 1263).
[c] Calculated using the paleolatitude calculator (http://www.paleolatitude.org) of van Hinsbergen et al. (2015) with the paleomagnetic reference frame from Torsvik et al. (2012).
[d] We use the shipboard composite depth scale for Site 1050 (Norris et al., 1998). The composite depth scales of Sites 1408 and 1410 used in this study are published in Boulila et al. (2018), whereas the revised shipboard composite depth scales of Sites 1409, 1260 and 1263 are from Hull et al. (2017), Westerhold and Röhl (2013) and Westerhold et al. (2015), respectively.

(Sites 1408, 1409, 1410 and 1263). Both species are thought to have been upper ocean mixed-layer dwellers (Pearson et al., 2006; Sexton et al., 2006c).

3.2. Age models

All ages are given in Myr relative to magnetochron boundary 20n/20r. This boundary is well documented in the magnetostratigraphies (e.g., inclination data) of all sites and serves as our primary age tie point (Ogg and Bardot, 2001; Erbacher et al., 2004; Edgar et al., 2007; Norris et al., 2014a, b, c; Westerhold et al., 2015). Age models for Sites 1408, 1410, 1260 and 1263 have been astronomically calibrated using XRF time series (Westerhold and Röhl, 2013; Westerhold et al., 2015; Hull et al., 2017; Boulila et al., 2018). However, the calibrated age model of Site 1260 was based on an older astronomical solution (Laskar et al., 2004; Westerhold and Röhl, 2013) in comparison to those of Sites 1408, 1410 and 1263 (Laskar et al., 2011a; Laskar et al., 2011b; Westerhold et al., 2015; Boulila et al., 2018). Therefore, we updated Site 1260′s age model by tuning its benthic $\delta^{13}C$ record to that from Site 1263 which shows excellent correlation with the La2010d eccentricity (Laskar et al., 2011a), resulting in a forward shift of absolute ages (younging) by 40 kyr (Fig. S3). Tuning benthic $\delta^{13}C$ at these two sites is considered reasonable because the pronounced cyclicities of (bulk and benthic) $\delta^{13}C$ in middle Eocene sequences have been observed to consistently covary with eccentricity and have thus been used for orbital tuning (e.g., Westerhold et al., 2015). The age model for Site 1409 was built in two steps: First, an age model was established based on linear interpolation between magnetostratigraphic dates (in Myr relative to 20n-20r boundary) on the GTS2012 timescale (Ogg, 2012; Vandenberghe et al., 2012). Second, Site 1409 was correlated to Site 1263, using the eccentricity cycles preserved in benthic foraminiferal $\delta^{13}C$ (Fig. S4; Table S1). At Site 1050, benthic foraminifera were not analysed, and planktic $\delta^{18}O$ and $\delta^{13}C$ values were deemed too variable for correlation. Therefore, the age model of Site 1050 was built based on the assumptions of linear sedimentation rates between the magnetochron boundaries (Ogg and Bardot, 2001) and magnetochron durations of GTS2012 (Ogg, 2012; Vandenberghe et al., 2012).

3.3. Sample preparation

Sediment samples (25 cm^3) from Sites 1409 (n = 72), 1410 (n = 50), 1050 (n = 50), 1260 (n = 50) and 1263 (n = 50) were freeze-dried and then wet-sieved through a 63 μm mesh at the University of Bergen, whereas samples from Site 1408 (30 cm^3, n = 65) were prepared for picking at Yale University (Hull et al., 2017). Planktic foraminifera were picked from a narrow size fraction from 250 μm to 355 μm. For benthic foraminifera, the range was extended (150–355 μm) to obtain enough specimens for isotope analysis.

As the goal of the study is to assess the impact of diagenesis on the application of foraminiferal Δ_{47} in paleoceanograhic research, samples were treated as commonly

done for paleoceanographic studies, mainly to remove infillings consisting of non-foraminiferal carbonate. To this end, we gently cracked specimens from each sample between two glass plates to open test chambers. After cracking, test fragments were rigorously cleaned as follows: Planktic foraminifera were ultrasonicated three times for 30 seconds in deionized water and one time for 30 seconds in methanol. The same cleaning protocol was used for benthic foraminifera but with only ten seconds of ultrasonication in methanol. Between each cleaning step, we brought test fragments into suspension, let the fragments settle and pipetted off the overlying solution which may contain potential contaminants (e.g., clay). After the last ultrasonication step, test fragments were rinsed at least three times (until the solute was clear and no longer milky) to remove any methanol and/or remaining clay particles. Before being weighed out for analysis, all samples were oven-dried at 50 °C and checked under the microscope for any remaining contaminants (e.g., black stains).

For SEM analysis, foraminiferal specimens were ultrasonicated in water for a few seconds, rinsed until the water became clear and then dried. Next, we mounted them on SEM stubs using adhesive carbon tabs. Coated with gold/palladium, they were photographed using a Zeiss Supra 55VP scanning electron microscope at the University of Bergen.

3.4. Measurement and processing of stable isotope data

The abundance of "clumped" carbonate ions containing both ^{13}C and ^{18}O isotopes is low (e.g., Ghosh et al., 2006). This low abundance leads to relatively large sample size requirements as the precision required for paleoclimate applications needs to be obtained by averaging over numerous replicate measurements (Thiagarajan et al., 2011; Meckler et al., 2014; Fernandez et al., 2017). Obtaining large sample amounts is challenging in foraminifera-based paleoceanography, where specimens of a given species are usually very limited in quantity. Yet recent advances in the analytical technique, especially in reducing sample size requirements, have greatly improved the applicability of this thermometer to foraminiferal tests (e.g., Meckler et al., 2014; Müller et al., 2017).

In this study, we use a recently developed measurement approach based on replicate measurements of very small (on the order of 100 μg) carbonate samples (e.g., Schmid and Bernasconi, 2010; Hu et al., 2014; Meckler et al., 2014). The necessary precision is achieved by pooling clumped isotope measurements of a large number of adjacent samples from a relatively stable climate interval (e.g., Grauel et al., 2013; Rodríguez-Sanz et al., 2017). We also average over a comparably large number of aliquot measurements within the time interval of interest to avoid aliasing and to maximize the overlap in time among the sites. Each clumped isotope sample value interpreted in this study is the average over 51–99 analyses of ~120 μg each (roughly 6–12 mg calcite per site and species in total). Some samples were measured more than once where foraminifera abundance allowed. In parallel with the average clumped isotope temperature for each climate interval, the method yields higher-resolution $\delta^{18}O$ and $\delta^{13}C$ data. Sample errors (precision) of Δ_{47} values are reported as the standard error of the mean (SE). ±1 SE and 68% confidence interval as well as ±2 SE and 95% confidence interval are almost indistinguishable, because of the large number of analyses for each reported clumped isotope temperature (>50 measurements). Δ_{47} values are given with four decimals to avoid rounding errors in further calculations.

All isotope analyses were carried out on a Thermo Scientific MAT 253 Plus mass spectrometer coupled to a Kiel IV carbonate preparation device (described in Schmid and Bernasconi, 2010). The Kiel device has been modified with a Porapak trap to eliminate organic contaminants. Clumped isotope compositions of foraminiferal calcites were measured in micro-volume mode with the long-integration dual-inlet (LIDI) method (Hu et al., 2014). We used the software "Easotope" (John and Bowen, 2016) for data processing. Clumped isotope values were standardized and monitored with four carbonate standards (ETH 1, 2, 3 and 4) of different composition and ordering state. Three of these carbonate standards were used to calculate Δ_{47} values from the background-corrected beam signals. A fourth carbonate standard was treated as a sample and used to monitor instrument performance. In every 23 h-run, 4–5 of each of these carbonate standards were included. The external reproducibilities (1σ standard deviation) of ETH 1, 2, 3 and 4 after correction range from 0.0308‰ to 0.0385‰. All carbonate $\delta^{18}O$ and $\delta^{13}C$ values are given relative to the VPDB scale and corrected with the same carbonate standards as used for clumped isotope corrections. Water $\delta^{18}O$ values are given relative to VSMOW. For $\delta^{18}O$ and $\delta^{13}C$, the mean 1σ external reproducibilities of the standards are 0.04–0.11‰ and 0.02–0.06‰, respectively. Sample and standard data are listed in Tables S2 and S3. Table S4 contains the reproducibilities of all standards for Δ_{47}, $\delta^{18}O$ and $\delta^{13}C$. Further details on the analysis of clumped isotopes and data correction can be found in Appendix A.1.

Clumped isotope paleotemperatures were calculated from the corrected mean Δ_{47} values using the travertine-based calibration of Kele et al. (2015), which was recalculated by Bernasconi et al. (2018). The recalculated travertine (Kele) calibration is based on similar analytical and data processing methods (e.g., Kiel device, Brand parameters, acid fractionation factor, standard values) as those employed at the University of Bergen, spans a large temperature range (6–95 °C) and shows a good agreement with an in-house calibration based on foraminifera (Piasecki et al., 2019). Calibration and analytical uncertainties in clumped isotope temperatures are fully propagated (see supporting information of Huntington et al. (2009) for description of error propagation procedure).

Eq. (1) of Bemis et al. (1998) is an oxygen isotope temperature calibration providing a good fit to modern *Cibicidoides* spp. and mixed layer dwelling planktic foraminifera. We used this calibration to calculate mean deep-sea water $\delta^{18}O$ compositions from benthic foraminiferal $\delta^{18}O$ and clumped isotope DST values measured on the same samples at each site. For that, we corrected our *Nuttalides truempyi* $\delta^{18}O$ data to *Cibicidoides* spp. with the correction factor for

$\delta^{18}O$ ((Nut + 0.10)/0.89) from Katz et al. (2003). The calibration error of Eq. (1) of Bemis et al. (1998) is not included in our calculations, due to the dominance of other major uncertainties inherent in the application of this equation to middle Eocene foraminifera (e.g., vital effects).

We also used Eq. (1) of Bemis et al. (1998) to calculate DST values from *N. truempyi* $\delta^{18}O$ values normalized to *Cibicidoides* spp. (Katz et al., 2003) and prescribed deep-sea water $\delta^{18}O$ values. Thereby, deep-sea water $\delta^{18}O$ compositions were assumed to be identical at all sites and approximated by the previously calculated deep-sea water $\delta^{18}O$ values averaged over all sites. We acknowledge some degree of circularity in these DST calculations based on benthic foraminiferal $\delta^{18}O$ and deep-sea water $\delta^{18}O$ values, leading to $\delta^{18}O$-based DSTs that are very similar to our Δ_{47} DSTs. However, due to the averaging of our deep-sea water $\delta^{18}O$ values across all sites, potential relative differences in DST between the sites should be preserved, allowing us to assess the effects of diagenesis on $\delta^{18}O$-based DST values.

Furthermore, we used the average of our deep-sea water $\delta^{18}O$ values as a basis to calculate surface water $\delta^{18}O$ values at each site following Eq. (1) of Zachos et al. (1994) to correct for latitudinal variation in surface $\delta^{18}O$, with the caveat that surface water $\delta^{18}O$ distributions during the Eocene are highly uncertain. Then, we calculated SSTs from surface water $\delta^{18}O$ and planktic foramininferal $\delta^{18}O$ values again with Eq. (1) of Bemis et al. (1998).

3.5. Modeling the effect of diagenesis

Similar to previous studies (e.g., Pearson et al., 2001; Tripati et al., 2003), we use the concept of a two component mixing line between a primary and secondary end-member to explore the effects of diagenesis on the isotopic composition of benthic and planktic foraminiferal tests, and hence their usefulness as a paleothermometer. This simple approach, based on the assumption of inorganic calcite precipitating in exchange with pore fluids (“open” system), is extended from the carbon and oxygen isotope systems to the clumped isotope system, and applied at Sites 1260 and 1263. At these carbonate-rich sites, foraminiferal tests show clear signs of diagenetic alteration, in contrast to the well-preserved foraminifera buried in the clay-rich sediments at Site 1409. Furthermore, isotope data measured on benthic foraminifera from Site 1260 as well as Site 1263 provide a basis to approximate the site-specific isotopic composition of secondary inorganic calcite (described in next paragraph). The calculated diagenetic trajectories across different preservation states provide constraints on the sensitivity of $\delta^{18}O$- and Δ_{47}-based paleotemperature estimates to diagenetic alteration, but do not factor in potential impacts purely from dissolution or the possibility of multiple or time-variant end-members.

The model assumes that diagenetic alteration occurs in the uppermost pore fluids, in keeping with other recent work (e.g., Rudnicki et al., 2001; Edgar et al., 2013; Voigt et al., 2016). Pore fluid $\delta^{18}O$ of the precipitating phase is estimated from benthic foraminiferal $\delta^{18}O$ (*N. truempyi* values normalized to *Cibicidoides* spp.) utilizing the calibration of Bemis et al. (1998) with site-specific benthic clumped isotope temperatures (Table 2). Then, pore fluid $\delta^{18}O$ is used to calculate inorganic calcite $\delta^{18}O$ values. For that, we follow two different temperature-dependent abiogenic calcite-water oxygen isotope fractionation relationships, determined by Watkins et al. (2013) and Kim and O’Neil (1997). The fractionation factor ($\alpha_{c\text{-}w}$) of Watkins et al. (2013) describes ^{18}O fractionation between water and carbonate corresponding to slow, equilibrium growth of inorganic calcite (Fantle and DePaolo, 2007). In contrast to Watkins et al. (2013), Kim and O’Neil (1997) derived their equilibrium curve from calcites that were grown at rates too high for equilibrium (Watkins et al., 2014). The fractionation factor of Kim and O’Neil (1997) thus describes non-equilibrium growth of calcite at higher growth rates in comparison to the fractionation factor of Watkins et al. (2013). Similar to previous studies on diagenesis (e.g., Schrag, 1999; Stolper et al., 2018), effects on $\alpha_{c\text{-}w}$ other than temperature (e.g., pH) are ignored for simplicity and owing to lack of constraints.

The inferred $\delta^{13}C$ signature of inorganic calcite precipitated in pelagic sediments with high carbonate but low organic matter content tends to be similar to bulk carbonate $\delta^{13}C$ values (e.g., Edgar et al., 2015; Voigt et al., 2016). Therefore, we approximate inorganic calcite $\delta^{13}C$ by bulk $\delta^{13}C$ values in our model (Table 2). We did not measure bulk $\delta^{13}C$ in this study. Bulk $\delta^{13}C$ data for Site 1263 were taken from Westerhold et al. (2015) and averaged over the study interval. For Site 1260, bulk $\delta^{13}C$ data were not available for the exact interval of this study. Therefore, bulk $\delta^{13}C$ values from Edgar et al. (2007) were averaged over a slightly younger interval (41.856 to 41.871 Ma, 75.485–75.785 m composite depth at their scale) before the Middle Eocene Climate Optimum, assuming values similar to the interval of this study. In addition, we tested our model using $\delta^{13}C$ values that are higher and lower than bulk $\delta^{13}C$ as well as our planktic $\delta^{13}C$ values to approximate inorganic $\delta^{13}C$. The latter approach has been previously applied by Edgar et al. (2015).

A major source of uncertainty for our model, as for previous modeling work, in correcting paleotemperature estimates for diagenetic effects is the amount of secondary inorganic calcite present in a frosty (*sensu* Sexton et al., 2006b) foraminiferal test (e.g., Tripati et al., 2003). Conventional SEM imagery does not allow for a quantitative assessment of diagenetic alteration. Indirect estimates for typical pelagic settings range widely, from around 15% to more than 50% secondary calcite (Pearson et al., 2001; Tripati et al., 2003; Kozdon et al., 2011; Edgar et al., 2015). Characterisation techniques such as electron backscatter diffraction (EBSD) have recently opened the possibility of more quantitatively estimating the fraction of diagenetic calcite in foraminiferal tests, and are currently being explored elsewhere (Tripati et al., 2017). With this future prospect in mind, we assess the sensitivity of our paleothermometers to various degrees of overprinting. We solve mass balance equations with diagenetic end-member contributions of 10, 20, 30, 40 and 50%. For $\delta^{18}O$, we assume linear mixing:

$$\delta^{18}O_{frosty} = F_{diag} \times \delta^{18}O_{diag} + (1 - F_{diag}) \times \delta^{18}O_{glassy} \quad (1)$$

Table 2
Hypothesized composition of inorganic calcite formed during early diagenesis. Inorganic calcite compositions used for our deep-sea temperature (DST) and sea surface temperature (SST) modeling are slightly different, because the overlapping time interval (and thus also the corresponding averaging interval) of our benthic isotope records is around 20 kyr longer than the overlapping interval of our planktic records (Figs. 4 and 5).

Site	Bottom water temperature[a] (°C)	Pore fluid $\delta^{18}O$[b] (‰)	$\alpha_{c\text{-}w}$ Watkins et al. (2013)[c]	$\alpha_{c\text{-}w}$ Kim and O'Neil (1997)	Inorg. calcite $\delta^{18}O$ Watkins et al. (2013) (‰)	Inorg. calcite $\delta^{18}O$ Kim and O'Neil (1997) (‰)	Inorg. calcite $\delta^{13}C$[d] (‰)	Inorg. calcite Δ_{47}[e] (‰)
Modeling of DSTs								
1260	12.6	−0.20	1.03285	1.03114	1.67	0.01	1.19	0.7167
1263	12.2	−0.17	1.03295	1.03124	1.80	0.14	2.02	0.7184
Modeling of SSTs								
1260	12.9	−0.15	1.03279	1.03108	1.65	0.00	1.19	0.7156
1263	12.5	−0.11	1.03288	1.03118	1.79	0.14	2.02	0.7173

[a] From the Δ_{47} signatures of benthic foraminifera averaged over relevant time interval.
[b] Derived from benthic foraminiferal $\delta^{18}O$ averaged over relevant time interval using Eq. (1) of Bemis et al. (1998).
[c] Based on $\alpha_{c\text{-}w}$ of Watkins et al. (2013), as shown in Eq. (19) of Watkins et al. (2014).
[d] Derived from bulk $\delta^{13}C$ (Edgar et al., 2007; Westerhold et al., 2015), as described in material and methods.
[e] Benthic foraminiferal Δ_{47} averaged over relevant interval.

F_{diag} is the fraction of the diagenetic end-member. Subscript text refers to the isotopic composition of measured frosty foraminiferal calcite (frosty), pristine glassy foraminiferal calcite (glassy) and inorganic diagenetic calcite (diag). Eq. (1) is then solved for $\delta^{18}O_{glassy}$ in order to estimate glassy foraminiferal $\delta^{18}O$ values. Similar calculations are carried out for $\delta^{13}C$.

In contrast to $\delta^{18}O$ and $\delta^{13}C$, Δ_{47} mixing is non-linear depending on the Δ_{47}, $\delta^{18}O$ and $\delta^{13}C$ values of the end-members (e.g., Eiler and Schauble, 2004; Defliese and Lohmann, 2015). We adopt the non-linear mixing model described in Defliese and Lohmann (2015) to calculate glassy foraminiferal Δ_{47} values from frosty foraminiferal Δ_{47} for different fractions of diagenetic calcite (see Appendix A.2 for further details). In order to test the sensitivity of the calculations to the type of mixing model, we additionally performed linear mixing calculations.

4. RESULTS

4.1. Foraminiferal preservation

Under the light microscope, benthic foraminifera from Site 1409 appear exceptionally well preserved (mostly translucent and glassy), whereas benthic foraminifera from Sites 1260 and 1263 are characterized by noticeably poorer (frosty) states of preservation (see Fig. S5 for preservation ranges of the benthic foraminiferal tests). This impression is confirmed by SEM analysis, which reveals much smoother surface textures of benthic foraminiferal tests at Site 1409 in comparison to Sites 1260 and 1263 (Fig. 2). Benthic foraminifera from Sites 1260 and 1263 are characterized by overgrowths of coarse inorganic crystallites with clearly visible crystal faces covering both surface and interior test walls (examples indicated by white arrows in Fig. 2e and g). The wall cross sections of *N. truempyi* from Site 1409 show calcite that is somewhat denser and more microgranular than at Sites 1260 and 1263 (Fig. 2g, h and i). However, benthic foraminiferal calcites from Sites 1260 and 1263 do not appear pervasively recrystallized. Additional SEM images documenting benthic foraminiferal preservation at each study site are shown in Fig. S6.

Planktic foraminifera from Sites 1050, 1260 and 1263 exhibit "blocky" textures and clear crystal faces (e.g., Pearson and Burgess, 2008), consistent with post-depositional alteration (Fig. 3). Crystallographic planes are most pronounced at Site 1263 and slightly less so at Site 1260, where fine wall structures such as tubular pore channels are visible in the wall cross section (Fig. 3h). Specimens from Site 1050 appear less granular in wall texture than those at Sites 1260 and 1263. Tests of *A. bullbrooki* examined at Sites 1408, 1409 and 1410 do not have large blocky crystals and do exhibit a number of fine wall structures, consistent with better calcite preservation. Some specimens show slightly uneven surfaces, covered by a thin layer of sub-micron crystals (Fig. 3m and n). These may be diagenetic in origin (cemented overgrowths) or could be part of the internal microstructure, exposed through minor partial dissolution (e.g., Pearson and Burgess, 2008). In contrast to the sites hosting frosty foraminifera, the Primary Organic

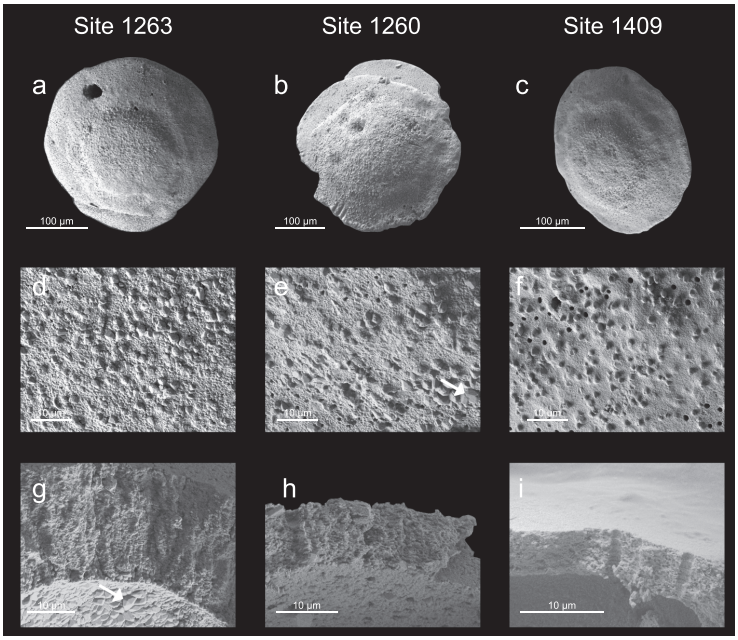

Fig. 2. SEM images showing the preservation state of benthic foraminifera *N. truempyi* at Sites 1263 (a, d, g), 1260 (b, e, h) and 1409 (c, f, i). Whole test images (a-c) do not reveal large differences in appearance, but when viewed in detail (d-i), the better preservation of the glassy benthic foraminiferal tests from Site 1409 is apparent. Scale bars are 100 µm (a-c) and 10 µm (d-i). The foraminifera were picked from samples 208-1263B-11H-4,91–93 (a, d, g), 207-1260B-10R-6,94–96 (b, e, h) and 342-U1409C-7H-4,110–112 (c, f, i). See Fig. S6 for additional images.

Membrane (POM) is clearly visible in the wall cross sections of the specimens from Sites 1408, 1409 and 1410 offshore Newfoundland (indicated by white arrows in Fig. 3p, q and r). Furthermore, many planktic foraminifera from these sites show substantial infillings (e.g., clay) in the aperture (Fig. 3k). However, our extensive cleaning protocol is designed to completely remove clay infillings before isotope analysis. In general, the foraminifera at Sites 1408, 1409 and 1410 exhibit broadly similar ranges of preservation (see Fig. S7 for preservation ranges of the planktic foraminiferal tests), despite their different subseafloor burial depths. This highlights the crucial role played by lithology (in this case, clay-rich sediments) in enhancing microfossil preservation (e.g., Sexton et al., 2006b; Sexton and Wilson, 2009). SEM images of further representative planktic foraminiferal specimens for each study site can be found in Figs. S8 and S9.

4.2. Foraminiferal $\delta^{18}O$, $\delta^{13}C$ and Δ_{47} values

Our high-resolution (~10 kyr) middle Eocene isotope records were used to define overlapping intervals for all benthic and planktic foraminiferal records (Figs. 4 and 5). The benthic isotope records overlap from approximately −0.17 Myr to +0.21 Myr around the 20n/20r boundary (marked by horizontal bar in Fig. 4), whereas the planktic records, which comprise more sites, overlap from approximately −0.15 Myr to +0.21 Myr (marked by horizontal bar in Fig. 5). To allow direct comparison, we only interpret averaged Δ_{47}- and $\delta^{18}O$-based temperature data from the abovementioned overlapping intervals.

Benthic $\delta^{18}O$ and $\delta^{13}C$ show synchronous low-frequency fluctuations (Fig. 4) following eccentricity cycles, especially pronounced from −0.1 Myr to +0.2 Myr at all sites. At times of high eccentricity (e.g., around +0.1 Myr), $\delta^{18}O$ values decrease, with an overall amplitude of roughly 0.2–0.3‰ (Fig. 4b). Using the equation of Bemis et al. (1998) and assuming no changes in global ice volume, these declines in $\delta^{18}O$ correspond to modest DST changes of approximately 1.0–1.5 °C. We observe slight offsets in mean benthic $\delta^{18}O$ (+0.1‰ to +0.3‰) and $\delta^{13}C$ (+0.2‰ to +0.4‰) values of Site 1263 in the South Atlantic relative to the more northern sites (Fig. 4b, c, S10a and S11a). As expected, the Δ_{47} signal appears very noisy in comparison to $\delta^{13}C$ and $\delta^{18}O$ (Fig. 4). Due to the large analytical uncertainty when measuring small samples, single measurements of Δ_{47} cannot be taken at face value. Average benthic foraminiferal Δ_{47} values for the overlapping time interval are 0.7145 ± 0.0028‰ (1SE) at Site 1409, 0.7167 ± 0.0042‰ at Site 1260 and 0.7184 ± 0.0045‰ at Site 1263.

Orbital-scale cyclicity appears less pronounced in the planktic $\delta^{18}O$ and $\delta^{13}C$ time series (Fig. 5) in comparison to benthic $\delta^{18}O$ and $\delta^{13}C$ (Fig. 4). Based on visual assessment, planktic $\delta^{13}C$ fluctuations are synchronous with eccentricity to a certain extent, especially at Sites 1410, 1260 and 1263, whereas changes in $\delta^{18}O$ are small (mostly < 0.5‰).

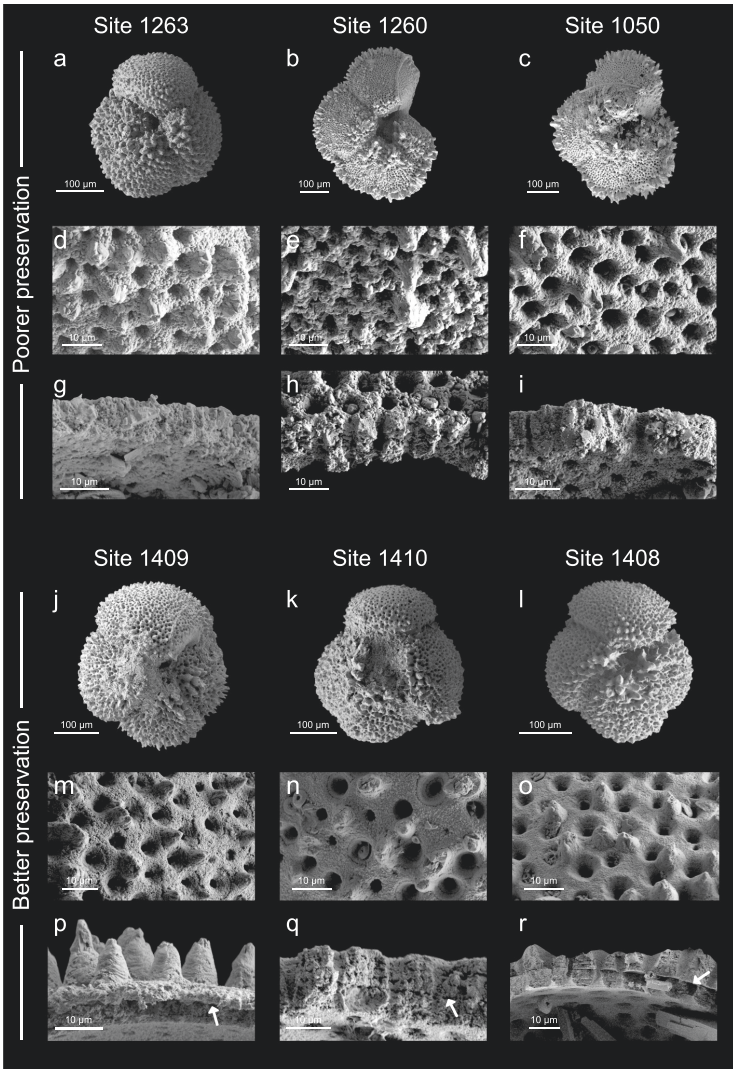

Fig. 3. SEM images showing planktic foraminiferal specimens of *M. coronatus* and *A. bullbrooki* representing the preservation states at Sites 1263 (a, d, g), 1260 (b, e, h). 1050 (c, f, i), 1409 (j, m, p), 1410 (k, n, q) and 1408 (l, o, r). Scale bars are 100 µm (a-c, j-l) and 10 µm (d-i, m-r). The foraminifera were picked from samples 208-1263B-11H-6,51–53 (a, d, g), 207-1260A-14R-5,146–148 (b, e, h), 171B-1050A-7H-5,102–104 (c, f, i), 342-U1409C-7H-2,136–138 (j, m, p), 342-U1410C-17X-4,46–48 (k, n), 342-U1410C-17X-3,73–75 (q), 342-U1408C-17H-3,37–39 (l, o) and 342-U1408B-18H-2,109–111 (r). See Figs. S8 and S9 for additional images.

Planktic foraminiferal Δ_{47} values averaged over the overlapping time interval are 0.6732 ± 0.0048 (1SE)‰ at Site 1408, 0.6767 ± 0.0044‰ at Site 1409, 0.6674 ± 0.0039‰ at Site 1410, 0.6677 ± 0.0047‰ at Site 1050, 0.6698 ± 0.0037‰ at Site 1260 and 0.6914 ± 0.0032‰ at Site 1263. Boxplots for benthic and planktic $\delta^{13}C$, $\delta^{18}O$ and Δ_{47} values at each site are shown in Figs. S10, S11 and S12.

4.3. Reconstructed deep-sea temperature and water $\delta^{18}O$ values

Benthic foraminiferal clumped isotope DSTs averaged over the studied interval (marked by horizontal bar in Fig. 4) amount to 13.2 ± 0.9 (1SE) °C at Site 1409, 12.6 ± 1.2 °C at Site 1260 and 12.2 ± 1.3 °C at Site 1263

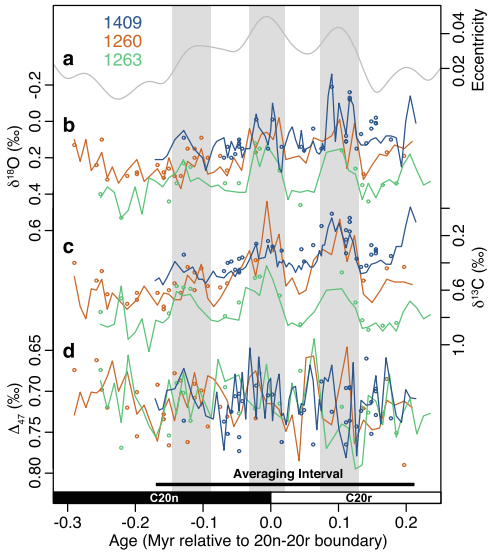

Fig. 4. Benthic $\delta^{18}O$ (b) and $\delta^{13}C$ (c) records of Sites 1409, 1260 and 1263 plotted with Δ_{47} (d) and eccentricity (a) of orbital solution La2010d (Laskar et al., 2011a). Lines are based on one measurement at each depth. Additional replicate measurements on some samples are shown as open circles and eccentricity maxima are highlighted with gray shading.

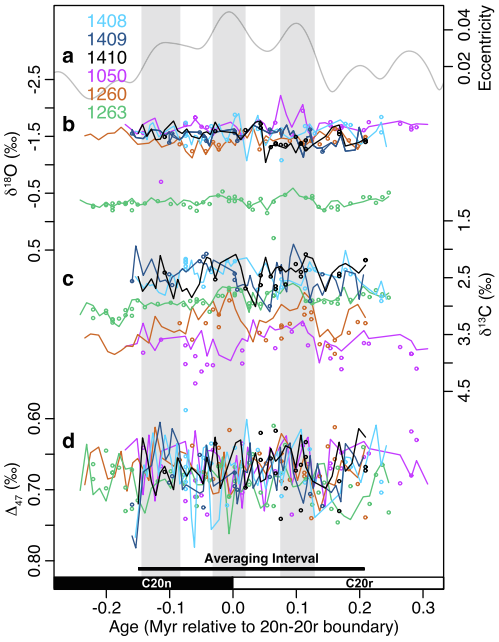

Fig. 5. (a) Eccentricity of orbital solution La2010d (Laskar et al., 2011a) as well as planktic foraminiferal (b) $\delta^{18}O$, (c) $\delta^{13}C$ and (d) Δ_{47} time series. Lines are based on one measurement at each depth. Additional replicate measurements on some samples are shown as open circles and eccentricity maxima are highlighted with gray shading.

(Fig. 6a). By combining mean clumped isotope temperature data with mean benthic $\delta^{18}O$, we estimate deep-sea water $\delta^{18}O$ compositions. Average deep-sea water $\delta^{18}O$ values at Sites 1409, 1260 and 1263 are -0.20 ± 0.19 (1SE)‰, -0.20 ± 0.26‰, and -0.17 ± 0.27‰, respectively (Fig. 6b). Our deep-sea water $\delta^{18}O$ values are in good agreement with each other, but are higher than the values from a global composite of reconstructed water $\delta^{18}O$ of approximately −0.60‰ (mean during study interval), based on combining benthic foraminiferal Mg/Ca and $\delta^{18}O$ values (Cramer et al., 2011). Using the average of our calculated $\delta^{18}O$ seawater values across the three sites (−0.19‰), DST values calculated from benthic $\delta^{18}O$ for each site, averaged over the studied interval, are 13.3 °C for Site 1409, 12.7 °C for Site 1260 and 12.1 °C for Site 1263 with absolute ranges of 2.9 °C, 2.1 °C and 1.8 °C, respectively (Fig. 6a).

4.4. Sea surface temperatures

Average clumped isotope SSTs are 24.7 ± 1.5 (1SE) °C, 23.6 ± 1.4 °C, 26.4 ± 1.3 °C, 26.3 ± 1.5 °C, 25.7 ± 1.2 °C and 19.5 ± 1.0 °C at Sites 1408, 1409, 1410, 1050, 1260 and 1263, respectively (Fig. 7). We also calculate $\delta^{18}O$-based SST values, acknowledging high uncertainty owing to our limited knowledge of past surface seawater $\delta^{18}O$ values. The latter are impacted by changes in the hydrological cycle, in addition to global ice-volume and temperature (e.g., Roberts et al., 2011). Here, we estimate surface water $\delta^{18}O$ values from deep water $\delta^{18}O$ (our mean Atlantic deep-sea water $\delta^{18}O = -0.19$‰), and correct for paleolatitude (Eq. (1) of Zachos et al. (1994)), with the caveat that latitudinal gradients may have shifted. Final adjusted surface water $\delta^{18}O$ estimates are 0.82‰, 0.65‰ and 0.42‰ at Sites 1050, 1260 and 1263, respectively, and 0.65‰ at Sites 1408, 1409 and 1410. Using these surface water $\delta^{18}O$ values to calculate mean $\delta^{18}O$-based SSTs for each site with the oxygen isotope paleotemperature equation of Bemis et al. (1998), we estimate average values at Sites 1408, 1409, 1410, 1050, 1260 and 1263 of 25.9 °C, 25.5 °C, 25.5 °C, 27.2 °C, 25.1 °C and 18.9 °C, respectively (Fig. 7). Due to the large, unquantifiable uncertainties associated with our estimates for surface water $\delta^{18}O$ compositions, we do not report error estimates for surface water $\delta^{18}O$ values and the resulting SSTs. Most $\delta^{18}O$-based SST values fall within the uncertainty of the respective mean clumped isotope temperature. In comparison to $\delta^{18}O$, Δ_{47} signatures indicate slightly higher SSTs at Sites 1410, 1260 and 1263, and slightly lower SSTs at Sites 1408, 1409 and 1050.

5. DISCUSSION

5.1. Impact of diagenesis on benthic foraminiferal $\delta^{18}O$ and Δ_{47} values

Orbital-scale variations in benthic $\delta^{18}O$ and $\delta^{13}C$ time series are evident in our benthic foraminiferal records (Fig. 4). During the middle Eocene these variations should

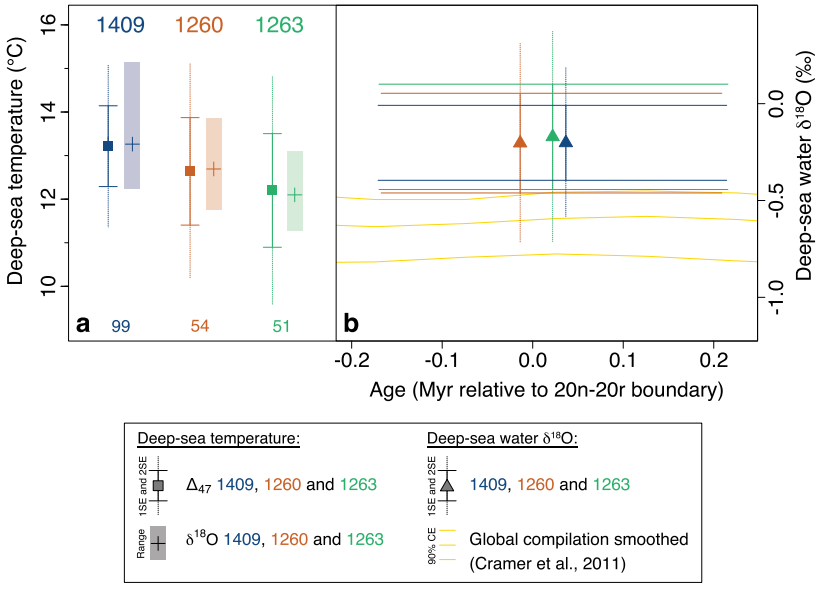

Fig. 6. (a) Comparison of benthic deep-sea temperatures based on Δ_{47} (squares) and $\delta^{18}O$ (plus signs) averaged over the overlapping time interval (illustrated in Fig. 4). For Δ_{47}-based temperatures, ±1SE and ±2SE are shown using solid and dotted lines, respectively. The number of measurements used for the calculation of each temperature value are listed below. Value ranges of $\delta^{18}O$-based temperatures are illustrated with shaded bars. (b) Calculated mean deep-sea water $\delta^{18}O$ (triangles). Here, an error bar represents the propagated analytical error in Δ_{47} and $\delta^{18}O$ (solid lines = ±1SE, dotted lines = ±2SE) and spans exactly the respective averaging time interval, with the location of a triangle indicating its mean age. In addition, we show a global deep-sea water $\delta^{18}O$ time series based on a compilation of Mg/Ca and $\delta^{18}O$ records (Cramer et al., 2011). The dataset of Cramer et al. (2011) is plotted with their 90% confidence envelope (CE).

include eccentricity modulation of bottom water conditions (e.g., Sexton et al., 2011; Westerhold and Röhl, 2013). Such variations are observed in the benthic $\delta^{18}O$ and $\delta^{13}C$ time series at all sites, despite contrasting burial histories (Fig. 4b and c), implying that diagenetic alteration did not occur to the extent that would erase this signal. Furthermore, mean $\delta^{18}O$- and Δ_{47}-based DST values derived from glassy benthic foraminifera at Site 1409 agree well with the corresponding temperatures measured on frosty foraminifera from Sites 1260 and 1263 (Fig. 6a). The agreement in mean deep-sea water $\delta^{18}O$ values is even better (Fig. 6b). These observations suggest a negligible impact of secondary diagenetic alteration on the $\delta^{18}O$ and Δ_{47} signatures of benthic foraminiferal calcites at Sites 1409, 1260 and 1263.

We acknowledge that gradients in deep-sea water $\delta^{18}O$ and/or DST between the different sites being examined could, in theory, mask some of the potential effects of differential diagenetic processes, but we consider this possibility as less likely. Our deep-sea water $\delta^{18}O$ values are higher in comparison to the values from the global composite record of Cramer et al. (2011), based on Mg/Ca. This difference could be due to water mass differences between the ocean basins, and/or additional effects on Mg/Ca such as carbonate ion concentration (e.g., Lear et al., 2010) or a varying Mg/Ca ratio of seawater.

Relatively minimal susceptibility of primary benthic foraminiferal $\delta^{18}O$ values in pelagic sediments towards diagenesis has been noted in previous studies (Edgar et al., 2013; Voigt et al., 2016). These authors attribute the robustness of benthic foraminiferal $\delta^{18}O$ values to diagenetic alteration occurring dominantly at shallow burial depths (<100 m) and very rapidly after deposition (<100 kyr) in a recrystallization environment similar to that of initial calcification. Their scenario of shallow diagenesis is supported by numerical modeling (e.g., Rudnicki et al., 2001). Additional complications can arise in settings with very low sedimentation rates and/or an overlying hiatus, where benthic foraminiferal $\delta^{18}O$ values can become severely altered (Sexton and Wilson, 2009).

None of the sites investigated in this study are marked by very low sedimentation rates or an overlying hiatus (Table 1). However, our modeled initial benthic foraminiferal calcification temperatures for different fractions of secondary inorganic calcite at Sites 1260 and 1263 (Fig. 8) indicate that, even in the case of shallow diagenesis, benthic foraminiferal $\delta^{18}O$ values and the resulting paleotemperatures can potentially be biased, depending on the amount of secondary inorganic calcite added, pore fluid chemistry and the rate of inorganic calcite precipitation. Modeled primary foraminiferal $\delta^{18}O$ (and $\delta^{13}C$) signatures for different fractions of diagenetic calcite are shown in Fig. S13.

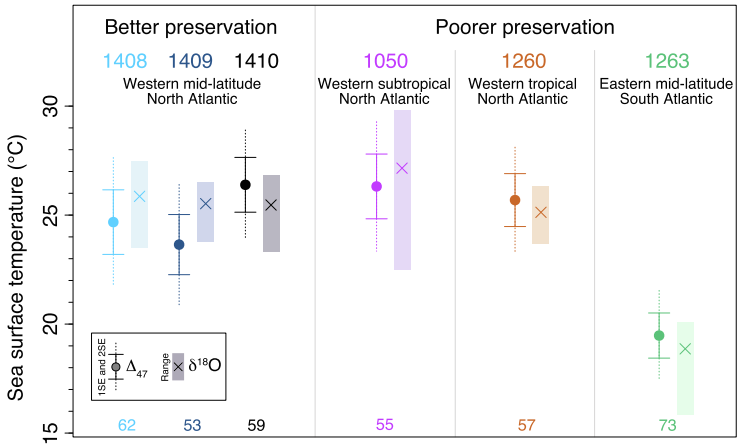

Fig. 7. Planktic Δ_{47}-based (circles) and $\delta^{18}O$-based (crosses) temperatures averaged over the overlapping time interval (illustrated in Fig. 5). The study sites from different oceanographic regimes are characterized by a wide range of preservation states. ±1SE and ±2SE of Δ_{47}-based temperatures are depicted by solid and dotted lines, respectively. Shaded bars show value ranges of $\delta^{18}O$-based temperatures. The number of measurements used for the calculation of the clumped isotope temperature values are listed at the bottom of the plots.

The temperature-dependence for ^{18}O uptake proposed by Watkins et al. (2013) is assumed to describe ^{18}O fractionation for slow inorganic calcite precipitation under near-equilibrium conditions, whereas the temperature-dependence proposed by Kim and O'Neil (1997) has been recently shown to reflect inorganic calcite growth rates, which are too high for isotopic equilibrium (Watkins et al., 2014). When using the fractionation factor of Watkins et al. (2013) for diagenetic calcite, our two-component mixing model indicates a potentially high susceptibility of $\delta^{18}O$-based paleotemperatures towards diagenesis (neomorphism and cementation), even in benthic foraminifera, with a bias of up to 2.0 °C for 20% diagenetic calcite and up to 8.0 °C for 50% diagenetic calcite (Fig. 8a). In the non-equilibrium regime described by Kim and O'Neil (1997), the bias is found to be significantly smaller (<1.0 °C for up to 50% diagenetic calcite).

We propose two possible explanations for the observed robustness of benthic foraminiferal $\delta^{18}O$ towards diagenesis: (1) Benthic foraminiferal tests at Sites 1260 and 1263 are generally unsusceptible to neomorphism, owing to their denser tests and their higher resistance to dissolution in comparison to planktic foraminiferal tests (e.g., Berger, 1973; Pearson et al., 2001). Therefore, contributions of secondary calcite during post-depositional diagenesis are minor. Although there is clear visible evidence for cementation with overgrowths of diagenetic calcite, in mass balance terms, this might be a proportionally minor component of whole test calcite, resulting in negligible $\delta^{18}O$ shifts of whole test $\delta^{18}O$ compositions. (2) Rates of inorganic calcite precipitation in sedimentary pore waters are too fast for isotopic equilibrium, e.g., as described by the equation of Kim and O'Neil (1997), and the fractionation of oxygen isotopes between inorganic calcite and water is similar to the fractionation in modern benthic foraminifera such as *Cibicidoides* spp. (the calibration equation used for *Cibicidoides* (Eq. (1), Bemis et al., 1998) and the inorganic calcite equation of Kim and O'Neil (1997) agree well, as documented in Bemis et al. (1998)). Together with our assumption of shallow burial diagenesis, this second potential explanation implies similar precipitation temperatures and $\delta^{18}O$ signatures of benthic foraminiferal (primary) and inorganic (secondary) calcites, and correspondingly small changes in benthic foraminiferal $\delta^{18}O$ through neomorphism and cementation. Our two explanations are not mutually exclusive. In fact, it is likely that the small impact of diagenesis on benthic foraminiferal $\delta^{18}O$ is caused by some combination of test robustness and inorganic calcite growth rates that are faster than those in equilibrium.

To the best of our knowledge, the sensitivity of primary Δ_{47} signatures of benthic foraminiferal tests to diagenetic alteration has not yet been tested. Our Δ_{47} results suggest no significant effect on benthic foraminiferal Δ_{47} values and DSTs derived therefrom (Figs. 4d and 6a). Isotope exchange reactions within carbonates as well as between carbonates and surrounding fluids seem to be of minor importance for isotope ordering of these calcites. This is in line with the view that C-O bond reordering in the solid mineral lattice of primary calcites is not substantial at burial temperatures below 100 °C for timescales from 10^6 to 10^8 years (Henkes et al., 2014). We show here that this holds true even in natural environments where the primary calcite is in permanent or semipermanent contact with water.

Similarly, our end-member modeling also suggests that clumped isotope paleotemperatures based on benthic foraminiferal Δ_{47} values are relatively insensitive to diagenetic processes such as neomorphism and cementation (bias of <1.2 °C for up to 50% diagenetic calcite), due to our assumption that DSTs can be used to approximate diagenetic calcite precipitation temperatures in a scenario of shallow burial diagenesis (Fig. 8b). We include two scenarios of deep diagenesis where diagenetic alteration occurs

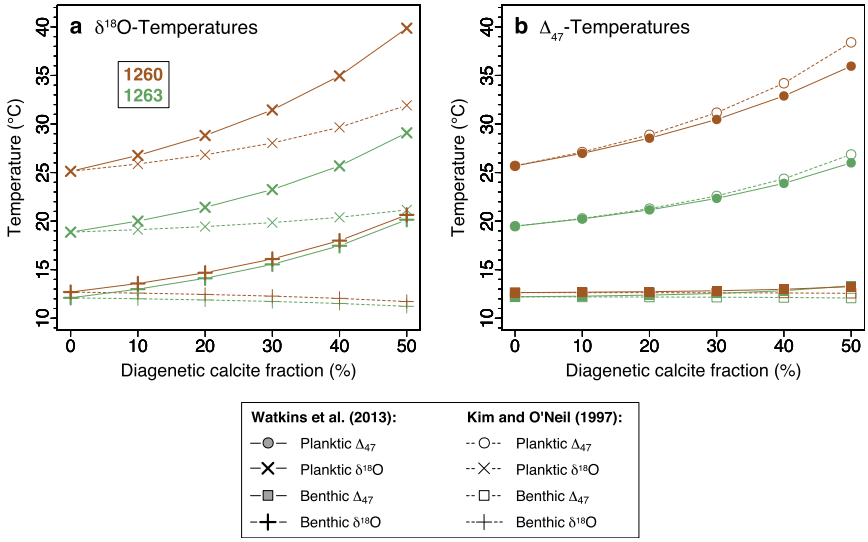

Fig. 8. Temperatures of initial biogenic calcification calculated for various assumed percentages of early diagenetic inorganic calcite at Sites 1260 (red) and 1263 (green). SEM images suggest substantial fractions of diagenetic calcite at Sites 1260 and 1263, in contrast to Site 1409. At the same time, both planktic and benthic isotope data are available at Sites 1260 and 1263. Panel (a) shows $\delta^{18}O$-based temperatures from planktic (crosses) and benthic (plus signs) foraminifera, whereas the values shown in (b) are based on the Δ_{47} signatures of planktic (circles) and benthic (squares) foraminifera. Starting points of the curves are the temperatures calculated from measured Δ_{47} and $\delta^{18}O$ (i.e., diagenetic calcite fraction = 0%). Calculations were performed using both the fractionation factor of Watkins et al. (2013) (solid lines) and the fractionation factor of Kim and O'Neil (1997) (dashed lines) for inorganic calcite.

near final burial depths (Fig. S14). In these cases, DSTs derived from $\delta^{18}O$ and Δ_{47} signatures of benthic foraminiferal tests may be biased to a larger degree, depending on pore fluid chemistry (Fig. S15). For example, the modeled diagenetic bias in foraminiferal Δ_{47}-based DSTs at Site 1260 is +3.2 °C, when assuming an extreme case of deep diagenesis near final burial depths under a middle Eocene geothermal gradient of 30 °C/km, 50% diagenetic calcite and ^{18}O fractionation during diagenetic calcite precipitation according to Watkins et al. (2013). However, our extreme scenarios of deep diagenesis are considered unlikely, based on numerical modeling and empirical data (e.g., Rudnicki et al., 2001; Edgar et al., 2013; Voigt et al., 2016), and should be seen as a sensitivity experiment only. We further note that effects on Δ_{47} values purely from dissolution have not yet been investigated.

5.2. Robustness of Δ_{47}- and $\delta^{18}O$-based sea surface temperature reconstructions

$\delta^{18}O$ signatures of shallow-dwelling planktic foraminifera are thought to be more susceptible to diagenesis than those of benthic foraminifera, primarily because of the contrast in carbonate precipitation environments (e.g., temperature, pH) between upper water column and bottom waters or sedimentary pore fluids (e.g., Edgar et al., 2013). Mean tropical SST values derived from frosty planktic foraminiferal $\delta^{18}O$ and Δ_{47} signatures are lower than 26 °C at tropical West Atlantic Site 1260 (Fig. 7). These reconstructed tropical SST values are thus substantially lower than previous middle Eocene (42–46 Ma) SST estimates of approximately 30–34 °C for other parts of the tropics (Evans et al., 2018). Moreover, they are similar to our $\delta^{18}O$- and Δ_{47}-based SST values from Sites 1408, 1409, 1410 and 1050 located at higher northern latitudes. Although we cannot exclude additional factors, such as differences in seasonality between the sites, we interpret the observed similarities between tropical and higher latitude SST values as primarily caused by partial diagenetic overprinting of tropical SST signatures in colder pore fluids.

End-member modeling supports this interpretation, indicating significant susceptibility of planktic foraminiferal calcite to diagenesis, both in terms of Δ_{47} and $\delta^{18}O$ values (Fig. 8). For Site 1260 in the tropical West Atlantic, our model calculations based on the assumptions listed in Table 2 and the ^{18}O fractionation factor of Watkins et al. (2013) indicate that assuming an inorganic calcite fraction of 20% would lead to a cold bias of −2.9 °C in SST derived from Δ_{47}, while a fraction of 50% would result in a bias of −10.3 °C. Using the fractionation factor of Kim and O'Neil (1997) to calculate inorganic calcite $\delta^{18}O$ compositions from pore fluid $\delta^{18}O$ values, we obtain similar cold biases for Δ_{47}-based SSTs amounting to −3.2 and −12.7 °C for 20 and 50% inorganic calcite, respectively. For $\delta^{18}O$-based SSTs, inorganic calcite fractions of 20 and 50% result in cold biases of −3.7 and −14.7 °C, when using the fractionation factor of Watkins et al. (2013), but only −1.7 and −6.8 °C, when using the factor of Kim and O'Neil

(1997). For comparison, Pearson et al. (2001) suggested that tropical SSTs derived from the $\delta^{18}O$ composition of planktic foraminiferal tests with 50% diagenetic calcite may be underestimated by roughly 10–15 °C.

In comparison to the tropics, the modeled effect of diagenetic alteration on stable isotopes in fossil planktic foraminiferal tests from middle latitudes is more modest (Fig. 8), due to smaller differences in isotopic composition between planktic foraminiferal and inorganic calcite (Fig. 5 and Table 2). For Δ_{47}-based SSTs at Site 1263 in the southern mid-latitude East Atlantic, cold biases calculated with the ^{18}O fractionation factor of Watkins et al. (2013) amount to −1.7 °C and −6.5 °C for inorganic calcite contributions of 20 and 50%, respectively. The values based on the factor of Kim and O'Neil (1997) are relatively similar at this site (−1.8 °C and −7.4 °C for 20% and 50%). For $\delta^{18}O$-based SSTs, modeled cold bias values diverge substantially when using different fractionation factors to calculate inorganic calcite $\delta^{18}O$, similar as observed for Site 1260 in the tropics, ranging from −0.6 °C to −2.6 °C for 20% inorganic calcite and from −2.3 °C to −10.2 °C for 50% inorganic calcite.

Because of their strong dependence on the $\delta^{18}O$ composition of pore fluids and inorganic calcite precipitated therefrom, the sensitivities of $\delta^{18}O$-based SSTs to diagenetic alteration are more uncertain than those of Δ_{47}-based SSTs. Our estimates for inorganic calcite $\delta^{18}O$ and $\delta^{13}C$ signatures (Table 2) are in the range of the values reported in previous studies (e.g., Pearson et al., 2001; Sexton and Wilson, 2009; Voigt et al., 2016). However, $\delta^{18}O$ and $\delta^{13}C$ compositions of diagenetic inorganic calcite are relatively poorly constrained in these and in our study, owing to a lack of direct measurements (e.g., acquired by in situ secondary ion mass spectrometry (SIMS) as documented in Kozdon et al. (2013)). Inorganic calcite $\delta^{18}O$, $\delta^{13}C$ and Δ_{47} values may be affected by "closed" system effects (i.e., limited exchange with pore fluids) and/or non-equilibrium isotope fractionation varying with salinity, pH and/or crystal growth rate (e.g., Hill et al., 2014; Watkins et al., 2014). Using the ^{18}O fractionation factor of Kim and O'Neil (1997) instead of Watkins et al. (2013) for inorganic calcite significantly lowers the sensitivity of foraminiferal $\delta^{18}O$ signatures to diagenetic alteration. In comparison, changing the ^{18}O fractionation factor has only a slight influence on the sensitivity of foraminiferal Δ_{47} values to diagenesis (due to different diagenetic end-member $\delta^{18}O$ compositions affecting non-linear mixing of Δ_{47}).

Furthermore, we note that if a simpler mixing model is used for estimating the effects of diagenesis on Δ_{47}, which does not consider non-linear mixing effects, then the modeled diagenetic effects would be larger. In this case, assuming 20% and 50% inorganic calcite result in cold biases of −3.5 °C and −14.6 °C at Site 1260 and −1.8 °C and −7.5 °C at Site 1263 (see Fig. S16 for a comparison between linear and non-linear Δ_{47} mixing). The magnitudes of these values are independent of the ^{18}O fractionation factor. The comparison between linear and non-linear mixing modeling demonstrates that the bias of Δ_{47}-based primary SST signals by diagenetic overprinting is partially mitigated by non-linear Δ_{47} mixing effects, which are caused by differences between the end-member isotopic compositions (e.g., Defliese and Lohmann, 2015). Thereby, the mixing offset is larger for large differences in $\delta^{18}O$ and/or $\delta^{13}C$ between the end-member compositions in comparison to small differences. Assuming small fractions of diagenetic calcite (20% and below), non-linear mixing effects on clumped isotope SST values appear generally small (<1 °C). For larger fractions of inorganic calcite, however, mitigation of diagenetic overprinting by non-linear mixing effects can be substantial in some settings. At Site 1260 in the tropics, for example, non-linear mixing effects reduce the modeled SST cold bias by 4.4 °C, when assuming an inorganic calcite fraction of 50% and equilibrium fractionation of ^{18}O in inorganic calcite (described by the ^{18}O fractionation factor of Watkins et al. (2013)).

We conducted a range of sensitivity analyses for different values of inorganic calcite $\delta^{18}O$ and $\delta^{13}C$ (Figs. S17 and S18). As expected, the sensitivity of Δ_{47}-derived paleotemperatures to diagenetic alteration is less affected by different values for inorganic calcite $\delta^{18}O$ in comparison to the sensitivity of $\delta^{18}O$-derived paleotemperatures, which even changes sign (Fig. S17). This makes it more difficult to correct paleotemperatures derived from the $\delta^{18}O$ signatures of foraminiferal tests for diagenetic alteration. Furthermore, utilizing mean planktic foraminiferal $\delta^{13}C$ values measured at each site (3.3‰ and 2.9‰ at Sites 1260 and 1263, respectively) instead of bulk $\delta^{13}C$ values (Table 2) to approximate inorganic calcite $\delta^{13}C$ values increases the sensitivity of Δ_{47}-based SSTs to diagenesis from 0.0 °C to 0.7 °C for 20% inorganic calcite and from 0.3 °C to 5.0 °C for 50% inorganic calcite, due to a weakening of non-linear mixing effects (Fig. S18). In contrast, inorganic calcite $\delta^{13}C$ values that are lower than bulk $\delta^{13}C$ (e.g., caused by organic carbon degradation) lead to stronger non-linear mixing effects and thus decreased sensitivity of primary Δ_{47} signatures to diagenetic alteration. Furthermore, diagenesis at deeper burial depths would imply a generally smaller cool bias in $\delta^{18}O$- and Δ_{47}-based SST values reconstructed from altered planktic foraminiferal tests (Figs. S14 and S15) than shallow diagenesis (shown in Fig. 8).

Comparison of samples from the clay-rich sedimentary sequences of Sites 1408, 1409 and 1410 provides an opportunity to assess if whole test $\delta^{18}O$ and Δ_{47} compositions of planktic foraminifera may be affected by the presence of very minor overgrowths of diagenetic calcite even in locations with generally good preservation of foraminifera (Fig. 3). Owing to the very close proximity of these Newfoundland sites to each other, planktic foraminiferal tests are assumed to reflect similar surface water conditions. In comparison to Site 1409, middle Eocene sediments at Sites 1408 and 1410 were deposited more rapidly and are more deeply buried (Table 1). After deposition, foraminiferal tests at Site 1409 thus stayed comparably long at shallow depths, where diffusive fluxes in pore fluids and reactive rates tend to be highest (e.g., Edgar et al., 2013). However, SEM images indicate only minor differences in preservation (Fig. 3), suggesting that these contrasting sedimentological facets of Sites 1408 and 1410 versus 1409 had minimal impact on differential diagenetic alteration.

In our isotope data, we find no evidence that Sites 1408, 1409 and/or 1410 might have been significantly affected by

diagenesis. Averages and ranges of $\delta^{18}O$-based SST values are similar at Sites 1408, 1409 and 1410 (Fig. 7). Planktic foraminiferal $\delta^{13}C$ values at Sites 1408, 1409 and 1410 are also in good agreement with each other (Fig. S11b). The observed range (~3 °C) among the average clumped isotope temperature results from Sites 1408, 1409 and 1410 is likely attributable to analytical uncertainties. Our findings imply that non-glassy planktic foraminiferal tests with minor signs of diagenetic calcite overgrowths but without visible neomorphism can be confidently used for $\delta^{18}O$- and Δ_{47}-based paleoclimate reconstructions.

5.3. Comparison with other estimates for middle Eocene temperatures

Fig. 9 shows the clumped isotope temperature estimates from this study plotted with existing SST and DST reconstructions from 42 to 46 Ma (Evans et al., 2018), representing an interval without major transitions or perturbations in global climate (e.g., Sexton et al., 2006a; Zachos et al., 2008). SST estimates based on foraminiferal $\delta^{18}O$ values are not shown, owing to their dependence on poorly constrained seawater $\delta^{18}O$. Mg/Ca-based SST values were compiled and recalculated by Evans et al. (2018), using seawater Mg/Ca data derived from the Δ_{47} and Mg/Ca signatures of shallow-dwelling large benthic foraminifera. In addition, we compare to clumped isotope SSTs derived from bivalve shells from Seymour Island, located in the South Pacific near the Antarctic Peninsula (Douglas et al., 2014).

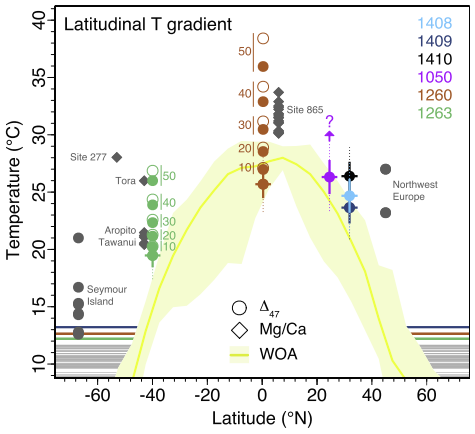

Fig. 9. Middle Eocene (42–46 Ma) SSTs and DSTs based on Δ_{47} and Mg/Ca compared to modern mean annual temperatures from the World Ocean Atlas 2013 (WOA, yellow, Locarnini et al., 2013). Reconstructed SST values from this study (circles) are shown with uncertainties (vertical solid lines = ±1SE, vertical dotted lines = ±2SE, horizontal solid lines = uncertainty in paleolatitude according to van Hinsbergen et al. (2015)). The Δ_{47}-based SST values derived from the frosty foraminiferal tests at Sites 1050, 1260 and 1263 are likely too low. Therefore, the range of SST values is illustrated for inorganic calcite fractions of 10, 20, 30, 40 and 50% for Sites 1260 and 1263. These values were calculated using either the ^{18}O fractionation factor of Watkins et al. (2013) (filled circles) or that of Kim and O'Neil (1997) (open circles). Mg/Ca SSTs (dark gray diamonds) from DSDP Site 277 as well as the localities Aropito, Tawanui and Tora in the Southwest Pacific area (Hines et al., 2017) and Site 865 in the equatorial Pacific (Tripati et al., 2003) were reevaluated by Evans et al. (2018). Dark gray circles are clumped isotope-based estimates from shallow-dwelling benthic foraminifera in Northwest Europe (Evans et al., 2018) and from bivalve shells from Seymour Island in the South Pacific (Douglas et al., 2014). Horizontal lines show DSTs measured in this study and the reconstruction of Cramer et al. (2011) for the interval from 42 to 46 Ma (light gray). Zonal mean and range in WOA SST (data from https://www.nodc.noaa.gov/cgi-bin/OC5/woa13/woa13.pl) are depicted by yellow lines and shading, respectively.

Δ_{47}-derived SST estimates from frosty foraminifera at Sites 1260 and 1263 are cooler than existing Mg/Ca-based SST values for similar paleolatitudes. The apparent cool bias at Site 1260 would be greatly reduced when correcting for secondary inorganic calcite fractions from 10 to 50%. For example, our Δ_{47}-based SST estimate corrected for 30–40% inorganic calcite at Site 1260 is in excellent agreement with Mg/Ca-based SSTs from ODP Site 865 in the western central equatorial Pacific (Tripati et al., 2003; Evans et al., 2018). The observed offset between SST values from Site 1263 in the eastern South Atlantic and DSDP Site 277 in the Southwest Pacific Ocean as well as the localities Aropito, Tawanui and Tora in eastern New Zealand (Hines et al., 2017; Evans et al., 2018) may be linked to differences in foraminiferal preservation and/or oceanographic regime between these distant sites. Given that Site 1263 is located near the eastern boundary of an ocean basin, comparably low SSTs at this site could have been caused by upwelling of cooler waters. However, low sedimentation rates observed at Site 1263 (Table 1) may indicate that there was no major upwelling at this site in the past, and the observed overgrowth on foraminifera used in this study does suggest that the colder temperature is at least in part due to diagenetic alteration. For Site 1050, the sensitivity of the SST value to diagenetic alteration was not modeled, as no benthic foraminiferal data were available to estimate the isotopic composition of inorganic calcite at this site. The uncorrected clumped isotope SST estimate for Site 1050 is likely too low, based on our assessment of planktic foraminiferal preservation at this site. In contrast, our new SST estimates derived from the well-preserved foraminiferal tests at Newfoundland Sites 1408, 1409 and 1410 indicate reasonable temperatures for the mid-latitudes, which were warmer than present during the middle Eocene greenhouse (Fig. 9).

Clumped isotope DSTs from Sites 1409, 1260 and 1263 appear higher (+0.6–4.3 °C) than the Mg/Ca-based DST values from the global compilation of Cramer et al. (2011). Mg/Ca DSTs (42–46 Ma) have been calculated by Cramer et al. (2011) based on seawater Mg/Ca values that are in good agreement with recent estimates for the middle Eocene (Evans et al., 2018), and have thus not been updated here. The offset observed between Δ_{47}-derived and Mg/Ca-derived DSTs may however be explainable by calibration uncertainty and/or possible vital effects in foraminiferal Mg/Ca compositions as well as inter-basin differences in DST and/or carbonate chemistry effects (e.g.,

saturation state) biasing Mg/Ca-based DSTs towards lower temperatures (e.g., Lear et al., 2010).

6. CONCLUSIONS

We used middle Eocene benthic and planktic foraminifera from six ODP/IODP sites in the Atlantic Ocean to test the effects of diagenesis on the stable and clumped isotopic compositions of foraminiferal calcites. SEM images revealed significant differences in carbonate fossil preservation between the sites. The clay-rich sediments from the Newfoundland Drifts host exceptionally well-preserved foraminiferal tests, whereas foraminifera from the more carbonate-rich pelagic settings, commonly used for Paleogene climate reconstructions, are characterized by poorer preservation states with clear diagenetic features. However, despite different burial histories and variable foraminiferal preservation, inter-site offsets in $\delta^{18}O$- and Δ_{47}-based DSTs from benthic foraminifera at the sites examined are negligible. Hence, primary benthic $\delta^{18}O$ and Δ_{47} signatures seem generally well preserved during post-depositional diagenesis under the conditions and timescales represented by our study sites. On the other hand, planktic foraminiferal tests from the carbonate-rich sediments showed clear signs of alteration. $\delta^{18}O$ and Δ_{47} compositions of these planktic tests both yield SSTs that are cooler than expected. The cool bias appears to be most pronounced at tropical Site 1260, and less so at mid-latitude Sites 1050 and 1263. This finding is consistent with our end-member mixing model results, which indicate that the susceptibility of planktic isotopic signatures to post-depositional alteration (neomorphism and cementation) is most visible in the tropics (where the seafloor temperatures under which diagenetic alteration occurs are most different from those of the overlying surface ocean where the planktic foraminifera lived). We furthermore find that diagenetic overprinting of primary Δ_{47} signals can be partially mitigated by non-linear Δ_{47} mixing effects, with the extent of this mitigating effect ranging from negligible to substantial depending on the setting and extent of overprinting. $\delta^{18}O$ and Δ_{47} compositions of the well-preserved planktic foraminiferal tests from the clay-rich sediments at Sites 1408, 1409 and 1410 located on Newfoundland Rise yield SST values with minimal impact of diagenetic alteration, despite slightly different burial histories.

In summary, we show that benthic foraminifera from deep-sea sediments and well preserved planktic foraminifera from clay-rich sediments may be used for $\delta^{18}O$- and Δ_{47}-based ocean temperature reconstructions, whereas SST reconstructions from planktic foraminiferal tests deposited in carbonate-rich settings can be compromised by diagenetic alteration, particularly in the tropics. We do not observe additional diagenetic effects altering Δ_{47} values beyond the effect of adding/replacing calcite at temperatures encountered in the deep-sea at the sites studied here. Rather, Δ_{47}-based SSTs are found to be similarly susceptible to diagenesis as those based on $\delta^{18}O$, with differences mostly depending on pore water chemistry and the amount of secondary inorganic calcite in a foraminiferal test. In the future, a means of estimating the percentage of inorganic calcite in fossil foraminiferal tests (e.g., by EBSD) would enable correction of planktic foraminiferal Δ_{47} (and to a lesser extent $\delta^{18}O$) signatures for post-depositional alteration, based on benthic Δ_{47} values and the modeling approach shown in this study. This approach offers paleoceanographers the potential to derive more accurate SST values from diagenetically altered planktic foraminifera.

ACKNOWLEDGEMENTS

We thank Pål Tore Mørkved, Enver Alagoz, Irene Heggstad, Andreas Rasmussen and Ulrike Proske for laboratory assistance, David De Vleeschouwer, Sevasti Modestou, Niklas Meinicke, Lisa Griem, Alvaro Fernandez Bremer, Joep van Dijk, Christina Ravelo and Reinhard Kozdon for insightful discussions as well as Pincelli M. Hull for discussions and sharing sample material from Site 1408. We also thank three reviewers and the associate editor for constructive comments that helped to improve the manuscript. This research used data and samples provided by the International Ocean Discovery Program (IODP). IODP is sponsored by the US National Science Foundation (NSF) and participating countries. This work was funded by the European Research Council (ERC) under the European Union's Horizon 2020 research and innovation programme (grant agreement No 638467) and by the Bergen Research Foundation. P.F.S. received support from a NERC grant (grant number NE/P019331). A.T. received support from the United States Department of Energy through a BES grant (grant number DE-FG02-13ER16402). The data from this study are archived in the supporting information.

APPENDIX A. SUPPLEMENTARY MATERIAL

Supplementary data to this article can be found online at https://doi.org/10.1016/j.gca.2019.05.005.

REFERENCES

Bemis B. E., Spero H. J., Bijma J. and Lea D. W. (1998) Reevaluation of the oxygen isotopic composition of planktonic foraminifera: Experimental results and revised paleotemperature equations. *Paleoceanography* **13**, 150–160.

Berger W. H. (1973) Deep-sea carbonates: pleistocene dissolution cycles. *J. Foramin. Res.* **3**, 187–195.

Bernasconi S. M., Müller I. A., Bergmann K. D., Breitenbach S. F. M., Fernandez A., Hodell D. A., Jaggi M., Meckler A. N., Millan I. and Ziegler M. (2018) Reducing uncertainties in carbonate clumped isotope analysis through consistent carbonate-based standardization. *Geochem. Geophys. Geosyst.* **19**, 2895–2914.

Boulila S., Vahlenkamp M., De Vleeschouwer D., Laskar J., Yamamoto Y., Pälike H., Kirtland Turner S., Sexton P. F., Westerhold T. and Röhl U. (2018) Towards a robust and consistent middle Eocene astronomical timescale. *Earth Planet. Sci. Lett.* **486**, 94–107.

Boyle P. R., Romans B. W., Tucholke B. E., Norris R. D., Swift S. A. and Sexton P. F. (2017) Cenozoic North Atlantic deep circulation history recorded in contourite drifts, offshore Newfoundland, Canada. *Mar. Geol.* **385**, 185–203.

Breitenbach S. F. M., Mleneck-Vautravers M. J., Grauel A.-L., Lo L., Bernasconi S. M., Müller I. A., Rolfe J., Gázquez F., Greaves M. and Hodell D. A. (2018) Coupled Mg/Ca and clumped isotope analyses of foraminifera provide consistent water temperatures. *Geochim. Cosmochim. Acta* **236**, 283–296.

Brown S. J. and Elderfield H. (1996) Variations in Mg/Ca and Sr/Ca ratios of planktonic foraminifera caused by postdepositional dissolution: Evidence of shallow Mg-dependent dissolution. *Paleoceanography* **11**, 543–551.

Cramer B. S., Miller K. G., Barrett P. J. and Wright J. D. (2011) Late Cretaceous-Neogene trends in deep ocean temperature and continental ice volume: Reconciling records of benthic foraminiferal geochemistry ($\delta^{18}O$ and Mg/Ca) with sea level history. *J. Geophys. Res.-Oceans* **116**, 1–23.

Crowley T. J. and Zachos J. C. (1999) Comparison of zonal temperature profiles for past warm time periods. In *Warm Climates in Earth History* (eds. B. Huber, K. Macleod and S. Wing). Cambridge University Press, New York, pp. 50–76.

Defliese W. F. and Lohmann K. C. (2015) Non-linear mixing effects on mass-47 CO_2 clumped isotope thermometry: Patterns and implications. *Rapid Commun. Mass Spectrom.* **29**, 901–909.

Delaney M. L. (1989) Temporal Changes in Interstitial Water Chemistry and Calcite Recrystallization in Marine Sediments. *Earth Planet. Sci. Lett.* **95**, 23–37.

Dhondt S. and Arthur M. A. (1996) Late cretaceous oceans and the cool tropic paradox. *Science* **271**, 1838–1841.

Douglas P. M. J., Affek H. P., Ivany L. C., Houben A. J. P., Sijp W. P., Sluijs A., Schouten S. and Pagani M. (2014) Pronounced zonal heterogeneity in Eocene southern high-latitude sea surface temperatures. *PNAS* **111**, 6582–6587.

Edgar K. M., Anagnostou E., Pearson P. N. and Foster G. L. (2015) Assessing the impact of diagenesis on $\delta^{11}B$, $\delta^{13}C$, $\delta^{18}O$, Sr/Ca and B/Ca values in fossil planktic foraminiferal calcite. *Geochim. Cosmochim. Acta* **166**, 189–209.

Edgar K. M., Pälike H. and Wilson P. A. (2013) Testing the impact of diagenesis on the $\delta^{18}O$ and $\delta^{13}C$ of benthic foraminiferal calcite from a sediment burial depth transect in the equatorial Pacific. *Paleoceanography* **28**, 468–480.

Edgar K. M., Wilson P. A., Sexton P. F. and Suganuma Y. (2007) No extreme bipolar glaciation during the main Eocene calcite compensation shift. *Nature* **448**, 908–911.

Eiler J. M. and Schauble E. (2004) $^{18}O^{13}C^{16}O$ in Earth's atmosphere. *Geochim. Cosmochim. Acta* **68**, 4767–4777.

Erbacher, J., Mosher, D.C., Malone, M.J. and the Expedition 207 Scientists (2004) Site 1260, Proceedings of the Ocean Drilling Program, Initial Reports Volume 207, pp. 1–113.

Evans D., Sagoo N., Renema W., Cotton L. J., Muller W., Todd J. A., Saraswati P. K., Stassen P., Ziegler M., Pearson P. N., Valdes P. J. and Affek H. P. (2018) Eocene greenhouse climate revealed by coupled clumped isotope-Mg/Ca thermometry. *PNAS* **115**, 1174–1179.

Fantle M. S. and DePaolo D. J. (2007) Ca isotopes in carbonate sediment and pore fluid from ODP Site 807A: The Ca^{2+}(aq)-calcite equilibrium fractionation factor and calcite recrystallization rates in Pleistocene sediments. *Geochim. Cosmochim. Acta* **71**, 2524–2546.

Fernandez A., Müller I. A., Rodríguez-Sanz L., van Dijk J., Looser N. and Bernasconi S. M. (2017) A reassessment of the precision of carbonate clumped isotope measurements: implications for calibrations and paleoclimate reconstructions. *Geochem. Geophys. Geosyst.* **18**, 4375–4386.

Ghosh P., Adkins J., Affek H., Balta B., Guo W., Schauble E. A., Schrag D. and Eiler J. M. (2006) ^{13}C–^{18}O bonds in carbonate minerals: A new kind of paleothermometer. *Geochim. Cosmochim. Acta* **70**, 1439–1456.

Golreihan A., Steuwe C., Woelders L., Deprez A., Fujita Y., Vellekoop J., Swennen R. and Roeffaers M. B. J. (2018) Improving preservation state assessment of carbonate microfossils in paleontological research using label-free stimulated Raman imaging. *PLoS ONE* **13**, 1–15.

Grauel A. L., Schmid T. W., Hu B., Bergami C., Capotondi L., Zhou L. and Bernasconi S. M. (2013) Calibration and application of the 'clumped isotope' thermometer to foraminifera for high resolution climate reconstructions. *Geochim. Cosmochim. Acta* **108**, 125–140.

Henkes G. A., Passey B. H., Grossman E. L., Shenton B. J., Perez-Huerta A. and Yancey T. E. (2014) Temperature limits for preservation of primary calcite clumped isotope paleotemperatures. *Geochim. Cosmochim. Acta* **139**, 362–382.

Henkes G. A., Passey B. H., Grossman E. L., Shenton B. J., Yancey T. E. and Perez-Huerta A. (2018) Temperature evolution and the oxygen isotope composition of Phanerozoic oceans from carbonate clumped isotope thermometry. *Earth Planet. Sci. Lett.* **490**, 40–50.

Hill P. S., Tripati A. K. and Schauble E. A. (2014) Theoretical constraints on the effects of pH, salinity, and temperature on clumped isotope signatures of dissolved inorganic carbon species and precipitating carbonate minerals. *Geochim. Cosmochim. Acta* **125**, 610–652.

Hines B. R., Hollis C. J., Atkins C. B., Baker J. A., Morgans H. E. G. and Strong P. C. (2017) Reduction of oceanic temperature gradients in the early Eocene Southwest Pacific Ocean. *Palaeogeogr. Palaeoclimatol. Palaeoecol.* **475**, 41–54.

Hu B., Radke J., Schlüter H. J., Heine F. T., Zhou L. and Bernasconi S. M. (2014) A modified procedure for gas-source isotope ratio mass spectrometry: the long-integration dual-inlet (LIDI) methodology and implications for clumped isotope measurements. *Rapid Commun. Mass Spectrom.* **28**, 1413–1425.

Hull, P.M., Bohaty, S.M., Cameron, A., Coxall, H.K., D'haenens, S., De Vleeschouwer, D., Elder, L.E., Friedrich, O., Kerr, K., Turner, S.K., Kordesch, W.E.C., Moriya, K., Norris, R.D., Opdyke, B.N., Penman, D.E., Pälike, H., Wilson, P.A., Sexton, P.F., Vahlenkamp, M., Wu, F. and Zachos, J.C., 2017. Data report: coarse fraction record for the Eocene megasplice at IODP Sites U1406, U1408, U1409, and U1411, Norris, R.D., Wilson, P.A., Blum, P., and the Expedition 342 Scientists, Proc. IODP, 342: College Station, TX (Integrated Ocean Drilling Program).

Huntington K. W., Eiler J. M., Affek H. P., Guo W., Bonifacie M., Yeung L. Y., Thiagarajan N., Passey B. H., Tripati A. K., Daeron M. and Came R. (2009) Methods and limitations of 'clumped' CO_2 isotope (Δ_{47}) analysis by gas-source isotope ratio mass spectrometry. *J. Mass Spectrom.* **44**, 1318–1329.

John C. M. and Bowen D. (2016) Community software for challenging isotope analysis: First applications of 'Easotope' to clumped isotopes. *Rapid Commun. Mass Spectrom.* **30**, 2285–2300.

Katz M. E., Katz D. R., Wright J. D., Miller K. G., Pak D. K., Shackleton N. J. and Thomas E. (2003) Early Cenozoic benthic foraminiferal isotopes: Species reliability and interspecies correction factors. *Paleoceanography* **18**.

Kele S., Breitenbach S. F. M., Capezzuoli E., Meckler A. N., Ziegler M., Millan I. M., Kluge T., Deák J., Hanselmann K., John C. M., Yan H., Liu Z. and Bernasconi S. M. (2015) Temperature dependence of oxygen- and clumped isotope fractionation in carbonates: A study of travertines and tufas in the 6–95 °C temperature range. *Geochim. Cosmochim. Acta* **168**, 172–192.

Killingley J. S. (1983) Effects of diagenetic recrystallization on $^{18}O/^{16}O$ values of deep-sea sediments. *Nature* **301**, 594–597.

Kim S. T. and O'Neil J. R. (1997) Equilibrium and nonequilibrium oxygen isotope effects in synthetic carbonates. *Geochim. Cosmochim. Acta* **61**, 3461–3475.

Kozdon R., Kelly D. C., Kita N. T., Fournelle J. H. and Valley J. W. (2011) Planktonic foraminiferal oxygen isotope analysis by

ion microprobe technique suggests warm tropical sea surface temperatures during the Early Paleogene. *Paleoceanography* **26**.

Kozdon R., Kelly D. C., Kitajima K., Strickland A., Fournelle J. H. and Valley J. W. (2013) In situ $\delta^{18}O$ and Mg/Ca analyses of diagenetic and planktic foraminiferal calcite preserved in a deep-sea record of the Paleocene-Eocene thermal maximum. *Paleoceanography* **28**, 517–528.

Laskar J., Fienga A., Gastineau M. and Manche H. (2011a) La2010: a new orbital solution for the long-term motion of the Earth. *Astron. Astrophys.* **532**.

Laskar J., Gastineau M., Delisle J.-B., Farrés A. and Fienga A. (2011b) Strong chaos induced by close encounters with Ceres and Vesta. *Astron. Astrophys.* **532**.

Laskar J., Robutel P., Joutel F., Gastineau M., Correia A. C. M. and Levrard B. (2004) A long-term numerical solution for the insolation quantities of the Earth. *Astron. Astrophys.* **428**, 261–285.

Lear Caroline H., Mawbey Elaine M. and Rosenthal Yai (2010) Cenozoic benthic foraminiferal Mg/Ca and Li/Ca records: Toward unlocking temperatures and saturation states. *Paleoceanography* **25**.

Locarnini, R.A., Mishonov, A.V., Antonov, J.I., Boyer, T.P., Garcia, H.E., Baranova, O.K., Zweng, M.M., Paver, C.R., Reagan, J.R., Johnson, D.R., Hamilton, M., Seidov, D., 2013. World Ocean Atlas 2013, Volume 1: Temperature. S. Levitus, Ed., A. Mishonov Technical Ed. NOAA Atlas NESDIS 73, 40.

Meckler A. N., Ziegler M., Millan M. I., Breitenbach S. F. M. and Bernasconi S. M. (2014) Long-term performance of the Kiel carbonate device with a new correction scheme for clumped isotope measurements. *Rapid Commun. Mass Spectrom.* **28**, 1705–1715.

Müller I. A., Fernandez A., Radke J., van Dijk J., Bowen D., Schwieters J. and Bernasconi S. M. (2017) Carbonate clumped isotope analyses with the long-integration dual-inlet (LIDI) workflow: scratching at the lower sample weight boundaries. *Rapid Commun. Mass Spectrom.* **31**, 1057–1066.

Norris, R.D., Kroon, D., Klaus, A. and the Expedition 171B Scientists (1998) Site 1050, Proceedings of the Ocean Drilling Program, Initial Reports, vol. 171B, pp. 93–169.

Norris, R.D., Wilson, P.A., Blum, P. and the Expedition 342 Scientists (2014a) Site U1408, Proceedings of the Integrated Ocean Drilling Program, volume 342, pp. 1–91.

Norris, R.D., Wilson, P.A., Blum, P. and the Expedition 342 Scientists (2014b) Site U1409, Proceedings of the Integrated Ocean Drilling Program, vol. 342, pp. 1–104.

Norris, R.D., Wilson, P.A., Blum, P. and the Expedition 342 Scientists (2014c) Site U1410, Proceedings of the Integrated Ocean Drilling Program, vol. 342, pp. 1–87.

Ogg J. G. (2012) Chapter 5 – Geomagnetic Polarity Time Scale. In *The Geologic Time Scale* (eds. F. M. Gradstein, J. G. Ogg, M. D. Schmitz and G. M. Ogg). Elsevier, Boston, pp. 85–113.

Ogg, J.G., Bardot, L., 2001. Aptian through Eocene magnetostratigraphic correlation of the Blake Nose Transect (Leg 171B), Florida continental margin, Kroon, D., Norris, R.D., Klaus, A., and the Expedition 171B Scientists, Proc. ODP, 171B, pp. 1–58.

Passey B. H. and Henkes G. A. (2012) Carbonate clumped isotope bond reordering and geospeedometry. *Earth Planet. Sci. Lett.* **351**, 223–236.

Pearson P. N. and Burgess C. E. (2008) Foraminifer test preservation and diagenesis: Comparison of high latitude Eocene sites. *Geol. Soc. Lond. Spec. Publ.* **303**, 59–72.

Pearson P. N., Ditchfield P. W., Singano J., Harcourt-Brown K. G., Nicholas C. J., Olsson R. K., Shackleton N. J. and Hall M. A. (2001) Warm tropical sea surface temperatures in the Late Cretaceous and Eocene epochs. *Nature* **414**, 481–487.

Pearson P. N., Olsson R. K., Huber B. T., Hemleben C., Berggren W. A. and Coxall H. K. (2006) Overview of Eocene Planktonic foraminiferal taxonomy, paleoecology, phylogeny, and biostratigraphy. *Cushman Found. Foraminiferal Res.*, 41.

Peral M., Daëron M., Blamart D., Bassinot F., Dewilde F., Smialkowski N., Isguder G., Bonnin J., Jorissen F., Kissel C., Michel E., Vázquez Riveiros N. and Waelbroeck C. (2018) Updated calibration of the clumped isotope thermometer in planktonic and benthic foraminifera. *Geochim. Cosmochim. Acta* **239**, 1–16.

Piasecki A., Bernasconi S. M., Grauel A. L., Hannisdal B., Ho S. L., Leutert T. J., Marchitto T. M., Meinicke N., Tisserand A. and Meckler A. N. (2019) Application of clumped isotope thermometry to benthic foraminifera. *Geochem. Geophys., Geosyst.* **20**.

Roberts C. D., LeGrande A. N. and Tripati A. K. (2011) Sensitivity of seawater oxygen isotopes to climatic and tectonic boundary conditions in an early Paleogene simulation with GISS ModelE-R. *Paleoceanography* **26**.

Rodríguez-Sanz L., Bernasconi S. M., Marino G., Heslop D., Müller I. A., Fernandez A., Grant K. M. and Rohling E. J. (2017) Penultimate deglacial warming across the Mediterranean Sea revealed by clumped isotopes in foraminifera. *Sci. Rep.* **7**.

Rudnicki M. D., Wilson P. A. and Anderson W. T. (2001) Numerical models of diagenesis, sediment properties, and pore fluid chemistry on a paleoceanographic transect: Blake Nose, Ocean Drilling Program Leg 171B. *Paleoceanography* **16**, 563–575.

Schauble E. A., Ghosh P. and Eiler J. M. (2006) Preferential formation of ^{13}C–^{18}O bonds in carbonate minerals, estimated using first-principles lattice dynamics. *Geochim. Cosmochim. Acta* **70**, 2510–2529.

Schmid T. W. and Bernasconi S. M. (2010) An automated method for 'clumped-isotope' measurements on small carbonate samples. *Rapid Commun. Mass Spectrom.* **24**, 1955–1963.

Schrag D. P. (1999) Effects of diagenesis on the isotopic record of late paleogene tropical sea surface temperatures. *Chem. Geol.* **161**, 215–224.

Sexton P. F., Norris R. D., Wilson P. A., Pälike H., Westerhold T., Röhl U., Bolton C. T. and Gibbs S. (2011) Eocene global warming events driven by ventilation of oceanic dissolved organic carbon. *Nature* **471**, 349–352.

Sexton P. F. and Wilson P. A. (2009) Preservation of benthic foraminifera and reliability of deep-sea temperature records: Importance of sedimentation rates, lithology, and the need to examine test wall structure. *Paleoceanography* **24**.

Sexton P. F., Wilson P. A. and Norris R. D. (2006a) Testing the Cenozoic multisite composite $\delta^{18}O$ and $\delta^{13}C$ curves: New monospecific Eocene records from a single locality, Demerara Rise (Ocean Drilling Program Leg 207). *Paleoceanography* **21**.

Sexton P. F., Wilson P. A. and Pearson P. N. (2006b) Microstructural and geochemical perspectives on planktic foraminiferal preservation: "Glassy" versus "Frosty". *Geochem. Geophys. Geosyst.* **7**.

Sexton P. F., Wilson P. A. and Pearson P. N. (2006c) Palaeoecology of late middle Eocene planktic foraminifera and evolutionary implications. *Mar. Micropaleontol.* **60**, 1–16.

Shenton B. J., Grossman E. L., Passey B. H., Henkes G. A., Becker T. P., Laya J. C., Perez-Huerta A., Becker S. P. and Lawson M. (2015) Clumped isotope thermometry in deeply buried sedimentary carbonates: The effects of bond reordering and recrystallization. *Geol. Soc. Am. Bull.* **127**, 1036–1051.

Stolper D. A., Eiler J. M. and Higgins J. A. (2018) Modeling the effects of diagenesis on carbonate clumped-isotope values in deep- and shallow-water settings. *Geochim. Cosmochim. Acta* **227**, 264–291.

Thiagarajan N., Adkins J. and Eiler J. M. (2011) Carbonate clumped isotope thermometry of deep-sea corals and implications for vital effects. *Geochim. Cosmochim. Acta* **75**, 4416–4425.

Torsvik T. H., Van der Voo R., Preeden U., Mac Niocaill C., Steinberger B., Doubrovine P. V., van Hinsbergen D. J. J., Domeier M., Gaina C., Tohver E., Meert J. G., McCausland P. J. A. and Cocks L. R. M. (2012) Phanerozoic polar wander, palaeogeography and dynamics. *Earth Sci. Rev.* **114**, 325–368.

Tripati, A., Vollmer, T., Perez-Huerta, A., 2017. A Quantitative Solution for the 'Cool Tropics' Paradox of Past Greenhouse Climates: Testing Diagenetic Hypotheses Combining Clumped Isotope and Electron Backscatter Diffraction Data on Foraminifera Goldschmidt Abstracts 3992.

Tripati A. K., Delaney M. L., Zachos J. C., Anderson L. D., Kelly D. C. and Elderfield H. (2003) Tropical sea-surface temperature reconstruction for the early Paleogene using Mg/Ca ratios of planktonic foraminifera. *Paleoceanography* **18**.

Tripati A. K., Eagle R. A., Thiagarajan N., Gagnon A. C., Bauch H., Halloran P. R. and Eiler J. M. (2010) ^{13}C–^{18}O isotope signatures and 'clumped isotope' thermometry in foraminifera and coccoliths. *Geochim. Cosmochim. Acta* **74**, 5697–5717.

Tucholke, B.E., Vogt, P.R., 1979. Western North Atlantic: sedimentary evolution and aspects of tectonic history. In: Tucholke, B.E., Vogt, P.R., et al., Init. Repts. DSDP, 43: Washington, DC (U.S. Govt. Printing Office), pp. 791–825.

van Hinsbergen D. J. J., de Groot L. V., van Schaik S. J., Spakman W., Bijl P. K., Sluijs A., Langereis C. G. and Brinkhuis H. (2015) A paleolatitude calculator for paleoclimate studies. *PLoS ONE* **10**, 1–21.

Vandenberghe N., Hilgen F. J., Speijer R. P., Ogg J. G., Gradstein F. M., Hammer O., Hollis C. J. and Hooker J. J. (2012) Chapter 28 – The Paleogene Period. In *The Geologic Time Scale* (eds. F. M. Gradstein, J. G. Ogg, M. D. Schmitz and G. M. Ogg). Elsevier, Boston, pp. 855–921.

Voigt J., Hathorne E. C., Frank M. and Holbourn A. (2016) Minimal influence of recrystallization on middle Miocene benthic foraminiferal stable isotope stratigraphy in the eastern equatorial Pacific. *Paleoceanography* **31**, 98–114.

Watkins J. M., Hunt J. D., Ryerson F. J. and DePaolo D. J. (2014) The influence of temperature, pH, and growth rate on the $\delta^{18}O$ composition of inorganically precipitated calcite. *Earth Planet. Sci. Lett.* **404**, 332–343.

Watkins J. M., Nielsen L. C., Ryerson F. J. and DePaolo D. J. (2013) The influence of kinetics on the oxygen isotope composition of calcium carbonate. *Earth Planet. Sci. Lett.* **375**, 349–360.

Westerhold T. and Röhl U. (2013) Orbital pacing of Eocene climate during the Middle Eocene Climate Optimum and the chron C19r event: Missing link found in the tropical western Atlantic. *Geochem. Geophys. Geosyst.* **14**, 4811–4825.

Westerhold T., Röhl U., Frederichs T., Bohaty S. M. and Zachos J. C. (2015) Astronomical calibration of the geological timescale: closing the middle Eocene gap. *Clim. Past* **11**, 1181–1195.

Wilson P. A. and Opdyke B. N. (1996) Equatorial sea-surface temperatures for the Maastrichtian revealed through remarkable preservation of metastable carbonate. *Geology* **24**, 555–558.

Zachos J. C., Dickens G. R. and Zeebe R. E. (2008) An early Cenozoic perspective on greenhouse warming and carbon-cycle dynamics. *Nature* **451**, 279–283.

Zachos, J.C., Kroon, D., Blum, P. and the Expedition 208 Scientists (2004) Site 1263, Proceedings of the Ocean Drilling Program, Initial Reports Volume 208, pp. 1–87.

Zachos J. C., Pagani M., Sloan L., Thomas E. and Billups K. (2001) Trends, rhythms, and aberrations in global climate 65 Ma to present. *Science* **292**, 686–693.

Zachos J. C., Stott L. D. and Lohmann K. C. (1994) Evolution of Early Cenozoic Marine Temperatures. *Paleoceanography* **9**, 353–387.

Associate editor: Jay Quade

Appendix

A.1 Further details on the analysis of clumped isotopes

The mass 47 anomaly is temperature-dependent and forms the basis of the clumped isotope thermometer (Wang et al., 2004; Eiler, 2007). It is reported as:

$$\Delta_{47}\ (‰) = [(R^{47} / R^{47*} - 1) - (R^{46} / R^{46*} - 1) - (R^{45} / R^{45*} - 1)] \times 1000 \quad (A.1)$$

where R^i are the measured ratios of the rare isotopologues with masses 45-47 to the most abundant isotopologue with mass 44. R^{i*} represents the corresponding ratios under stochastic (or random) distribution of the isotopes among all possible isotopologues and is calculated from the measured abundances of ^{13}C and ^{18}O. The measured enrichment of the mass 47 isotopologue is defined as:

$$\delta^{47}\ (‰) = (R^{47}{}_{Sample} / R^{47}{}_{Reference} - 1) \times 1000 \quad (A.2)$$

Sample measurements were done in a randomized manner spanning an extended period of time (November 2016 to February 2018). Mass 44-49 ion beams of sample and reference CO_2 gas were collected in six Faraday cups. We used reference gas from two commercial compressed gas tanks: (1) $\delta^{18}O_{VPDB}$ = -5.38 ‰ and $\delta^{13}C_{VPDB}$ = -4.45 ‰ from October 2016 to October 2017, (2) $\delta^{18}O_{VPDB}$ = -5.61 ‰ and $\delta^{13}C_{VPDB}$ = -3.54 ‰ from October 2017 to March 2018. Samples were reacted with phosphoric acid at 70°C. During a measurement run, the Porapak trap (Schmid et al., 2012) was cooled to -20°C in order to trap contaminants (e.g., Halocarbons, Hydrocarbons), and baked out (120°C) for at least 1 h after each run. The signals of m/z 48 and 49 were monitored to detect possible contamination (e.g., Bernasconi et al., 2013).

For the measuring interval from October 2016 to October 2017, we used the carbonate standards ETH 1, 3 and 4 for correction and the carbonate standard ETH 2 for monitoring. From November 2017 to March 2018, ETH 1, 2 and 3 were utilized for correction and ETH 4 for monitoring. Using the software "Easotope" (John and Bowen, 2016), the measured $\delta^{18}O$ values were corrected for drift using "stretching" based on the three correction standards and a correction interval of 30-40 standard replicates before and after each sample analysis. $\delta^{13}C$ values were also corrected for drift with the same standards, but without stretching. Δ_{47} was corrected for composition (δ^{47})-dependent (negative baseline) and composition-independent (scale compression) mass spectrometer effects using the same three standards. In order to characterize the pressure-sensitive baseline (PBL) on all Faraday cups and determine the dependence of the PBL on the m/z 44 intensity for the other masses, we performed high-voltage peak scans at 5 different m/z 44 signal intensities on a daily basis. The dependence of the PBL on the m/z 44 intensity was then used to do a PBL correction on the raw beam signals accounting for negative baseline/non-linearity effects caused by the formation of secondary electrons (He et al., 2012; Bernasconi et al., 2013; Meckler et al., 2014). The PBL corrected signals were used to calculate $\delta^{18}O_{VPDB}$, $\delta^{13}C_{VPDB}$ and raw Δ_{47} values with the "Brand" isotopic parameters (Brand et al., 2010; Daëron et al., 2016). The empirical transfer function based on the three correction standards corrects for scale compression caused by fragmentation/recombination reactions in the electron ionization impact source and standardizes Δ_{47} data for inter-laboratory comparison (Dennis et al., 2011). Application of the empirical transfer function obtained from the correlation of raw and accepted Δ_{47} values of the three standards converted our Δ_{47} to the absolute

reference frame. For that, we used standard replicate measurements from a correction interval of ±30-40 standards and the accepted standard Δ_{47} values from Bernasconi et al. (2018). Finally, we added an acid fractionation correction of +0.062 ‰ (Defliese et al., 2015) to the Δ_{47} value in the absolute reference frame, in order to transfer our data into a more common acid fractionation framework (from 70°C to 25°C digestion). To account for ^{18}O fractionation during calcite digestion at 70°C, an acid fractionation factor of 1.00871 was applied (Kim et al., 2007).

For the period from October 2016 to October 2017, mean Δ_{47} and external reproducibility (1σ standard deviation) of ETH 2 after correction were 0.2516±0.0334 ‰ (n=901) (Tables S3 and S4). The external reproducibilities of ETH 1, 3 and 4 were ±0.0351 ‰ (n=907), ±0.0325 ‰ (n=911) and ±0.0308 ‰ (n=918), respectively. From November 2017 to March 2018, mean Δ_{47} and external reproducibility of ETH 4 after correction were 0.5145±0.0385 ‰ (n=456), whereas the external reproducibilities of ETH 1, 2 and 3 were ±0.0365 ‰ (n=458), ±0.0340 ‰ (n=402) and ±0.0356 ‰ (n=460), respectively. All standard measurement data are listed in Table S3.

A.2 Δ_{47} end-member calculations

Δ_{47} end-member calculations to derive glassy foraminiferal Δ_{47} were carried out in R. Following the procedure described in Defliese and Lohmann (2015), we calculated δ^{45}, δ^{46} and δ^{47} from Δ_{47}, $\delta^{13}C$ and $\delta^{18}O$ for both frosty foraminiferal calcite (δ^{i}_{frost}) and inorganic calcite (δ^{i}_{diag}, as derived from benthic foraminiferal calcite). For that, we utilized the ^{18}O acid fractionation correction of Kim et al. (2007), the Δ_{47} acid fractionation correction of Defliese et al. (2015), the parameters recommended by Daëron et al. (2016) and the following reference gas: $\delta^{18}O_{VPDB}$ = -5.38 ‰ and

$\delta^{13}C_{VPDB}$ = -4.45 ‰ (all clumped isotope measurements included in the non-linear mixing calculations were measured with the same reference gas).

In a CO_2 mixture, end-members of different isotopic composition have been shown to mix linearly with respect to δ^{45}, δ^{46} and δ^{47} (e.g., Affek and Eiler, 2006; Defliese and Lohmann, 2015). Therefore, we used a simple linear mixing equation to derive glassy foraminiferal δ^i values (δ^i_{glassy}):

$$\delta^i_{glassy} = (\delta^i_{frosty} - F_{diag} \times \delta^i_{diag}) / (1 - F_{diag}) \quad (A.3)$$

Glassy foraminiferal Δ_{47} was then calculated from glassy foraminiferal δ^{45}, δ^{46} and δ^{47}. This necessitates the estimation of a hypothetical ETF slope and intercept for glassy calcite. For each calculation, we assumed that the ETF slope from the clumped isotope measurement on frosty material represents the mean (weighted with the fraction of diagenetic calcite) of the hypothetical glassy calcite ETF slope and the ETF slope of the benthic clumped isotope measurement that was used to approximate diagenetic inorganic calcite. Accordingly, a mean glassy calcite ETF slope was calculated from the mean ETF slopes of the measurements on frosty and benthic foraminifera. The same approach was applied to the ETF intercept. Code in R format is provided upon request.

References

Affek, H. and Eiler, J. (2006) Abundance of mass 47 CO_2 in urban air, car exhaust, and human breath. *Geochimica et Cosmochimica Acta* **70,** 1-12.

Bernasconi, S.M., Hu, B., Wacker, U., Fiebig, J., Breitenbach, S.F.M. and Rutz, T. (2013) Background effects on Faraday collectors in gas-source mass spectrometry and implications for clumped isotope measurements. *Rapid Communications in Mass Spectrometry* **27,** 603-612.

Bernasconi, S.M., Müller, I.A., Bergmann, K.D., Breitenbach, S.F.M., Fernandez, A., Hodell, D.A., Jaggi, M., Meckler, A.N., Millan, I. and Ziegler, M. (2018) Reducing uncertainties in carbonate clumped isotope analysis through consistent carbonate-based standardization. *Geochemistry, Geophysics, Geosystems* **19,** 2895-2914.

Brand, W.A., Assonov, S.S. and Coplen, T.B. (2010) Correction for the ^{17}O interference in $\delta^{13}C$ measurements when analyzing CO_2 with stable isotope mass spectrometry (IUPAC Technical Report). *Pure and Applied Chemistry* **82,** 1719-1733.

Daëron, M., Blamart, D., Peral, M. and Affek, H.P. (2016) Absolute isotopic abundance ratios and the accuracy of Δ_{47} measurements. *Chemical Geology* **442,** 83-96.

Defliese, W.F., Hren, M.T. and Lohmann, K.C. (2015) Compositional and temperature effects of phosphoric acid fractionation on Δ_{47} analysis and implications for discrepant calibrations. *Chemical Geology* **396,** 51-60.

Defliese, W.F. and Lohmann, K.C. (2015) Non-linear mixing effects on mass-47 CO_2 clumped isotope thermometry: Patterns and implications. *Rapid Communications in Mass Spectrometry* **29,** 901-909.

Dennis, K.J., Affek, H.P., Passey, B.H., Schrag, D.P. and Eiler, J.M. (2011) Defining an absolute reference frame for 'clumped' isotope studies of CO_2. *Geochimica et Cosmochimica Acta* **75,** 7117-7131.

Eiler, J.M. (2007) “Clumped-isotope” geochemistry—The study of naturally-occurring, multiply-substituted isotopologues. *Earth and Planetary Science Letters* **262,** 309-327.

He, B., Olack, G.A. and Colman, A.S. (2012) Pressure baseline correction and high-precision CO_2 clumped-isotope (Δ_{47}) measurements in bellows and micro-volume modes. *Rapid Communications in Mass Spectrometry* **26,** 2837-2853.

John, C.M. and Bowen, D. (2016) Community software for challenging isotope analysis: First applications of ‘Easotope' to clumped isotopes. *Rapid Communications in Mass Spectrometry* **30,** 2285-2300.

Kim, S.T., Mucci, A. and Taylor, B.E. (2007) Phosphoric acid fractionation factors for calcite and aragonite between 25 and 75 ˚C: Revisited. *Chemical Geology* **246,** 135-146.

Meckler, A.N., Ziegler, M., Millan, M.I., Breitenbach, S.F.M. and Bernasconi, S.M. (2014) Long-term performance of the Kiel carbonate device with a new correction scheme for clumped isotope measurements. *Rapid Communications in Mass Spectrometry* **28,** 1705-1715.

Schmid, T.W., Radke, J. and Bernasconi, S.M. (2012) Clumped-isotope measurements on small carbonate samples with a Kiel IV carbonate device and a MAT 253 mass spectrometer. *Thermo Fisher Application Note*.

Wang, Z., Schauble, E.A. and Eiler, J.M. (2004) Equilibrium thermodynamics of multiply substituted isotopologues of molecular gases. *Geochimica et Cosmochimica Acta* **68,** 4779-4797.

Supplementary figures

Sensitivity of clumped isotope temperatures in fossil benthic and planktic foraminifera to diagenetic alteration

Thomas J. Leutert[a]*, Philip F. Sexton[b], Aradhna Tripati[c,d], Alison Piasecki[a,e], Sze Ling Ho[a,f] and A. Nele Meckler[a]

[a]Bjerknes Centre for Climate Research and Department of Earth Science, University of Bergen, 5007 Bergen, Norway

[b]School of Environment, Earth & Ecosystem Sciences, The Open University, Milton Keynes MK7 6AA, UK

[c]Department of Earth, Planetary, and Space Sciences, Department of Atmospheric and Oceanic Sciences, Institute of the Environment and Sustainability, Center for Diverse Leadership in Science, University of California, Los Angeles, CA 90095, USA

[d]European Institute of Marine Sciences (IUEM), Université de Brest, UMR 6538, Domaines Océaniques, Rue Dumont D'Urville, and IFREMER, Laboratoire Géophysique et enregistrement Sédimentaire, 29280 Plouzané, France

[e]Department of Earth and Planetary Sciences, Harvard University, Cambridge, MA 02138, USA

[f]Institute of Oceanography, National Taiwan University, 10617 Taipei, Taiwan

Contents: 33 pages, 18 figures and captions

*Corresponding author:

E-mail: Thomas.Leutert@uib.no

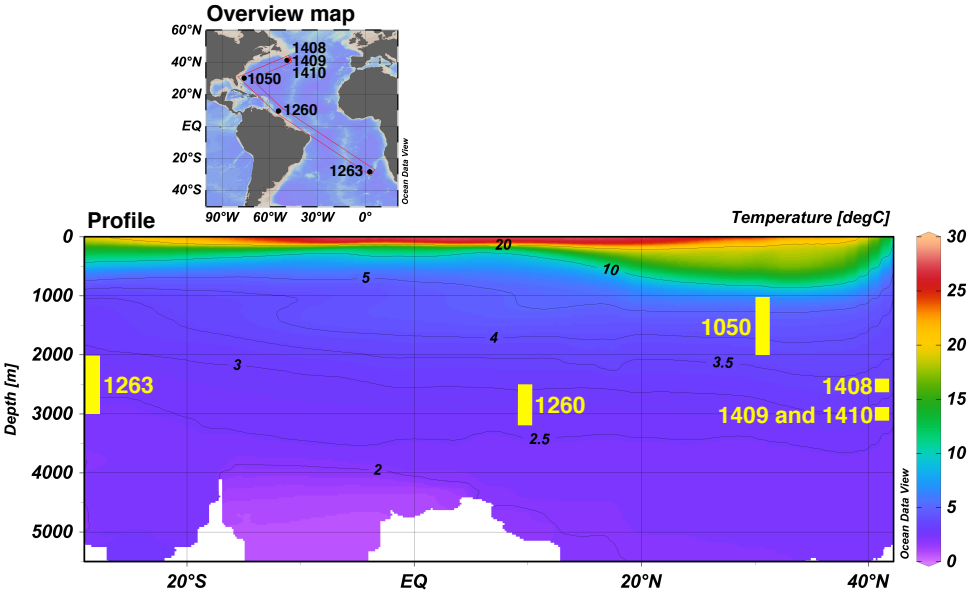

Fig. S1: Modern (1955-2012) mean annual temperature cross profile through all study sites. Estimated paleodepth ranges (Table 1) are marked in yellow. We analysed benthic foraminiferal material from Sites 1409, 1260 and 1263. At these sites, mean annual bottom water temperatures in the modern Atlantic Ocean range between around 2.5-3.5 °C, supporting our assumption of similar temperatures during benthic foraminiferal calcification. This figure was created using Ocean Data View (ODV) with temperature data from the World Ocean Atlas 2013 (Locarnini et al., 2013).

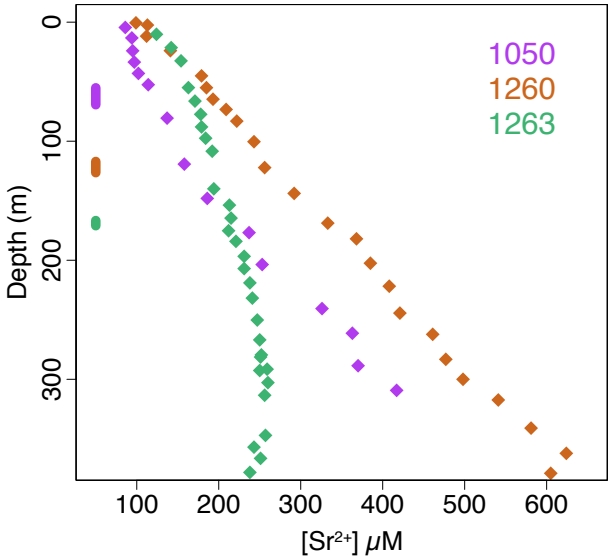

Fig. S2: Comparison of pore fluid Sr^{2+} profiles at Sites 1050 (Norris et al., 1998), 1260 (Erbacher et al., 2004) and 1263 (Zachos et al., 2004). At Sites 1408, 1409 and 1410, pore fluid Sr^{2+} concentrations were not measured. Pore fluid Sr^{2+} is traditionally used as an indicator of diagenetic alteration, as dissolution and reprecipitation processes expel strontium in the coexisting pore fluids (e.g., Baker et al., 1982; Schrag et al., 1995). Sites 1050, 1260 and 1263 all show increases in pore fluid [Sr^{2+}] with depth in the sampling intervals. The observed increases with depth may be symptomatic for ongoing diagenetic alteration. However, this interpretation of Sr^{2+} profiles in terms of diagenetic alteration is complicated by upward Sr^{2+} diffusion from the basement, making it difficult to draw firm conclusions about the extent of diagenetic alteration of foraminiferal calcites (e.g., Edgar et al., 2013). Sample depth ranges at Sites 1050, 1260 and 1263 are shown by vertical lines. Our stable isotopic compositions as well as pore fluid Sr^{2+} values from Site 1050 were measured on the

sediments of Hole A. Therefore, pore fluid Sr^{2+} values are plotted against Hole A depth (Norris et al., 1998), whereas the pore fluid Sr^{2+} values at Sites 1260 and 1263 are plotted against the respective shipboard composite depths (Erbacher et al., 2004; Zachos et al., 2004).

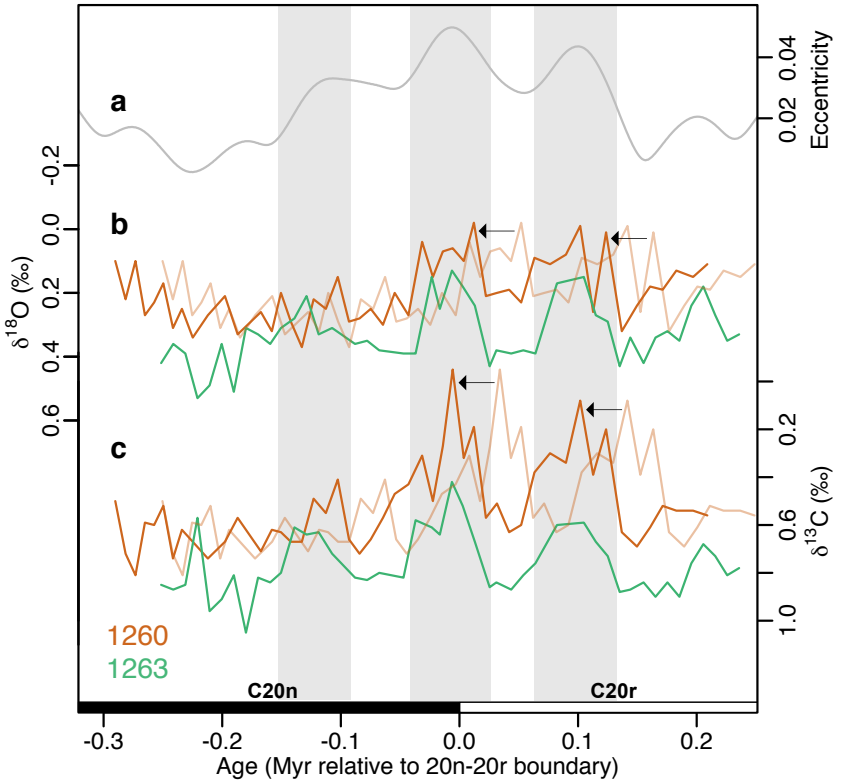

Fig. S3: (a) Eccentricity of orbital solution La2010d (Laskar et al., 2011) as well as benthic foraminiferal (b) $\delta^{18}O$ and (c) $\delta^{13}C$. In case of Site 1260, the semitransparent curves represent the age model of Westerhold and Röhl (2013), whereas the nontransparent curves the age model of this study. The agreement in both $\delta^{18}O$ and $\delta^{13}C$ between Site 1260 and 1263 as well as between Site 1260 and eccentricity is significantly improved by shifting the Site 1260-age model of Westerhold and Röhl (2013) 40 kyr forward in time. Lines are based on one measurement at each depth.

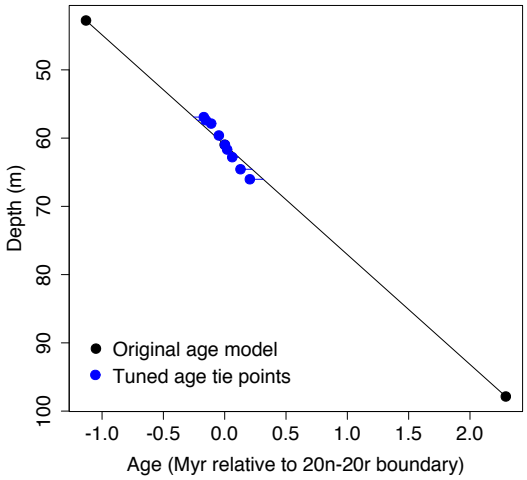

Fig. S4: Tuned age points used for linear interpolation at Site 1409 (blue) in comparison to the magnetochron boundary-based age model using GTS2012 (black) (Ogg, 2012; Vandenberghe et al., 2012). $\delta^{13}C$ increases and decreases at Site 1409 were tuned to those at Site 1263, using the software AnalySeries 2.0 (Paillard et al., 1996). Tuning depths can be found in Table S1.

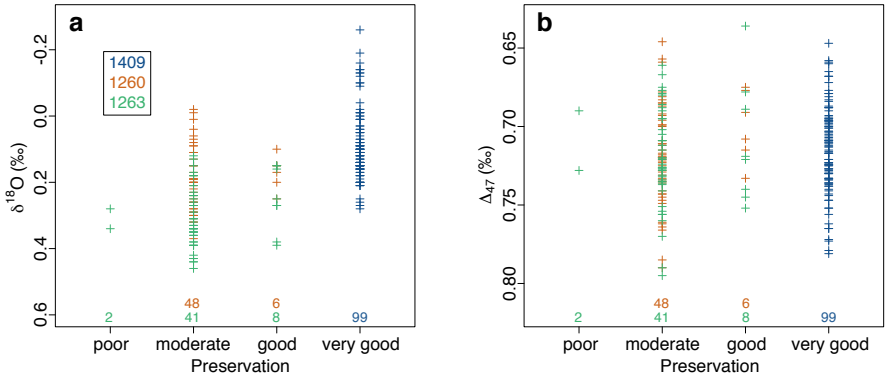

Preservation classes for benthic foraminifera

poor: moderate to extensive recrystallization visible, abundant overgrowth of large inorganic calcite crystals and/or signs of major dissolution

moderate: no to minor recrystallization, increased inorganic calcite overgrowth and/or signs of dissolution

good: no visible recrystallization, limited inorganic calcite overgrowth and/or dissolution

very good: no visible recrystallization, very limited amount of inorganic calcite overgrowth, no to very minor effects of dissolution visible

Fig. S5: Benthic $\delta^{18}O$ (a) and Δ_{47} (b) values of poorly, moderately, well and very well preserved foraminiferal tests. We rely on these qualitative classification classes in the current absence of a tool to quantify the amount of diagenetic calcite in a foraminiferal test. For each site, the number of observations per preservation class are listed at the bottom of the plots. Benthic foraminifera were first roughly classified under the light microscope based on test surface texture (preservation of microscale features such as pores), degree of translucence and test fragmentation. Then, a number of representative specimens from each site were further examined under the SEM to confirm and visualize potential dissolution, inorganic calcite overgrowths and recrystallization, and make the final classification. Note that we did the classification

in categories based on overall preservation of *N. truempyi* tests in each sample, although every sample typically includes a range of preservation states. SEM images documenting benthic foraminiferal preservation ranges at Sites 1409, 1260 and 1263 (including examples of poorly, moderately, well and very well preserved surface textures) are shown in Fig S6.

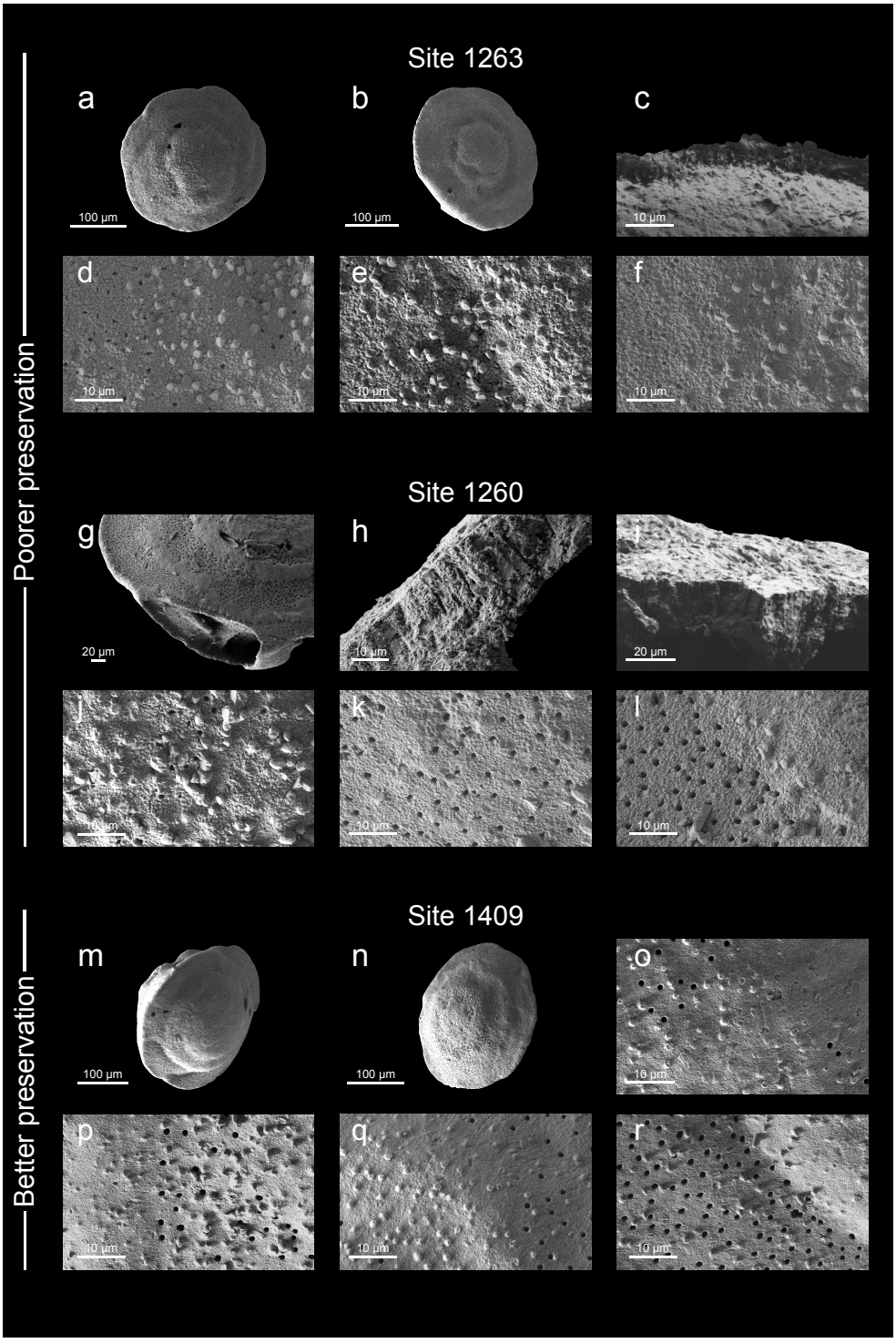
Site 1263
Site 1260
Site 1409
Poorer preservation
Better preservation
a
b
c
d
e
f
g
h
i
j
k
l
m
n
o
p
q
r
100 µm
10 µm
20 µm

Fig. S6: Additional SEM images illustrating preservation states and preservation ranges of benthic foraminifera *N. truempyi* at Sites 1263 (a-f), 1260 (g-l) and 1409 (m-r). For each site, a number of different representative specimens are shown. As an example, the benthic foraminiferal wall texture shown in (e) appears poorly preserved. Here, pores are largely obscured by abundant overgrowths of inorganic calcite crystals. In comparison to (e), inorganic calcite crystals on the moderately preserved specimen shown in (d) are slightly smaller, overgrowths less extensive and pores mostly visible. The comparably well preserved wall texture shown in (k) is characterized by limited inorganic calcite overgrowth with only small crystallites. The very well preserved texture shown in (r) appears smooth without visible crystal faces or pore etching. The foraminifera were picked from samples 208-1263B-11H-4,91-93 (a-f), 207-1260B-10R-6,94-96 (g-l) and 342-U1409C-7H-4,110-112 (m-r).

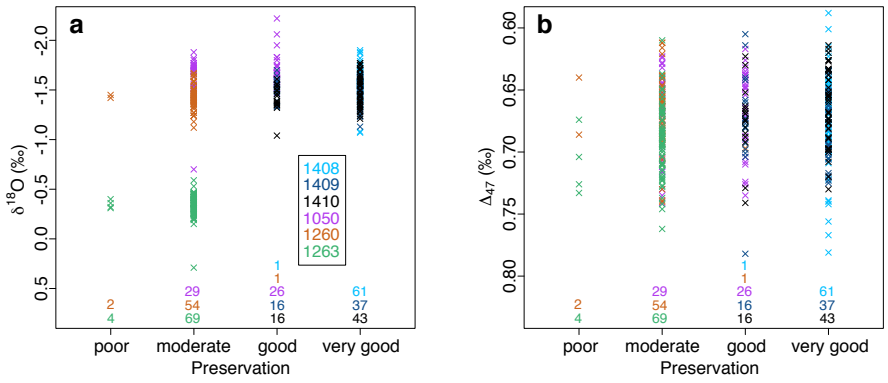

Preservation classes for planktic foraminifera

poor: extensive recrystallization, ubiquitous and massive inorganic calcite overgrowths and/or signs of major dissolution

moderate: some recrystallization, small inorganic calcite overgrowths and/or signs of dissolution

good: no visible recrystallization, signs of minor inorganic calcite overgrowths and/or minimal dissolution

very good: no visible recrystallization, no to very minor signs of inorganic calcite overgrowths, no effects of dissolution visible

Fig. S7: Planktic $\delta^{18}O$ (a) and Δ_{47} (b) values of poorly, moderately, well and very well preserved foraminiferal tests. For each site, the number of measurement values per preservation class are listed at the bottom of the plots. Similar to the classification of benthic foraminiferal preservation, the classification of planktic foraminiferal preservation states was done based on light microscopy in combination with SEM images of selected representative planktic foraminiferal tests. Note that planktic and benthic foraminiferal preservation classes are not identical. SEM images documenting planktic foraminiferal preservation ranges at each site are shown in Figs. S8 and S9. These figures include examples of poorly, moderately, well and very well preserved surface textures.

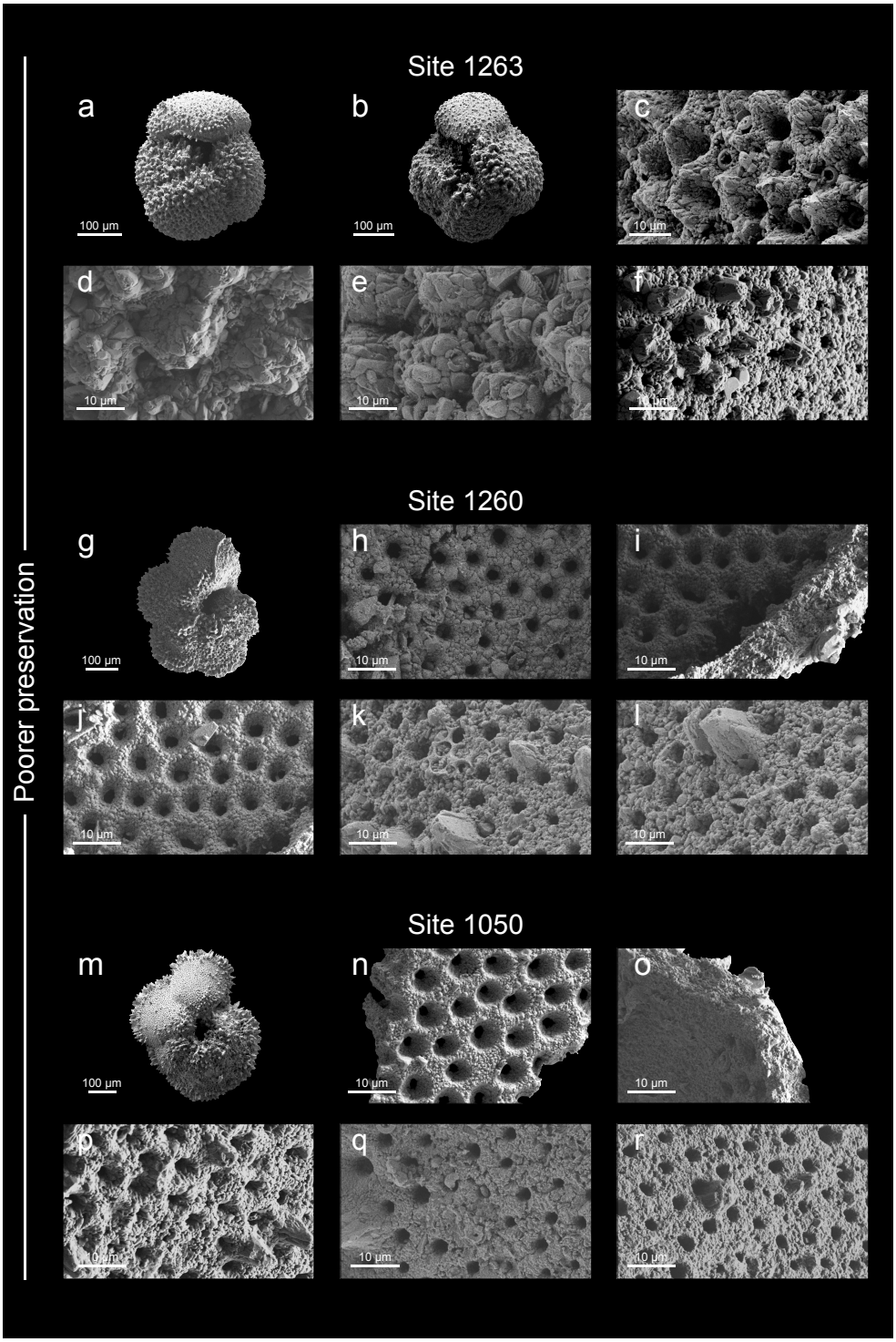
Site 1263
a
100 µm
b
100 µm
c
10 µm
d
10 µm
e
10 µm
f
10 µm
Site 1260
g
100 µm
h
10 µm
i
10 µm
j
10 µm
k
10 µm
l
10 µm
Site 1050
m
100 µm
n
10 µm
o
10 µm
p
10 µm
q
10 µm
r
10 µm
Poorer preservation

Fig. S8: Additional SEM images illustrating preservation states and preservation ranges of planktic foraminifera *A. bullbrooki* and *M. coronatus* at Sites 1263 (a-f), 1260 (g-l) and 1050 (m-r). For each site, a number of different representative specimens are shown. (d) and (e) display examples of poorly preserved planktic foraminiferal wall textures with ubiquitous overgrowths of massive calcite crystals, whereas calcite crystals covering the moderately preserved primary textures shown in (f) and (l) are smaller. Examples of well and very well preserved wall textures are presented in Fig. S9. The foraminifera were picked from samples 208-1263B-11H-6,51-53 (a, c, f), 208-1263B-11H-3,106-108 (b, d, e), 207-1260A-14R-5,146-148 (g-l), 171B-1050A-7H-5,102-104 (m, q, r) and 171B-1050A-7H-6,11-13 (n, o, p).

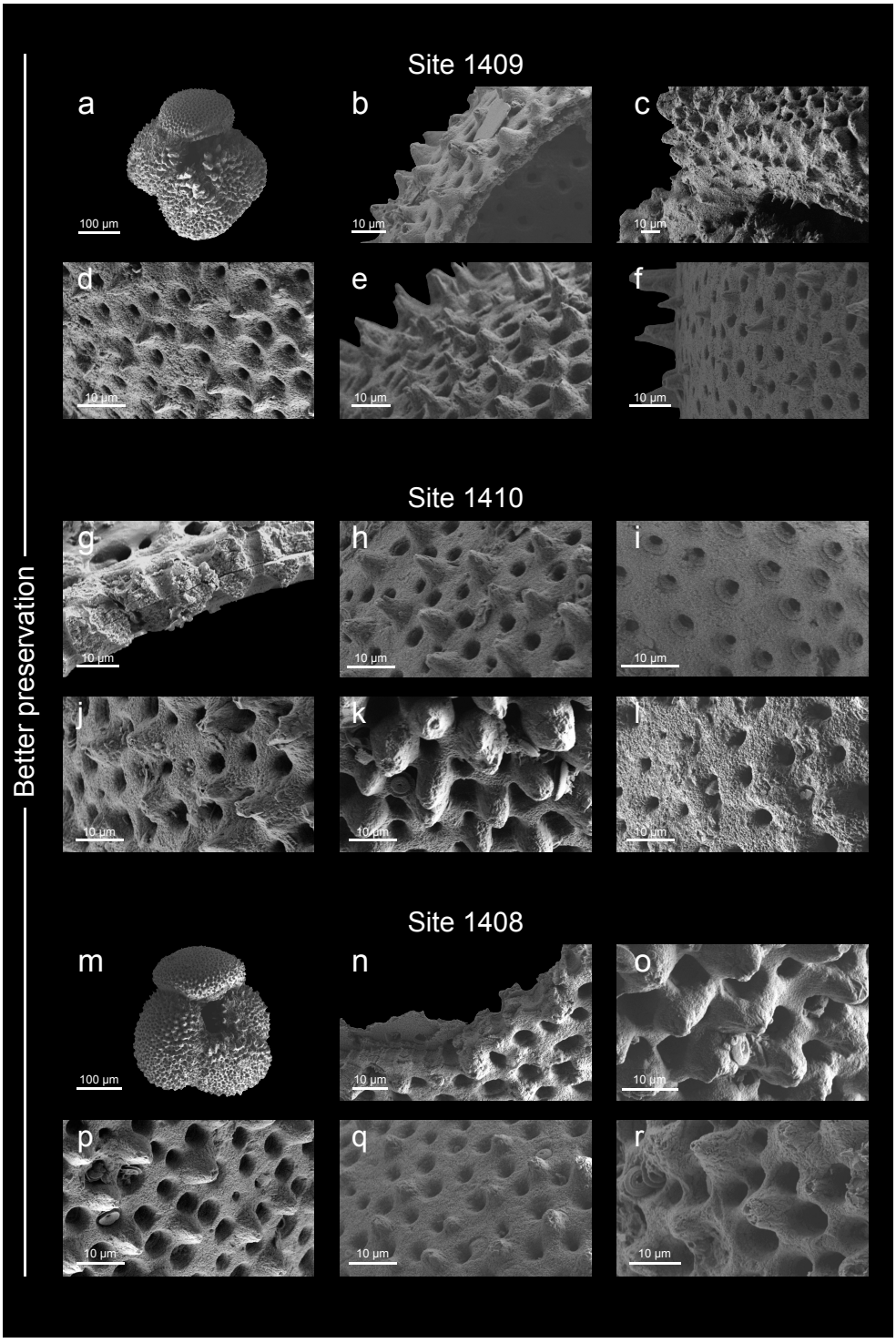
Site 1409
a
b
c
d
e
f
Site 1410
g
h
i
j
k
l
Site 1408
m
n
o
p
q
r
100 µm
10 µm
Better preservation

Fig. S9: Additional SEM images illustrating preservation states and preservation ranges of planktic foraminifera *A. bullbrooki* at Sites 1409 (a-f), 1410 (g-l) and 1408 (m-r). For each site, a number of different representative specimens are shown. Examples of well preserved wall textures are illustrated in (d) and (l). These wall textures appear slightly uneven (e.g., caused by dissolution) but exhibit only very small, hardly identifiable inorganic calcite crystals. For comparison, (o) and (p) show examples of very good preservation with purely biogenic surfaces and no visible signs of post-depositional alteration. The foraminifera were picked from samples 342-U1409C-7H-2,136-138 (a, c, d), 342-U1409C-7H-2,123-125 (b, e, f), 342-U1410C-17X-4,46-48 (g, h), 342-U1410C-17X-3,147-149 (i, j, k), 342-U1410C-17X-3,73-75 (l), 342-U1408C-17H-3,37-39 (m, n, o, q, r) and 342-U1408B-18H-2,109-111 (p).

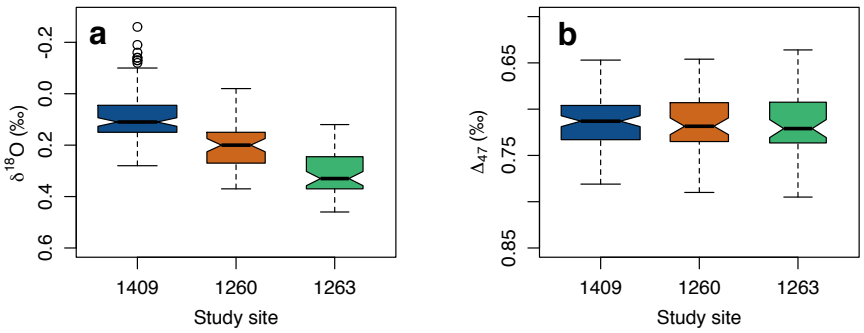

Fig. S10: Boxplots for benthic $\delta^{18}O$ (a) and Δ_{47} (b) values from -0.17 Myr to +0.21 Myr around the 20n/20r boundary. Boxes indicate lower and upper quartiles. Bold horizontal lines represent the median, whereas the lines extending vertically from the boxes (whiskers) illustrate the value ranges excluding outliers (circles). The boxplots were created using R with standard settings. Colors as defined in Fig. 1.

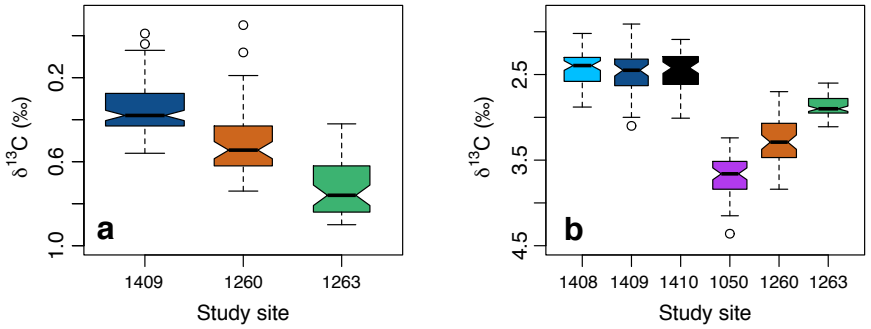

Fig. S11: Boxplots for benthic (a) and planktic (b) $\delta^{13}C$ values. Benthic and planktic data cover -0.17 Myr to +0.21 Myr and -0.15 Myr to +0.21 Myr around the 20n/20r boundary, respectively. The boxplots were created using R with standard settings. Colors as defined in Fig. 1.

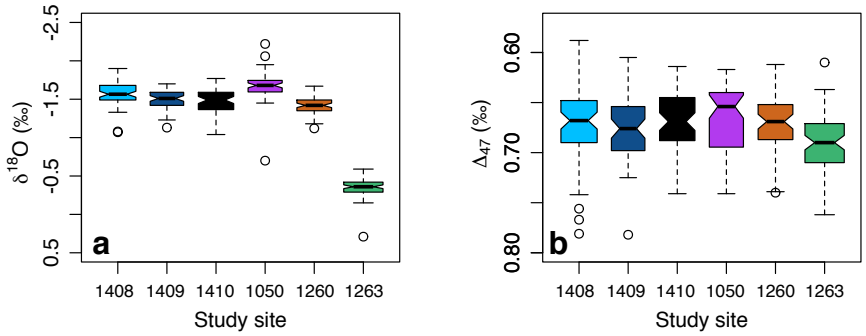

Fig. S12: Boxplots for planktic $\delta^{18}O$ (a) and Δ_{47} (b) covering -0.15 Myr to +0.21 Myr around the 20n/20r boundary. The boxplots were created using R with standard settings. Colors as defined in Fig. 1.

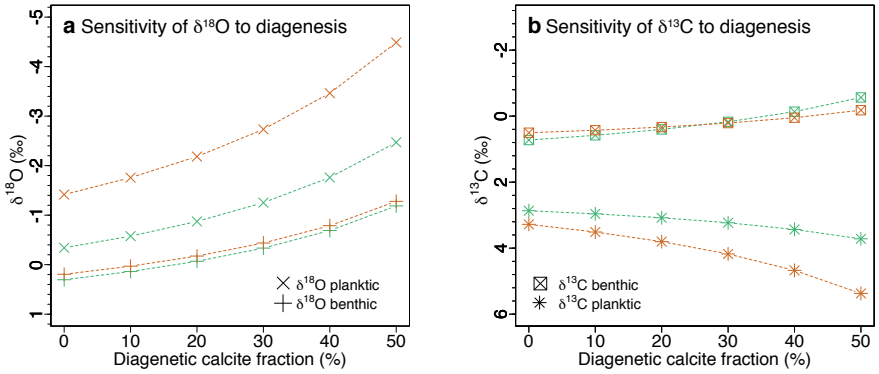

Fig. S13: Sensitivities of foraminiferal $\delta^{18}O$ and $\delta^{13}C$ values to diagenesis. Initial biogenic $\delta^{18}O$ (a) and $\delta^{13}C$ (b) signatures were modeled for different fractions of inorganic calcite. For this modeling, we utilized the ^{18}O fractionation factor of Watkins et al. (2013). Similar to $\delta^{18}O$, planktic $\delta^{13}C$ seems to be more susceptible to diagenetic alteration than benthic $\delta^{13}C$. Colors as defined in Fig. 1.

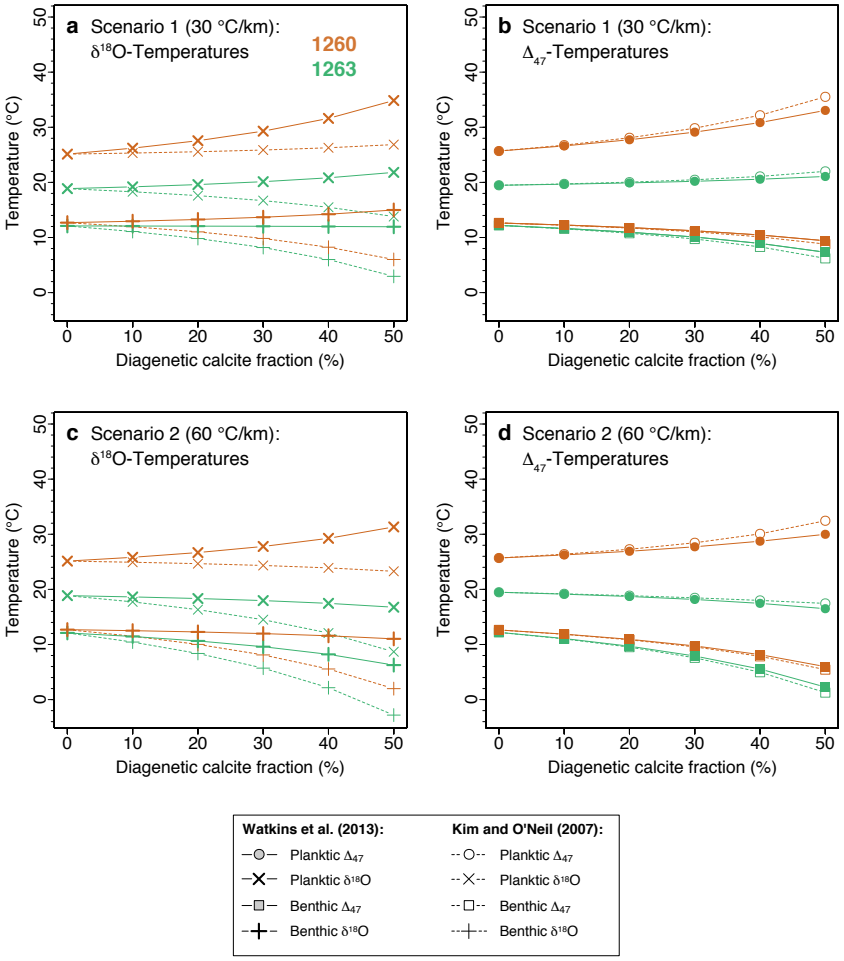

Fig. S14: Effects of late diagenesis near final sediment burial depths on modeled biogenic calcification temperatures ($\delta^{18}O$ and Δ_{47}). Similar to Sexton et al. (2006), two different geothermal gradient estimates were used to approach the geothermal gradient during the middle Eocene and define two scenarios of late (deep) diagenesis: (1) 30 °C/km (a, b) and (2) 60 °C/km (c, d) (Zwart et al., 1996; Rao et al., 2001; Stolper et al., 2018). In addition, we utilized a pore fluid $\delta^{18}O$ gradient of -2.5

‰/km (Lawrence and Gieskes, 1981; Sexton and Wilson, 2009) and our site-specific clumped isotope DSTs averaged over the relevant interval (temperatures at 0 m below sea floor) to calculate pore fluid $\delta^{18}O$ and temperatures at final sediment burial depths in both scenarios of deep diagenesis. Constant gradients in pore fluid $\delta^{18}O$ and temperature were assumed, due to a lack of better constraint for Sites 1260 and 1263 during the middle Eocene. For the same reason, pore fluid $\delta^{13}O$ gradients in these high carbonate, low organic matter sediments were assumed to be 0 ‰/km. Sediments from Site 1260 were taken from around 117 m to 129 m burial depth and sediments from Site 1263 were taken from around 170 m to 174 m burial depth (Table 1). In both scenarios, deep diagenesis at Sites 1260 and 1263 is assumed to occur in depths of 117 m and 170 m, respectively (approximate locations of uppermost samples at each site). For the modeling of DSTs at Site 1260, calculated temperatures of diagenetic calcite precipitation are 16.1 °C and 19.7 °C in Scenarios 1 and 2, respectively. Furthermore, diagenetic calcite $\delta^{18}O$ compositions in Scenarios 1 and 2 are 0.62 ‰ and -0.12 ‰, respectively, when assuming the ^{18}O fractionation factor of Watkins et al. (2013), and -1.04 ‰ and -1.79 ‰, respectively, when assuming the ^{18}O fractionation factor of Kim and O'Neil (1997). At Site 1263, diagenetic calcite precipitation temperatures are 17.3 °C and 22.4 °C in Scenarios 1 and 2, whereas diagenetic calcite $\delta^{18}O$ compositions are 0.28 ‰ and -0.78 ‰ for ^{18}O fractionation according to Watkins et al. (2013), and -1.39 ‰ and -2.46 ‰ for ^{18}O fractionation according to Kim and O'Neil (1997). Similar to the scenario of early burial diagenesis described in Table 2, inorganic calcite precipitation temperature and $\delta^{18}O$ values used for SST modeling are very similar to the values used for DST modeling, and thus not listed explicitly. Deep and shallow diagenesis values are compared in Fig. S15.

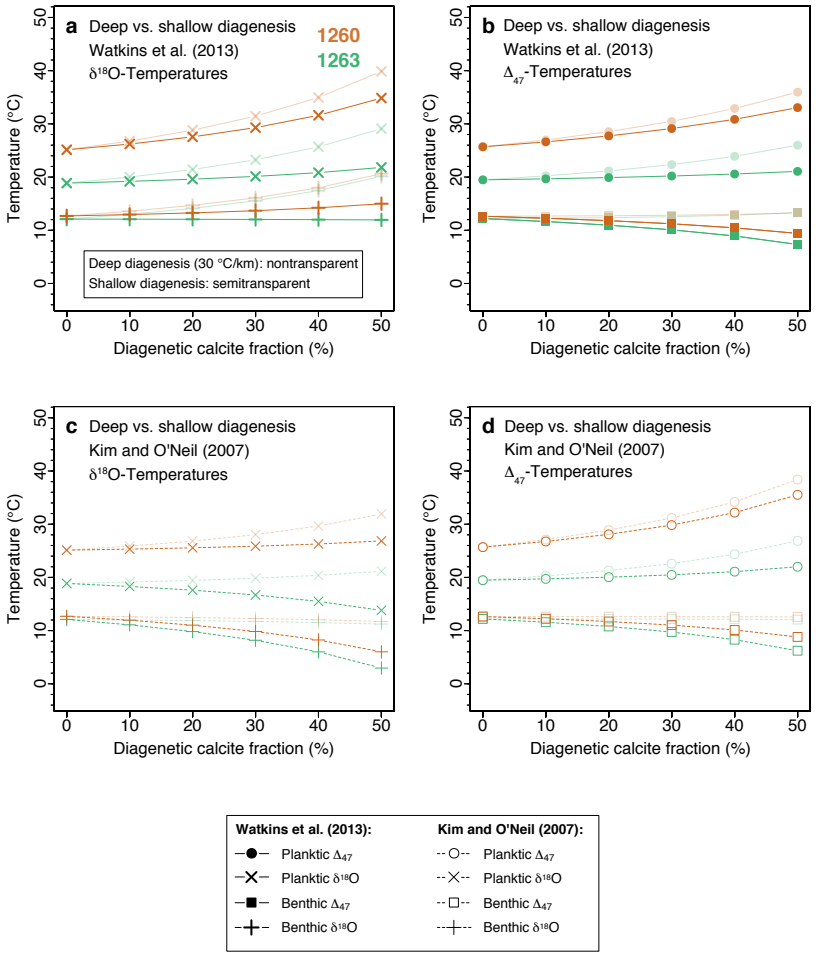

Fig. S15: Comparison of deep (nontransparent) and shallow (semitransparent) diagenetic effects on modeled biogenic calcification temperatures ($\delta^{18}O$ and Δ_{47}). $\delta^{18}O$-based temperature values are shown in (a) and (c), whereas Δ_{47}-based temperatures are shown in (b) and (d). The deep diagenesis values are identical to the values shown in Figs. S14a and S14b (geothermal gradient of 30 °C/km), whereas the shallow diagenesis values are identical to the values shown in Fig. 8. In

comparison to shallow diagenesis, deeper diagenesis would imply a smaller cool bias in SSTs reconstructed from the $\delta^{18}O$- and Δ_{47}-signatures of planktic foraminiferal tests and benthic foraminiferal DSTs that are potentially too high.

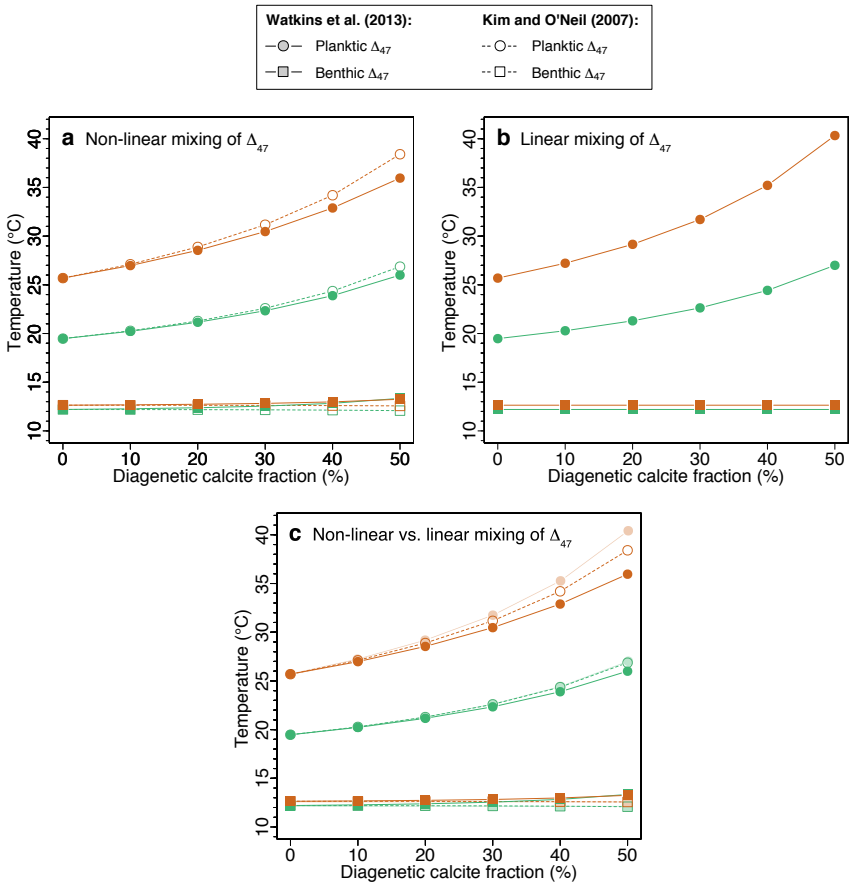

Fig. S16: Effects of non-linear mixing on modeled Δ_{47}-based temperatures. Temperatures of initial biogenic calcification are plotted for (a) non-linear and (b) linear Δ_{47} mixing. Panel (c) shows non-linear (nontransparent) vs. linear (semitransparent) mixing of Δ_{47}. (a) is identical to Fig. 8b. We used the ^{18}O fractionation factors of Watkins et al. (2013) (filled circles) and Kim and O'Neil (1997) (open circles) for our non-linear mixing calculations. The curves in (b) visualizing linear mixing have been calculated based on the assumption that the Δ_{47} values of frosty foraminiferal tests represent weighted averages (linear mixing) of the Δ_{47}

values of glassy biogenic calcite and inorganic calcite formed during post-depositional diagenesis. Therefore, these values are independent of the ^{18}O fractionation factor. The comparison of non-linear and linear mixing of Δ_{47} (c) shows a reduced susceptibility of planktic foraminiferal Δ_{47} to diagenesis when considering non-linear mixing effects. Colors as defined in Fig. 1.

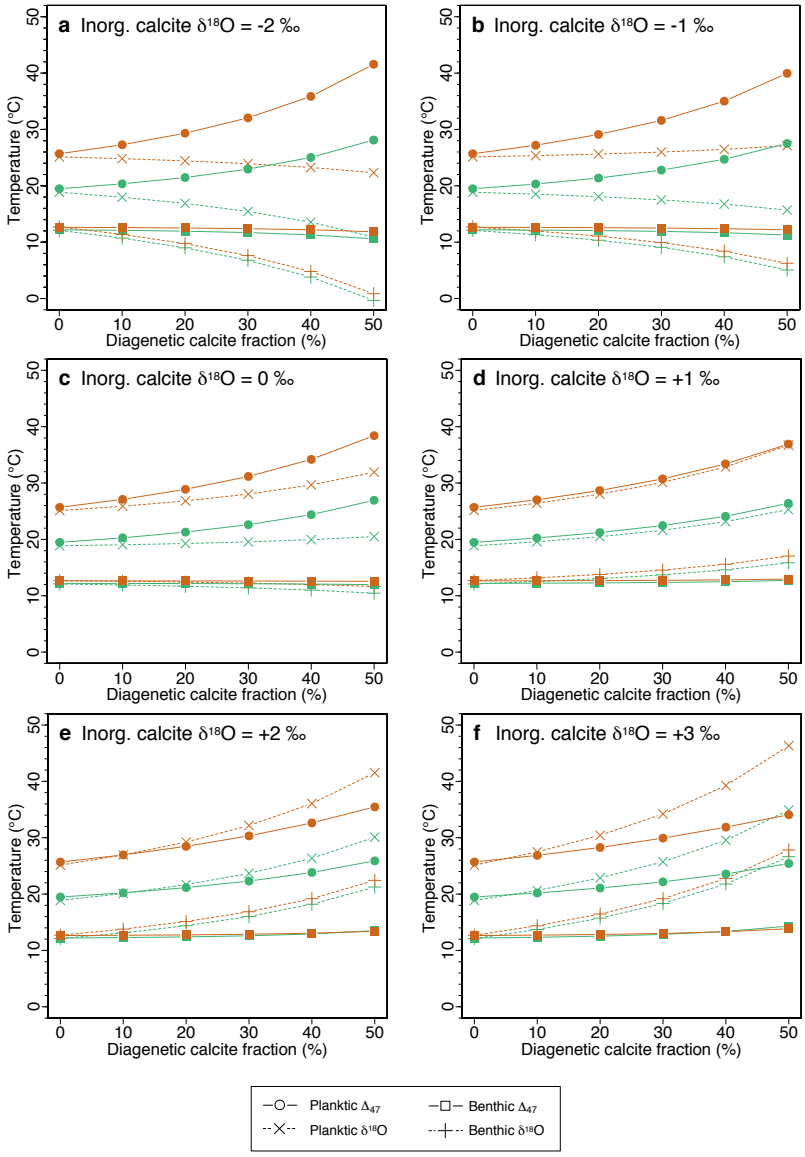

Fig. S17: Sensitivity of modeled biogenic calcification temperatures ($\delta^{18}O$ and Δ_{47}) to different inorganic $\delta^{18}O$ compositions. $\delta^{18}O$ values of pore fluids and inorganic calcite precipitated during early diagenesis may be influenced by local effects and thus

difficult to estimate without direct measurements. Therefore, inorganic calcite $\delta^{18}O$ values of (a) -2 ‰, (b) -1 ‰, (c) 0 ‰, (d) +1 ‰, (e) +2 ‰ and (f) +3 ‰, spanning the range of published values (e.g., Pearson et al., 2001; Tripati et al., 2003; Kozdon et al., 2013; Voigt et al., 2016), were used to test the effect of inorganic calcite $\delta^{18}O$ on diagenetic alteration. Temperature values are based on planktic (crosses) and benthic (plus signs) foraminiferal $\delta^{18}O$ as well as on planktic (circles) and benthic (squares) foraminiferal Δ_{47}. For this sensitivity test, the ^{18}O fractionation factor does not matter, as inorganic calcite $\delta^{18}O$ is prescribed. Colors as defined in Fig. 1.

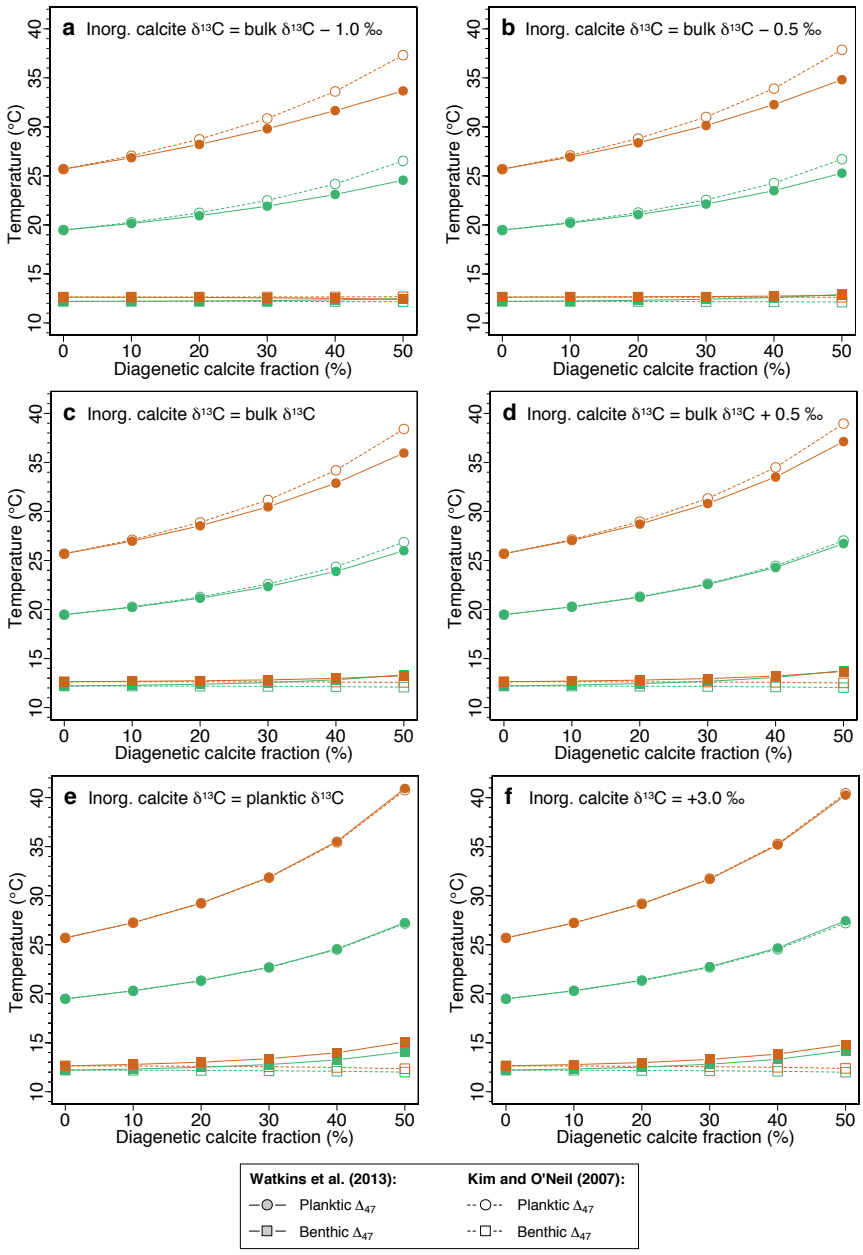

Fig. S18: Sensitivity of modeled biogenic calcification temperatures (Δ_{47}) to different inorganic $\delta^{13}C$ compositions. The approximation of inorganic calcite $\delta^{13}C$ by bulk

$\delta^{13}C$ (Table 2) may be complicated by local effects. Furthermore, bulk $\delta^{13}C$ values for Site 1260 (Edgar et al., 2007) were taken from a slightly different time interval during the middle Eocene (roughly 42 Ma). Using the ^{18}O fractionation factors of Watkins et al. (2013) (filled circles) and Kim and O'Neil (1997) (open circles), we performed a sensitivity study to test the effect of different assumptions for inorganic calcite $\delta^{13}C$ on the susceptibility of clumped isotope temperatures to diagenesis. For that, we assumed inorganic calcite $\delta^{13}C$ values that are (a) 1.0 ‰ lower than bulk $\delta^{13}C$, (b) 0.5 ‰ lower than bulk $\delta^{13}C$ and (d) 0.5 ‰ higher than bulk $\delta^{13}C$. In addition, we used (e) site-specific planktic $\delta^{13}C$ averaged over the overlapping time interval to approximate inorganic calcite $\delta^{13}C$ as well as (f) absolute inorganic calcite $\delta^{13}C$ equals 3.0 ‰, similar to Pearson et al. (2001). (c) is identical to Fig. 8b. Temperature values are based on planktic (circles) and benthic (squares) foraminiferal Δ_{47}. Colors as defined in Fig. 1.

References

Baker, P.A., Gieskes, J.M. and Elderfield, H. (1982) Diagenesis of Carbonates in Deep-Sea Sediments - Evidence from Sr/Ca Ratios and Interstitial Dissolved Sr^{2+} Data. *Journal of Sedimentary Petrology* **52,** 71-82.

Edgar, K.M., Pälike, H. and Wilson, P.A. (2013) Testing the impact of diagenesis on the $\delta^{18}O$ and $\delta^{13}C$ of benthic foraminiferal calcite from a sediment burial depth transect in the equatorial Pacific. *Paleoceanography* **28,** 468-480.

Edgar, K.M., Wilson, P.A., Sexton, P.F. and Suganuma, Y. (2007) No extreme bipolar glaciation during the main Eocene calcite compensation shift. *Nature* **448,** 908-911.

Erbacher, J., Mosher, D.C., Malone, M.J. and the Expedition 207 Scientists (2004) Site 1260, *Proceedings of the Ocean Drilling Program, Initial Reports Volume 207*, pp. 1-113.

Kim, S.T. and O'Neil, J.R. (1997) Equilibrium and nonequilibrium oxygen isotope effects in synthetic carbonates. *Geochimica et Cosmochimica Acta* **61,** 3461-3475.

Kozdon, R., Kelly, D.C., Kitajima, K., Strickland, A., Fournelle, J.H. and Valley, J.W. (2013) In situ $\delta^{18}O$ and Mg/Ca analyses of diagenetic and planktic foraminiferal calcite preserved in a deep-sea record of the Paleocene-Eocene thermal maximum. *Paleoceanography* **28,** 517-528.

Laskar, J., Fienga, A., Gastineau, M. and Manche, H. (2011) La2010: a new orbital solution for the long-term motion of the Earth. *Astronomy & Astrophysics* **532**.

Lawrence, J.R. and Gieskes, J.M. (1981) Constraints on Water Transport and Alteration in the Oceanic Crust from the Isotopic Composition of Pore Water. *Journal of Geophysical Research* **86,** 7924-7934.

Locarnini, R.A., Mishonov, A.V., Antonov, J.I., Boyer, T.P., Garcia, H.E., Baranova, O.K., Zweng, M.M., Paver, C.R., Reagan, J.R., Johnson, D.R., Hamilton, M. and Seidov, D. (2013) World Ocean Atlas 2013, Volume 1: Temperature. S. Levitus, Ed., A. Mishonov Technical Ed. *NOAA Atlas NESDIS 73***,** 40.

Norris, R.D., Kroon, D., Klaus, A. and the Expedition 171B Scientists (1998) Site 1050, *Proceedings of the Ocean Drilling Program, Initial Reports, Vol. 171B*, pp. 93-169.

Ogg, J.G. (2012) Chapter 5 – Geomagnetic Polarity Time Scale, in: Gradstein, F.M., Ogg, J.G., Schmitz, M.D., and Ogg, G.M. (Eds.), *The Geologic Time Scale*. Elsevier, Boston, pp. 85-113.

Paillard, D., Labeyrie, L. and Yiou, P. (1996) Macintosh program performs time-series analysis. *Eos Trans. AGU* **77,** 379.

Pearson, P.N., Ditchfield, P.W., Singano, J., Harcourt-Brown, K.G., Nicholas, C.J., Olsson, R.K., Shackleton, N.J. and Hall, M.A. (2001) Warm tropical sea surface temperatures in the Late Cretaceous and Eocene epochs. *Nature* **414,** 481-487.

Rao, Y.H., Subrahmanyam, C., Sharma, S.R., Rastogi, A.A. and Deka, B. (2001) Estimates of geothermal gradients and heat flow from BSRs along the Western Continental Margin of india. *Geophysical Research Letters* **28,** 355-358.

Schrag, D.P., DePaolo, D.J. and Richter, F.M. (1995) Reconstructing Past Sea-Surface Temperatures - Correcting for Diagenesis of Bulk Marine Carbonate. *Geochimica et Cosmochimica Acta* **59,** 2265-2278.

Sexton, P.F. and Wilson, P.A. (2009) Preservation of benthic foraminifera and reliability of deep-sea temperature records: Importance of sedimentation rates, lithology, and the need to examine test wall structure. *Paleoceanography* **24**.

Sexton, P.F., Wilson, P.A. and Pearson, P.N. (2006) Microstructural and geochemical perspectives on planktic foraminiferal preservation: "Glassy" versus "Frosty". *Geochemistry Geophysics Geosystems* **7**.

Stolper, D.A., Eiler, J.M. and Higgins, J.A. (2018) Modeling the effects of diagenesis on carbonate clumped-isotope values in deep- and shallow-water settings. *Geochimica et Cosmochimica Acta* **227,** 264-291.

Tripati, A.K., Delaney, M.L., Zachos, J.C., Anderson, L.D., Kelly, D.C. and Elderfield, H. (2003) Tropical sea-surface temperature reconstruction for the early Paleogene using Mg/Ca ratios of planktonic foraminifera. *Paleoceanography* **18**.

Vandenberghe, N., Hilgen, F.J., Speijer, R.P., Ogg, J.G., Gradstein, F.M., Hammer, O., Hollis, C.J. and Hooker, J.J. (2012) Chapter 28 – The Paleogene Period, in: Gradstein, F.M., Ogg, J.G., Schmitz, M.D., and Ogg, G.M. (Eds.), *The Geologic Time Scale*. Elsevier, Boston, pp. 855-921.

Voigt, J., Hathorne, E.C., Frank, M. and Holbourn, A. (2016) Minimal influence of recrystallization on middle Miocene benthic foraminiferal stable isotope stratigraphy in the eastern equatorial Pacific. *Paleoceanography* **31,** 98-114.

Watkins, J.M., Nielsen, L.C., Ryerson, F.J. and DePaolo, D.J. (2013) The influence of kinetics on the oxygen isotope composition of calcium carbonate. *Earth and Planetary Science Letters* **375,** 349-360.

Westerhold, T. and Röhl, U. (2013) Orbital pacing of Eocene climate during the Middle Eocene Climate Optimum and the chron C19r event: Missing link found

in the tropical western Atlantic. *Geochemistry Geophysics Geosystems* **14,** 4811-4825.

Zachos, J.C., Kroon, D., Blum, P. and the Expedition 208 Scientists (2004) Site 1263, *Proceedings of the Ocean Drilling Program, Initial Reports Volume 208*, pp. 1-87.

Zwart, G., Moore, J.C. and Cochrane, G.R. (1996) Variations in temperature gradients identify active faults in the Oregon accretionary prism. *Earth and Planetary Science Letters* **139,** 485-495.

Graphic design: Communication Division, UiB / Print: Skipnes Kommunikasjon AS

uib.no

ISBN: 9788230846919 (print)
9788230860656 (PDF)